Aalto-yliopisto
Aalto-universitetet
Aalto University

Master's Programme in Building Technology

Finnish Bridge Fatigue Load Model Calibration from Recorded Traffic Data in Kaarina

Max Abrahamsson

Master's thesis
2025

Aalto-yliopisto
Aalto-universitetet
Aalto University

Author Max Abrahamsson	
Title of thesis Finnish Bridge Fatigue Load Model Calibration from Recorded Traffic Data in Kaarina	
Programme Building Technology	
Thesis supervisor Prof. Weiwei Lin	
Thesis advisor Dr. Rui Hao	
Date 18.02.2025	**Number of pages** 102+2	**Language** English

Abstract

In 2013, a new regulation was implemented that increased the allowable vehicle weights in Finland. However, heavier vehicles increase stress ranges, which can affect the fatigue life of bridges. Eurocodes provide five Fatigue Load Models for fatigue verification. However, these Load Models were derived from Central European traffic in the 1980s. Two of the Fatigue Load Models are used in this analysis, FLM3 and FLM4. Furthermore, this analysis includes recorded traffic data from two separate years, 2014 and 2016. The traffic data was measured in Southwest Finland during a larger measurement campaign. Eurocodes provide two fatigue verification methods. That is the cumulative damage method and the damage equivalent method. The first is used with the recorded traffic and FLM4, whereas the latter is used with FLM3.

The effect of the regulation change and the accuracy of the Fatigue Load Models are inspected for four case bridges with varying span lengths. The required elastic section modulus for each case bridge and span length is calculated. The section modulus obtained for the 2016 recorded traffic is compared with the ones obtained for 2014 traffic to see how the regulations have affected bridge fatigue. The comparison between Fatigue Load Models and actual traffic is done by comparing the section modulus obtained for FLM3 and FLM4 with the 2016 recorded traffic. A new Fatigue Load Model is also calibrated based on FLM3, given in the Eurocodes. The calibration is done using the 2016 measured traffic data.

The results obtained clearly show how the regulation change has affected bridge fatigue. The traffic recorded in 2016 requires a higher elastic section modulus than the 2014 traffic. This is due to heavier vehicles and a higher traffic volume, causing larger stress ranges and more stress cycles. The Fatigue Load Models give conservative results compared to actual traffic, even when the vehicle weights have increased. With the calibrated Fatigue Load Model, the accuracy improved substantially compared to measured traffic. This is due to the new FLM and fatigue vehicle representing the traffic they were calibrated from.

Keywords Fatigue; Bridge fatigue; Fatigue Load Model; FLM3; FLM4; Elastic section modulus; B-WIM; WIM; Recorded traffic

Aalto-yliopisto
Aalto-universitetet
Aalto University

Tekijä Max Abrahamsson

Työn nimi Suomalaisen väsymiskuormakaavion kalibrointi Kaarinassa mitattujen liikennetietojen perusteella

Koulutusohjelma Building Technology

Vastuuopettaja/valvoja Prof. Weiwei Lin

Työn ohjaaja Toht. Rui Hao

Päivämäärä 18.02.2025 **Sivumäärä** 102+2 **Kieli** Englanti

Tiivistelmä

Vuonna 2013 otettiin käyttöön uusi säädös, joka kasvatti sallittuja ajoneuvopainoja suomessa. Raskaammat ajoneuvot kuitenkin kasvattavat jännitysvaihteluvälejä, mikä voi siten vaikuttaa siltojen väsymiskestävyyteen. Eurokoodit tarjoavat viisi väsymiskuormakaaviota väsymistarkastelua varten. Nämä kuormakaaviot on kuitenkin kalibroitu Keski-Euroopan 1980-luvulla mitatusta liikenteestä. Tässä analyysissä käytetään kahta väsymiskuormakaaviota, FLM3 ja FLM4. Tämä analyysi sisältää myös mitattuja liikennetietoja kahdelta eri vuodelta, 2014 ja 2016. Lisäksi Eurokoodit tarjoavat kaksi väsymistarkastelumenetelmää, kumulatiivisen vauriomenetelmän ja vaurioekvivalenttimenetelmän. Ensimmäistä käytetään todellisen liikenteen ja FLM4-mallin kanssa, kun taas jälkimmäistä käytetään FLM3-mallin kanssa.

Säädösmuutosten vaikutusta ja väsymiskuormakaavioiden tarkkuutta tutkitaan neljän esimerkkisillan sekä usean jännepituuden avulla. Kullekin esimerkkisillalle ja jännepituudelle lasketaan tarvittava taivutusvastus. Vuoden 2016 mitatun liikenteen perusteella saatu taivutusvastus vertaillaan vuoden 2014 liikenteestä saatuihin arvoihin, jotta voidaan arvioida säädösmuutosten vaikutusta siltojen väsymiseen. Väsymiskuormakaavioiden ja todellisen liikenteen välinen vertailu tehdään vertaamalla FLM3- ja FLM4-malleilla saatua taivutusvastusta vuoden 2016 mitattuun liikenteeseen. Lisäksi FLM3-malliin perustuva uusi väsymiskuormakaavio kalibroidaan käyttäen vuoden 2016 mitattuja liikennetietoja.

Saadut tulokset osoittavat selvästi, kuinka säädösmuutos on vaikuttanut siltojen väsymiseen. Vuoden 2016 mitattu liikenne vaatii suuremman taivutusvastuksen kuin vuoden 2014 liikenne. Tämä johtuu raskaammista ajoneuvoista ja suuremmasta liikennemäärästä, jotka aiheuttavat laajempia jännitysvaihteluita ja enemmän jännityssyklejä. Väsymiskuormakaaviot antavat todelliseen liikenteeseen verrattuna varovaisempia tuloksia, vaikka ajoneuvojen painot ovat kasvaneet. Kalibroidun väsymiskuormakaavion avulla tarkkuus parani merkittävästi mitattuun liikenteeseen verrattuna.

Avainsanat Väsyminen; Sillan väsyminen; Väsymiskuormakaavio; FLM3; FLM4; Taivutusvastus; B-WIM; Mitattu liikenne

Aalto-yliopisto
Aalto-universitetet
Aalto University

Författare Max Abrahamsson

Titel Finsk broutmattningslastmodellkalibrering baserad på uppmätt trafikdata i Kaarina

Utbildningsprogram Building Technology

Ansvarslärare Prof. Weiwei Lin

Handledare Dr Rui Hao

Datum 18.02.2025 **Sidantal** 102+2 **Språk** Engelska

Sammandrag

År 2013 implementerades en ny föreskrift som ökade de tillåtna fordonsvikterna i Finland. Tyngre fordon leder dock till större utmattningsspänningsvariationer, vilket i sin tur kan påverka broars utmattningslivslängd. Eurokoderna tillhandahåller fem utmattningslastmodeller för verifiering av utmattning. Dessa lastmodeller härstammar dock från den centraleuropeiska trafiken från 1980-talet. Två av utmattningsmodellerna används i denna analys, FLM3 och FLM4. Vidare inkluderar analysen uppmätt trafikdata från två separata år, 2014 och 2016. Dessutom tillhandahåller Eurokoderna två metoder för verifiering av utmattning, den kumulativa skademetoden och den ekvivalenta skademetoden. Den förstnämnda används med de uppmätta trafikdata och FLM4, medan den senare används med FLM3.

Effekten av föreskriftsändringen samt noggrannheten av utmattningslastmodellerna undersöks för fyra exempel bron med varierande spannlängder. Den nödvändiga elastiska sektionsmodulen beräknas för varje bro och spannlängd. Sektionsmodulen som erhålls från den uppmätta trafikdata från 2016 jämförs med motsvarande värden från 2014 för att analysera hur föreskriftsändringen har påverkat broarnas utmattning. Jämförelsen mellan utmattningsmodellerna och den riktiga trafiken görs genom att jämföra sektionsmodulen som erhålls för FLM3 och FLM4 med de uppmätta trafikdata från 2016. Dessutom kalibreras en ny utmattningsmodell baserat på FLM3. Kalibreringen görs med hjälp av de uppmätta trafikdata från 2016.

Resultaten visar tydligt hur föreskriftsändringen har påverkat broarnas utmattning. Trafiken som mättes 2016 kräver en högre elastisk sektionsmodul än trafiken från 2014. Detta beror på tyngre fordon och en högre trafikvolym, vilket orsakar större spänningsvariationer och fler belastningscyklar. Utmattningsmodellerna ger konservativa resultat jämfört med den riktiga trafiken, även när fordonsvikterna har ökat. Med den kalibrerade utmattningsmodellen förbättrades noggrannheten avsevärt i jämförelse med de uppmätta trafikdata.

Nyckelord Utmattning; Utmattningsmodell; FLM3; FLM4; Sektionsmodul; B-WIM; Trafikdata

Table of contents

Preface and acknowledgements

This thesis has been a long and challenging journey, with several obstacles, particularly during the calculation phase. However, despite many difficulties, the learning process has been incredibly rewarding. Through this experience, I have gained valuable new skills that I previously had no knowledge of and hope to apply them in the future. However, most importantly, I gained a deeper understanding of myself.

I would like to express my sincere gratitude to Professor Weiwei Lin and Dr. Rui Hao for providing me with the opportunity to undertake this thesis and for their constructive feedback, continuous guidance and support throughout this thesis process.

Helsinki, 18 February 2025
Max Abrahamsson

Symbols and abbreviations

Symbols

D	cumulative damage
F_{axle}	axle force
N	number of cycles
N_i	number of cycles to failure at i:th stress
Q_{ik}	concentrated loads
R	stress ratio; ratio
S	stress range; stress amplitude
W; W,el	elastic section modulus
a	intercept value at the axis of representing cycles
edges	bin edge
m, m_i	slope parameter
n_i	number of cycles for a given stress range
q_{ik}	uniformly distributed loads
q_{rk}	uniformly distributed loads
t_r	crossing time
α_{qi}	α-factor for uniformly distributed loads
α_{Qi}	α-factor for concentrated loads
γ_{Ff}	partial fatigue safety factor
γ_{MF}	material safety factor
$\Delta\sigma$	stress range
$\Delta\sigma_c$	detail category

$\Delta\sigma_D$	constant amplitude fatigue limit
$\Delta\sigma_{E2}$	damage equivalent stress range at 2 million cycles
$\Delta\sigma_i$	a certain stress range
$\Delta\sigma_L$	cut-off limit
$\Delta\sigma_p$	stress range according to FLM3
λ	damage equivalent factor
σ	stress
σ_a	stress amplitude
σ_m	mean stress
σ_{max}	maximum stress
σ_{min}	minimum stress
ϕ_2	damage equivalent impact factor

Abbreviations

ASTM	American Society for Testing and Materials
B-WIM	Bridge Weigh-in-Motion
CAL	Constant Amplitude Load
DAF	Dynamic Amplification Factor
DLDR	Double Linear Damage Rule
ERS	Electrical Resistance Strain
FLM	Fatigue Load Model
GVW	Gross Vehicle Weight
HCF	High Cycle Fatigue

HS-WIM	High-Speed Weigh-in-Motion
IL	Influence Line
LCF	Low Cycle Fatigue
LDR	Linear Damage Rule
LM	Load Model
LS-WIM	Low-Speed Weigh-in-Motion
MFI	Moving Force Identification
NA	National Annex
NLDR	Non-Linear Damage Rule
RC	Reinforced Concrete
RMSE	Root Means Square Error
SFS	Suomen Standardisoimisliitto
UDL	Uniformly Distributed Load
VAL	Variable Amplitude Load
WIM	Weigh-in-Motion

1 Introduction

Bridges are a main part of the infrastructure that connects cities and people. The main purpose of a bridge is to make the journey easier from point A to point B, by overcoming obstacles. A bridge can be classified by different criteria, from span length to span type or by structural form. As of 2024, there are roughly 15160 bridges on the Finnish road network (Väylävirasto, 2024). As bridges can be very long structures with a large clearance to the ground, a failure could have significant economic and life losses. Thus, the design, construction, and maintenance should be well executed. The designed life span of a bridge in Finland is usually 100 years apart from some extreme cases like the Kruunuvuori bridge, with a designed 200-year service life (Tompuri, 2023). Although the life span of a bridge is very long, maintenance and reparations are frequently needed due to regulation changes and environmental changes, which can drastically impact the service life.

1.1 Background

The weight of vehicles has altered through the years and will continue to alter in the years to come. The evolution of vehicle weights has been somewhat significant in Finland, where the maximum gross vehicle weight (GVW) has been regulated to 76 tonnes. This can be observed from Figure 1. Earlier, the maximum weight was 60 tonnes. Furthermore, the maximum allowable vehicle mass for different axle combinations has increased. (Pöyskö, et al., 2014)

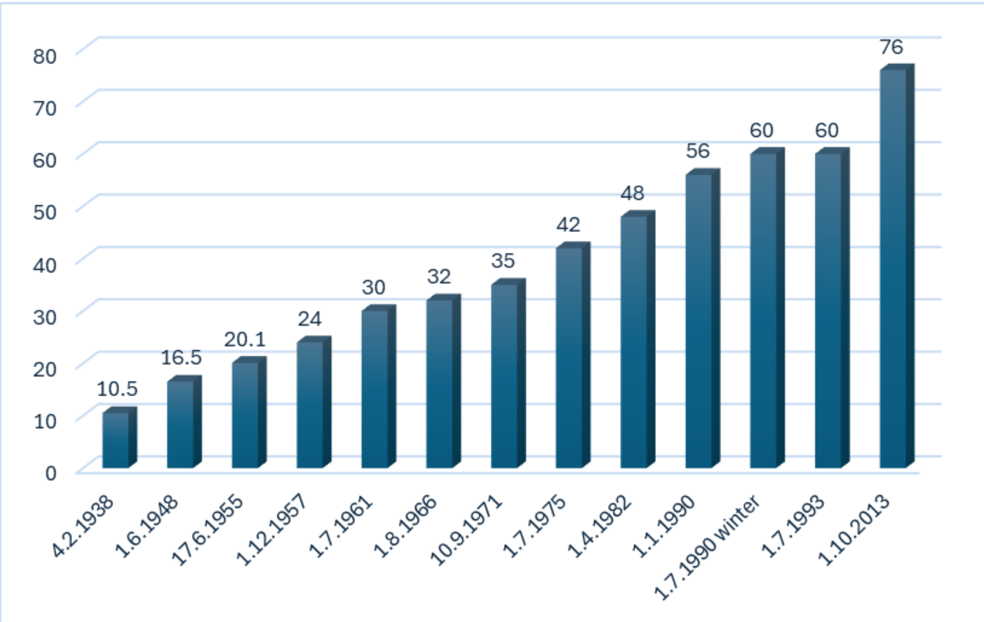

Figure 1. Evolution of maximum allowable vehicle weights in Finland. (Toikka & Virtala, 2015, modified)

Vehicle weights has increased due to regulation changes implemented in 2013, allowing heavier and larger vehicles on the Finnish road network. The main goals of these regulation changes were to decrease transportation costs and environmental impact. By increasing the unit size and weight of the transportation, the number of transportations was expected to decrease. Additionally, the changes were estimated to positively impact the overall traffic safety. (Rauhanen, 2015, presentation)

The increase in allowable vehicle mass does not directly mean that the vehicles themselves are getting heavier, but the load they carry is allowed to be larger. Still, the changes have put pressure on bridges in Finland. Due to the new regulations, the number of bridges with a weight limit has been increased. Before the regulation was presented in 2013, the number of bridges with a weight limit in Finland was 144, and it was estimated that that number would increase to 250-300 bridges (Pöyskö, et al., 2014). In 2021, the number of bridges with a weight limit was 387 (Väylävirasto, 2023).

The evolution of vehicle weights in Finland can be seen from traffic measurements conducted in Kaarina, located in Southwest Finland. Figure 2 shows the difference between two different measurement years, 2014 and 2016. For both years, the measurements were done during a one-week measurement period. With only two years apart, the gross vehicle weights have increased substantially. In 2014, the largest vehicle weight was 657kN, while only two years later, the largest weight had increased with over 300kN to a little shy of 974kN. Furthermore, in 2016, 294 heavier vehicles were recorded that were heavier than the heaviest vehicle two years prior.

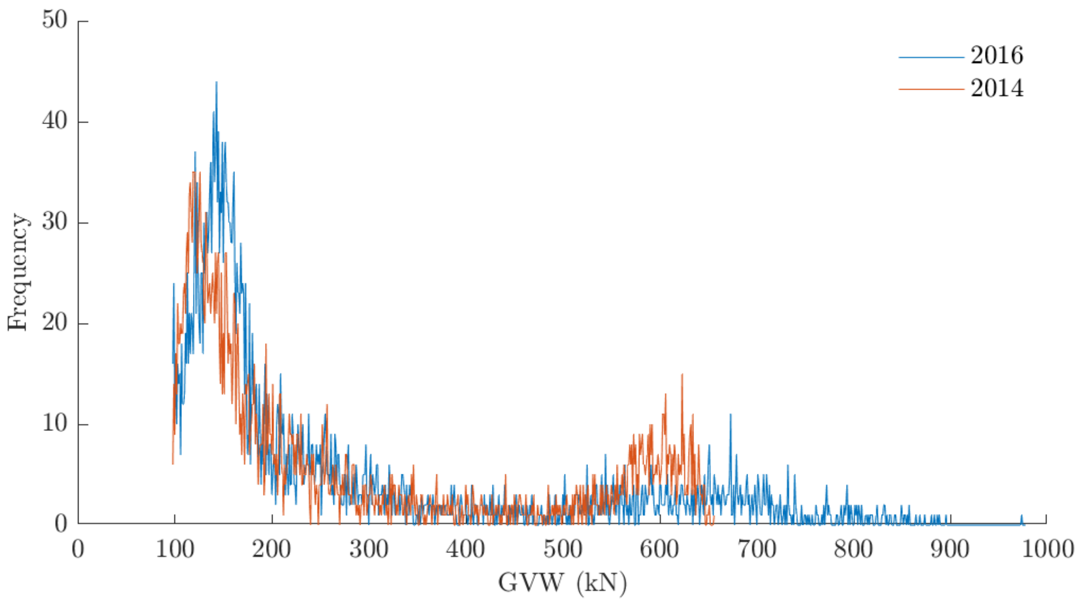

Figure 2. Frequency of GVW for years 2014 and 2016 in Kaarina.

The increase in vehicle weights has been somewhat of a trend across Europe. In 1996 the maximum allowable weight in the EU for national and international road transport was set to 40 tonnes (Council Directive 96/53/EC, 1996). However, the weight limits will increase in the years to come. In 2024, the European Parliament agreed to increase the weight limit to 44 tonnes due to the desire to increase the number of zero-emission heavy vehicles (Willets, 2024). Furthermore, because countries are moving towards electric vehicles with heavy batteries, the vehicle masses will increase compared to cars with petrol engines (Fernandes, et al., 2020).

1.1.1 Traffic measurement

The measurement of traffic and vehicle weights has multiple benefits. The measuring data can be used for pavement and bridge design, monitoring, and improving regulations. As traffic volumes and vehicle weights can be considered heterogeneous between countries and regions, the measurement becomes necessary to find risk factors and, furthermore, review the design codes and improve upon them.

One of the main advantages of weight measurements is the monitoring of overloaded vehicles. These vehicles pose a significant threat to road safety and have a big impact on the degradation of the road surface as well as the main infrastructure, including bridges (Rygula, et al., 2019). Overloaded vehicles are a common global problem. Karim, et al. (2012) reported that 21,5% of commercial vehicles in Malaysia exceeded the permissible GVW limits. In Bosnia and Herzegovina, 24,2% of the vehicles measured were overloaded, as Kulovic, et al. (2017) reported. Meanwhile, approximately 10% of vehicles in Switzerland had axle loads greater than the allowable legal limit (Mayer, et al., 2010).

Overloaded vehicles also threaten the fatigue life of bridges as stress ranges increase due to heavier traffic, and thus the fatigue damage increases. Aggarwal & Parameswaran (2015) studied the effect of overloaded vehicles on the accumulated fatigue damage of a bridge. The results were significant, as a 53% increase in accumulated fatigue damage was reported. Furthermore, the same study reported that a 50% increase in vehicle weight increases the accumulated fatigue damage by 80%. This study was performed for a longitudinal steel girder. Meanwhile, Jang & Mohammadi (2018) reported a decrease in fatigue life when vehicle weights increase.

Deng & Yan (2018) studied the relationship between GVW and cumulative fatigue damage. The study used a fatigue vehicle with a GVW of 320kN and five different overloaded vehicles. The calculations were done by utilising a 2D and 3D bridge model. A large increase in cumulative fatigue damage when GVW increased was reported. For a 13% increase in GVW, the corresponding increase in fatigue damage was 44%. Furthermore, it was reported that the increase in traffic volume increases the fatigue damage linearly. This is due to the use of a linear damage model.

1.2 Measurement technologies

There are practically two systems that can be used for measuring vehicle weights. These systems are called static and dynamic. With static weighing, the gross vehicle weights and axle loads are measured when vehicles are stationary. In contrast, dynamic measurement systems measure loads and other parameters when a vehicle is in motion. (Kim, et al., 2021)

Furthermore, dynamic systems or Weigh-in-Motion (WIM) technologies can be divided into two general categories. These are low-speed WIM (LS-WIM) and high-speed WIM (HS-WIM). In LS-WIM, the vehicles are weighed in motion while travelling, usually between 5 and 15 km/h. With HS-WIM, the vehicles are weighed at full speed. (Richardson, et al., 2014).

1.2.1 Static weighing

The static scale is the most accurate of the weighing methods, however it can be quite unmanageable. Static scales can be classified as Fixed, Semi-Portable, or Portable Systems. The Fixed System is generally installed on the pavement of a reinforced concrete (RC) platform. The Semi-Portable Systems are portable scales installed only during the weighing period. For this system, grooves and permanent road installations are used. Meanwhile, the fully Portable system uses wheel or axle scales placed on the pavement surface. (Richardson, et al., 2014)

While the static weighing system is the most accurate of the three methods, the data gathered from the two WIM systems are usually more representative due to the biases of the data from static measurement campaigns, as truck operators or drivers may try to avoid the scales (Cottrell, 1992). This has been enabled due to queues forming at the weighing sites due to high traffic volumes and the long time it takes to weigh multiple vehicles selected for checking (Jacob & La Beaumelle, 2010).

1.2.2 Weigh-in-Motion

The WIM systems were developed to decrease the required time to get the weight and other vehicle parameters compared to the time it takes with static weighing. Furthermore, by automating the weighing process, an increase in efficiency at checking points was possible. (Jacob & La Beaumelle, 2010).

One of the first attempts of WIM development was done in the early 1950s by the United States Bureau of Public Roads. While some electronic scales had already been used to weigh vehicles at low speeds, any successful attempts to weigh vehicles at full speed had not yet been made. Thus, the first test with real traffic was done in 1951, when a pit with load cells was installed in Virginia. The weighing system consisted of a floating slab built on the pavement surface. The slab was supported by load cells with columns, where the wire strain gauges were attached. (Norman & Hopkins, 1952)

Compared to Static scales, with LS-WIM, the time required to weigh a vehicle is shorter. LS-WIM typically consist of wheel or axle scales equipped with load cells. These scales are positioned on reinforced concrete or asphalt platforms. The wheel and axle loads are calculated by the data processing system that analyses the signal from the load cells. High-speed WIM systems measure the vehicles directly in the traffic lanes. This way, the axle weights can be calculated when vehicles travel at full speed. The devices used for measurement are installed in the pavement or the underside of a bridge. Thus, B-WIM or pavement-based devices, like bending plates, strip sensors, and multiple strip sensors, can be used for HS-WIM measurement. (Richardson, et al., 2014)

1.2.3 Bridge Weigh-in-Motion

The development of the Bridge Weigh-in-Motion (B-WIM) system began during the 1970s when Moses (1979) introduced the first system where bridge strain histories estimated the axle loads. The system included strain gauges, an operator, tape switches, and an instrument van. The operator alerted the system of an oncoming vehicle. The tape switches installed on the pavement recorded the speed, axle spacings, and positions when the vehicle passed over the switches. The strain gauge installed on the bridge soffit measured the strains caused by the passing vehicle. The signals from the tape switches and strains from the strain gauges were sent to a van underneath the bridge. Later B-WIM developments were presented by Peters (1984) when the AXWAY system was introduced. The AXWAY system determined axle and gross vehicle weights with an instrumented bridge. However, the operation and data gathering cost was expensive as the AXWAY was a manned system. Therefore, Peters (1986) introduced CULWAY, an unmanned system. Instead of a bridge, the CULWAY system measured axle loads by using culverts. The inaccuracies of B-WIM measurements are practically non-existent with the CULWAY system, as the dynamic effects and vibrations are damped by the soil between the culverts and the pavement. (Richardson, et al., 2014)

A B-WIM system provides a few advantages, like unbiased data on traffic measurements. Additionally, one of the bigger advantages of the system is its non-destructive application. A B-WIM system estimates the attributes of passing traffic loads by measuring the deformation of a bridge under live loading. Sensors utilised in this system are placed and installed on the soffit of an existing bridge (Lydon, et al., 2016). Other advantages of the B-WIM systems are that the sensors used for measuring traffic can be reinstalled on a different bridge and for determining the performance of the bridge itself (Al-Qadi, et al., 2016).

1.2.4 Static and dynamic algorithms

B-WIM algorithms can typically be divided into two categories. That is static and dynamic algorithms. The goal of the static algorithm is to obtain the static axle weight. Whereas the goal of dynamic algorithms, otherwise known as moving force identification (MFI) methods, is to get the time history of axle forces. (Yu, et al., 2016)

The algorithm presented by Moses is the base of most static algorithms. The strains measured by the sensors are related to the bending moment, and thus, the total bending moment can be obtained by summing the strain sensors placed in a longitudinal location. The strain sensors are usually located at the midspan. With this method, the axle detection and calculation of vehicle speed plays a crucial role, as the GVW is obtained by summing the axle weights. (Lydon, et al., 2016)

Ojio & Yamada (2002) developed a method to calculate the GVW with a strain signal area or influence area. In this method, the system was calibrated with vehicles passing the bridge with a known GVW. From this an influence line was obtained, after which the influence area and the GVW of unknown vehicles could then be calculated. (Lydon, et al., 2016)

A few years later, Ojio & Yamada (2005) presented a method where the axle weights are obtained by reaction forces located at the supports of a simply supported bridge. Thus, it can be called the reaction force method. As the largest value in the reaction force influence line appears when a vehicle first enters the bridge, the influence line gets a sharp edge. Furthermore, because the edge is caused by the axle force, the load of the axle can be assumed to be the height of the influence line edge. (Yu, et al., 2016)

Moving force identification (MFI) is a method where the forces are obtained by minimising the difference between theoretical calculations and practical measurements. With MFI, the complete time history of axle forces caused by vehicles passing a bridge can be obtained. MFI allows static axle loads to be calculated by removing the dynamic effects caused by vehicles with the help of the complete time history. (Yarnold, et al., 2023)

In a comprehensive state-of-the-art review, Yu, et al. (2016) presented different MFI methods that have been proposed through the years. The first MFI method introduced by O'Connor & Chan (1988) uses an interpretive analysis, where data for displacement, bending moment, or acceleration can be used to measure the dynamic vehicle loads. In this method, a bridge consisting of lumped masses is modelled where the masses are interconnected by massless elastic beam elements. If vehicle velocities and accelerations are known, a numerical differential method can be used to obtain the nodal displacements and bending moments. When the moments and displacements are obtained, the axle forces can be solved with a least-square method.

Meanwhile, as presented by Chan, et al. (1999), the moving axle forces can be obtained with the Euler-Bernoulli beam theory instead of the beam element method. With this method, the mode shape function is substituted with Euler's beam equation, after which the modal displacement can be solved. When the displacement caused by moving loads is known, the forces of each load can be obtained. Similarly to the method developed by O'Connor & Chan (1988), the axle forces can be obtained by applying the least-square method.

Several other MFI methods have been proposed through the years, like the time domain method by Law, et al. (1997) and the frequency-time domain method by Law, et al. (1999). However, while MFI has been studied a lot and has great potential for accuracy, the MFI algorithms still lack in some areas. Most of the studies regarding MFI have been done with simple beams or plates. Additionally, gathering real-time axle weights can be difficult as it is resource intensive. This means that MFI algorithms require a large amount of computational power. Because of the complexity of MFI algorithms, static methods like Moses' algorithm are more optimal compared to B-WIM systems. (Yu, et al., 2016)

1.2.5 Application of B-WIM

A modern B-WIM system usually consists of strain gauges for measuring strain, sensors for axle detection, a system for collecting data, and a computer. The most common system for strain measurement is the electrical resistance strain (ERS) gauge. These gauges consist of metallic foil and are applied in a Wheatstone configuration to increase the signal, as the measured strain is usually low. ERS gauges can be reused if fixed with a transducer. However, the gauges can also be installed on the structure directly. The advantage of ERS gauges is their affordability and somewhat good accuracy. Because of these advantages, the gauges are most suitable for short-term measurements. However, they lack durability and are influenced by weather changes and electromagnetic interference (Lydon, et al., 2016) (Yu, et al., 2016)

Vibrating wire strain gauges can also be used for strain measurement. These gauges can be installed in two separate ways, by mounting on the structure's surface or by placing them in concrete. When the strain changes, so does the tension in the wire, which simultaneously changes the wire's resonant frequency. The good durability and low amount of preparation needed give the vibrating wire strain gauges some advantages over other strain measurement systems. However, recording dynamic responses caused by high-speed vehicles can be difficult due to its low scanning rate. (Yu, et al., 2016)

Fibre optic sensors, otherwise known as FBG sensors, are widely used for health monitoring. Compared to the previously explained strain gauges, the fibre optic sensors are not influenced by any electromagnetic interferences and can be used for long-term measurements due to their great durability. Furthermore, due to the small size of the sensors, the installation of multiple sensors is easier on larger structures. The strain is measured by the relationship between the change in wavelength and the strain caused by a load or fluctuation in temperature. (Yarnold, et al., 2023)

Axle detection plays a crucial role in the B-WIM system, as vehicle speed and axle distances affect the results in weight calculations. Usually, axle detectors can be divided into two categories. These are removable and permanent detectors. The first category includes axle detectors like tape switches or road hoses and the latter contains sensors that are installed in the pavement, like piezoceramic sensors. The sensors are installed either on the bridge or before the bridge. However, some developments have been made by replacing traditional axle detectors with strain recordings. (O'Brien, et al., 2001)

1.3 Background of the Fatigue Load Models

The Eurocodes originated in the 1970s when the Commission of the European community wanted to eliminate any technical obstacles to trading and wanted to establish harmonised technical rules for the design in construction (EN 1990, 2002). Since then, multiple Eurocodes have been introduced for the design of different materials and structures. For the design of bridges, there are several codes that one should follow depending on the material being used. Figure 3 shows the Eurocodes required for the design of bridges.

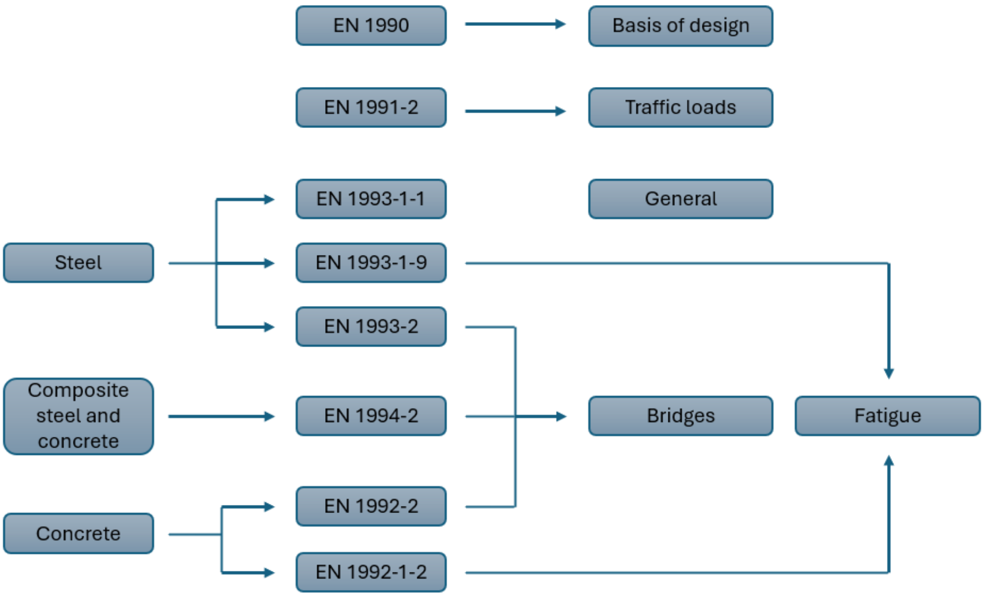

Figure 3. Eurocodes used for the design of bridges.

For fatigue design, the Fatigue Load Models (FML: s) presented in Eurocodes (SFS-EN 1991-2) have been calibrated from old traffic data that were recorded in several European countries on two separate occasions, first between the years 1977 and 1982 and later in the years 1986 and 1987. In the latter measurement campaign, countries like France, Germany, Italy, and Spain provided broader information about the vehicles, including axle forces and axle spacings, and distances between heavy vehicles. (Bruls, et al., 1996)

All the recorded data were intended to be used to create a sample of European traffic. However, it was concluded that the traffic data recorded in France near Auxerre would be used, as it was already considered as European traffic or as uniform traffic. The traffic data from other countries would only be used for possible corrections (Bruls, et al., 1996). While the traffic recorded in Auxerre was not the heaviest, or the time of measurement was not the longest, the frequency of heavy axle weights made the traffic most suitable to use for the calibration of the Fatigue Load Models (Al-Emrani & Aygul, 2014).

Because the calibration of the Fatigue Load Models originates from Central European traffic, countries like Finland with higher GVW may make the fatigue design more unpredictable. Additionally, the traffic densities vary between countries. The unpredictability in fatigue design may occur if only Eurocodes are used for the design. This is why countries have their own National Annexes (NA: s), where parameters and other information left open in Eurocodes can be determined. In Finland, when the new traffic regulations came into effect in 2013, the National Annexes were adjusted to match the new weight limits (Qvisen, 2020).

1.4 Aim and Scope

The increase in vehicle weights has an impact on bridge fatigue. Additionally, as the Fatigue Load Models used today were derived from traffic measured in the 1980s, they should be compared against today's traffic. For the comparison, this study includes measured traffic from two separate years, 2014 and 2016. Therefore, the goals for this thesis are:

1. To see how the regulations implemented in 2013 have affected bridge fatigue. This is done by comparing the required elastic section modulus ($W_{,el}$) between years 2014 and 2016. The section modulus represents a design life of 100 years.

2. To compare recorded traffic with Fatigue Load Models presented in the Eurocodes. This is done by comparing the required elastic section modulus between FLM3 and the 2016 B-WIM database as well as FLM4 and the 2016 B-WIM database.

3. To calibrate a new Fatigue Load Model based on the 2016 recorded traffic data. The goal is to calibrate a new Fatigue Load Model that represents today's traffic.

The comparison between real traffic and the Fatigue Load Models can be evaluated with several methods. The recorded traffic data can be simulated on one lane or several lanes. Furthermore, the verification can be done with multiple vehicles being on a bridge simultaneously, either travelling in the same lane or side by side on different lanes. However, for simplification purposes, this thesis is limited to the study of:

1. Roadway bridges with a span length of 10-80m,

2. Single lane traffic conditions,

3. one-directional traffic flow,

4. one-by-one crossing.

These limitations consider mainly the simulations of the recorded traffic data, as FLM3 includes a single fatigue vehicle, and the verification of FLM4 is performed with equivalent lorries crossing the bridge one-by-one, as specified in SFS-EN 1991-2.

It should be noted that this thesis does not include a fatigue life assessment of any existing bridge. Hence, the recorded traffic data or Fatigue Load Models are not used to determine the fatigue life of any sort. The comparisons and calibration are done with an equal fatigue life for all calculations. That is, a 100-year design life is used. Furthermore, this study does not examine the accuracy of the Fatigue Load Models, as the Load Models are supposed to be inaccurate. This is because the Load Models are used to determine the safety of a structure. Additionally, while other cumulative damage methods are presented in this thesis, the comparison of these damage methods is not included.

Furthermore, the reader should know that the measured traffic used in the calculations in this thesis is referred to as recorded traffic, actual traffic, B-WIM, and WIM.

1.5 Structure of the Thesis

This thesis is divided into five chapters, including the current chapter. Chapter 2 gives the reader a theoretical background about fatigue, including fatigue stresses and parameters, fatigue loads, methods to simplify complex loading situations, and fatigue strength.

Chapter 3 explains fatigue verification according to Eurocodes. Furthermore, minor differences between the Eurocodes and NCCI codes are identified. Two fatigue verification methods, the cumulative damage method, and the equivalent damage method, are explained. Additionally, possible limitations concerning both methods are described. The cumulative fatigue verification is done with the Miner's linear damage rule. However, different cumulative fatigue verification rules are presented in this chapter.

Chapter 4 includes the analysis and results obtained from comparing recorded traffic with the Fatigue Load Models. Additionally, the effect of the regulation change is investigated in this chapter. This chapter explains the method and the analysis setting for each calculation.

Chapter 5 shows the calibration of the new Fatigue Load Model, including the calibration of the new fatigue vehicle. Furthermore, results obtained with the new FLM are presented in this chapter. The calibrated Load Model improves the accuracy when compared to actual traffic.

Chapter 6 summarises and concludes the results obtained from Chapter 4 and Chapter 5. Additionally, limitations related to the analysis are explained, and possible future work is proposed.

2 Fatigue

Fatigue can be described as failure caused by repeated loading affecting a structure over a longer or shorter time (Peres, 2004). Skoglund (2021) describes fatigue as accumulated damage in specific areas caused by fluctuating loads over time. Fatigue is one of the leading causes of damage to steel structures, where the damage shows as cracks that are usually located near structural details (Skoglund, 2021). Fatigue damage can be divided into three phases:

1. crack initiation
2. crack propagation
3. final rapture

During crack initiation, small fatigue cracks are formed when stress levels at a certain location exceed the average stresses. Crack propagation occurs after the crack has initiated. The final rapture occurs when the external load exceeds the strength of the section. (Skoglund, 2021)

Fatigue can be caused by several different natural phenomena, e.g., wind or waves (Croce, 2001). For structures on a road network like bridges, fatigue is mostly caused by heavy traffic like lorries. Because the collapse of a bridge caused by fatigue damage can be sudden, the designer should be aware of the traffic volume and vehicle weights present at the location to correctly determine the fatigue life.

2.1 Fatigue stresses

When designing against fatigue, it is important to understand the stresses and their parameters. For the fatigue design of steel bridges, the two most important parameters are stress range and the number of stress cycles caused by vehicles passing a bridge (Wang, et al., 2015). In addition, as fatigue damage is ruled by the stress fluctuations, the stress range, stress amplitude, and mean stress are more significant than the maximum stress itself (Pedersen, 2018). Loads applied to a specimen during fatigue testing are determined by a stress range or stress amplitude (Lee, et al., 2005). Stress range $\Delta\sigma$ is obtained by calculating the difference between the maximum stress and minimum stress. Meanwhile, stress amplitude σ_a is half of the stress range. Hence, the stress range and the stress amplitude are obtained with equations (1) and (2),

$$\Delta\sigma = \sigma_{max} - \sigma_{min} \tag{1}$$

$$\sigma_a = \frac{\Delta\sigma}{2} \tag{2}$$

Mean stress σ_m is important as it is connected to the stress amplitude. That is when stress amplitude increases, so does the mean stress (Pedersen, 2018). Additionally, both mean stress and stress ratio are significant, as tensile stresses cause more damage than compressive stresses. However, these parameters are rarely calculated as most structures are subjected to residual stresses instead of tensile or compressive stresses (Skoglund, 2021). Nevertheless, mean stress σ_m and the stress ratio R are expressed with equations (3) and (4),

$$\sigma_m = \frac{\sigma_{max} + \sigma_{min}}{2} \tag{3}$$

$$R = \frac{\sigma_{min}}{\sigma_{max}} \tag{4}$$

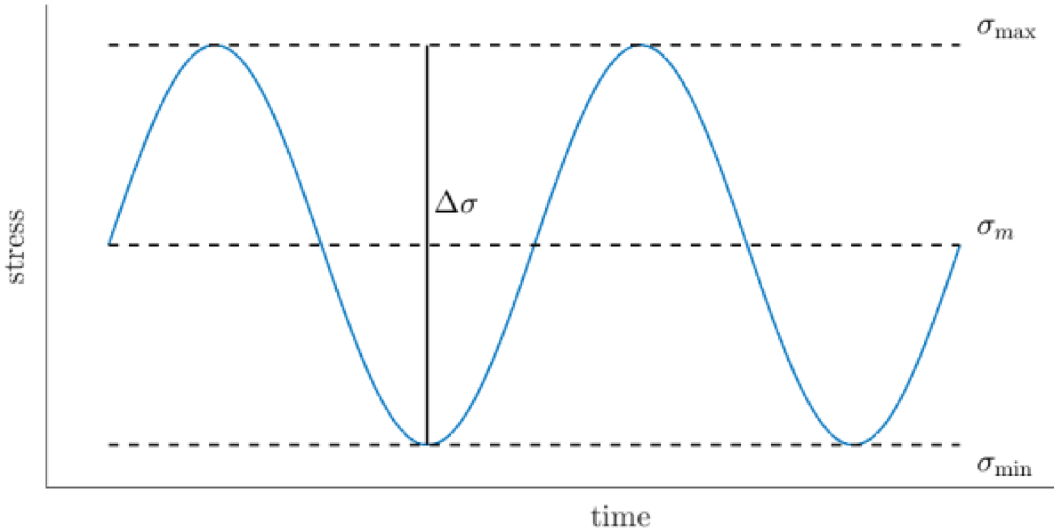

Figure 4. Illustration of stress range, mean stress, and maximum and minimum stress.

2.1.1 Residual and mean stresses

Residual stresses are represented in welded structures and result from the welding process itself. More specifically, the residual stresses result from both tensile and compressive stresses existing in the weld and its surrounding area, where these stresses can also be called residual tensile stresses and residual compressive stresses (Mertz, 2022). This means that the residual stresses are in equilibrium and can exist without applied external loads (Skoglund, 2021). Both tensile and compressive stresses occur as the weld tries to contract when it cools, which leads to the welded part trying to hinder the weld as both must maintain the same length (Mertz, 2022).

The distribution of residual tensile stresses and residual compressive stresses have a significant effect on the welded structures, as the residual tensile stresses can reach material yield strength. These residual tensile stresses are present in locations of the welded structures where fatigue crack growth is most likely to occur. This means that parts with defections are already subjected to initial stresses even before any external loads are applied. Thus, the stress range is the main parameter that affects the fatigue crack growth, as the initial stresses are usually near the yield stress level. (Mertz, 2022) (Russo, et al., 2016)

As demonstrated in equation (3), mean stress is the average of the maximum and minimum stresses. While mean stresses are seldom important in fatigue design as structures are mainly influenced by residual stresses, mean stresses have an important role in structures where residual stresses are absent, and more specifically tensile mean stresses. This is because tensile mean stresses are more damaging than compressive mean stresses (Skoglund, 2021). The significance of mean stresses can also be demonstrated by the fact that when mean stress increases, fatigue life decreases, and when mean stress decreases, fatigue life increases (Pedersen, 2018).

2.2 Fatigue loads

A structure can be influenced by constant amplitude loading (CAL) or variable amplitude loading (VAL). The load cycles in the former have the same stress range (Figure 5a) while the stress ranges in the latter are mostly of different magnitudes for the load cycles (Figure 5b). However, it is extremely unlikely that a structure is subjected to CAL, even if the S-N curves presented in the Eurocodes have been established by experimental data gathered from constant amplitude loading. (Skoglund, 2021)

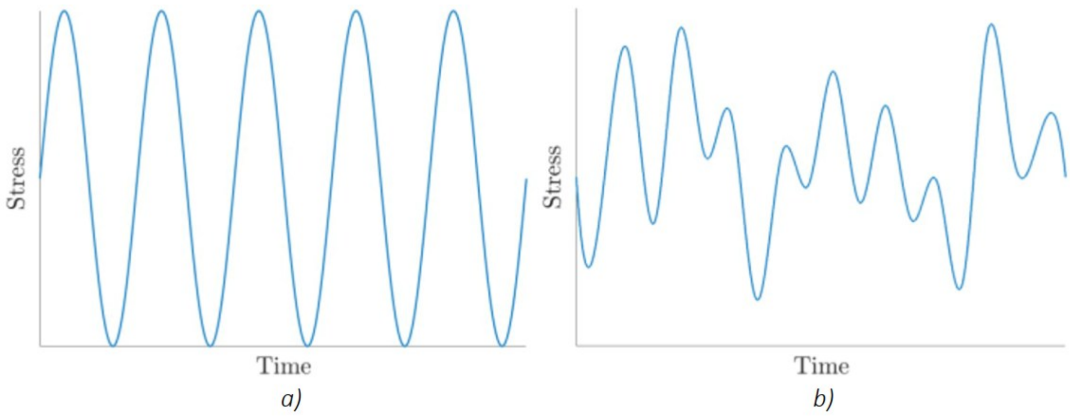

Figure 5. a) Illustration of constant amplitude loading and b) illustration of variable amplitude loading.

Because variable amplitude loading is very complex, it needs to be converted to a simpler loading situation, like constant amplitude loading. This means that the complex loads should be portrayed as constant amplitude loads that will result in similar fatigue damage as the original load history. The transformation can be done with a cycle counting method, like the "Rainflow" or "Reservoir" method. (Al-Emrani & Aygul, 2014) (Hobbacher, et al., 2008)

2.3 Cycle counting

There are different techniques for extracting cycles from a stress history and for simplifying the loading situation. As stated earlier, the stress-time history is typically very complex. Thus, it needs to be transformed into peaks and valleys. The highest peaks and lowest valleys are connected directly with straight lines. This creates a simplified stress history that reflects the general trend but ignores the minor fluctuations between the highest and lowest values. Figure 6 and Figure 7 illustrates this procedure.

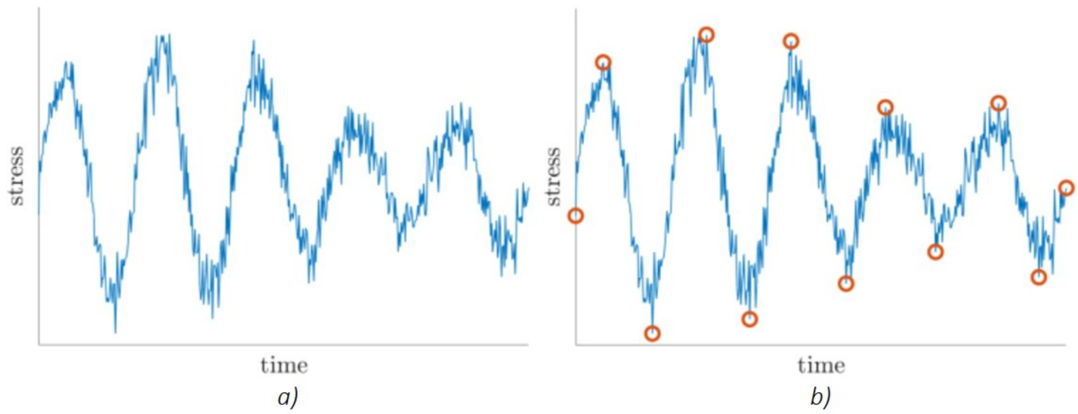

Figure 6. a) Illustration of stress-time history. b) red circles show the highest peaks and lowest valleys.

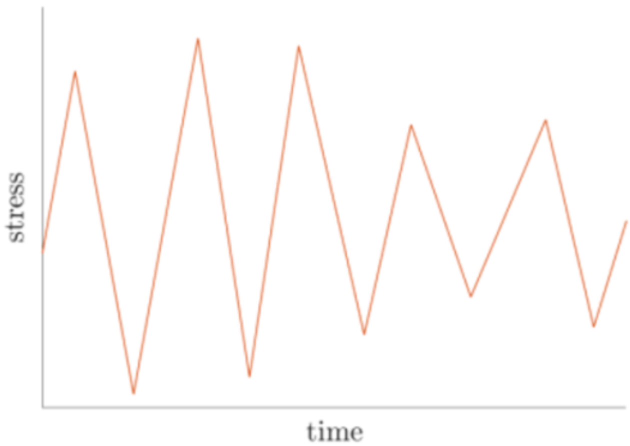

Figure 7. Highest peaks and lowest valleys are connected to create a simplified stress history.

Some cycle counting methods require rearranging of the reduced time history, either by moving the highest peak to the ends or by rotating the time history. The following chapters explain two different cycle counting methods, “Rainflow” and “Reservoir” counting method.

2.3.1 Rainflow counting method

Rainflow counting is a simple method that can be illustrated with rain dropping on a roof. When using the rainflow counting method, the stress history is rotated 90° so that time is shown vertically and stress horizontally. This makes the stress histogram replicate a Japanese-styled pagoda roof. After the stress history is rotated, imaginary rain falls on the roof and drips from one roof edge to another. The distance a single drop travels can be considered as a stress range. To obtain the stress ranges, both positive and negative half-cycles need to be counted. Figure 8 illustrates the rainflow counting procedure. The positive half-cycles are obtained when the rain drips from left to right in Figure 8. Negative half-cycles are obtained when rain is dripping from right to left in Figure 8. The rain flow only stops when it encounters a greater peak or valley than where it started, drips from the last roof edge, or encounters an existing drop. (Pedersen, 2018)

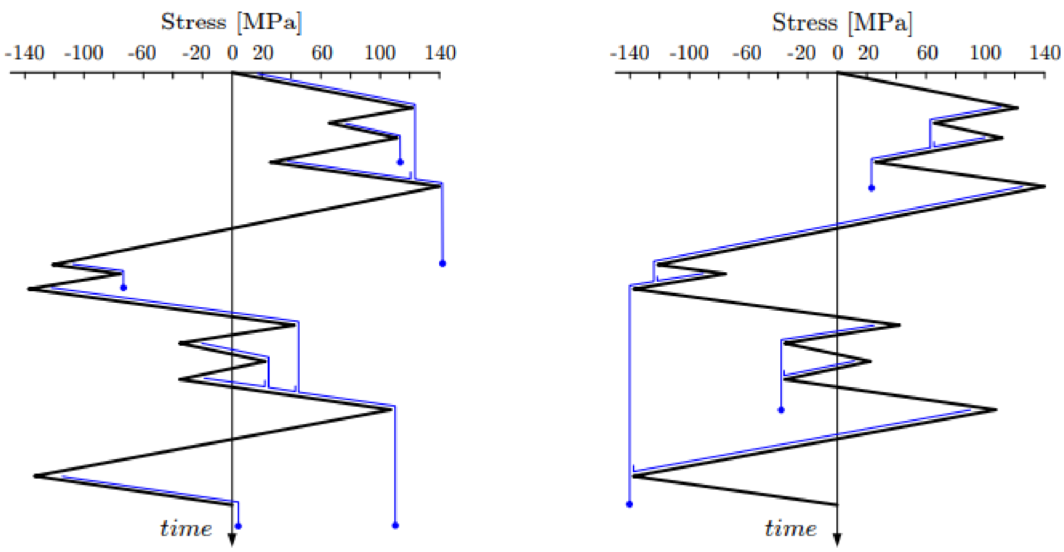

Figure 8. Illustration of rainflow counting method. (Pedersen, 2018)

2.3.2 Reservoir counting method

The reservoir counting method includes several steps to convert a complex stress history into multiple stress ranges and stress cycles. The conversion is done by splitting and rearranging the original stress-time history by finding the peak stress and placing it on both ends of the stress spectrum. The new stress spectrum is filled, e.g., with imaginary water to create a so-called "reservoir". The lowest point is identified from the newly rearranged stress spectrum, and the "water" is drained from that point. The stress range is obtained by subtracting the stress at the highest level of the imaginary water with the stress level located at the lowest point where the "water" was drained. This procedure is repeated until the "water" is fully drained. (Skoglund, 2021)

Below is an example illustration of the reservoir counting method. Figure 9 a) shows the original stress history with three points appointed. Points p1 and p2 are located at both ends of the stress history, and p3 represents the highest peak. Figure 9 b) shows how the original stress history has been rearranged so that the peak value (p3) has been placed on both ends, and the ends of the original history (p1, p2) now connect in the middle. Furthermore, a new point (p4) has been assigned, and the stress history has been filled with "water".

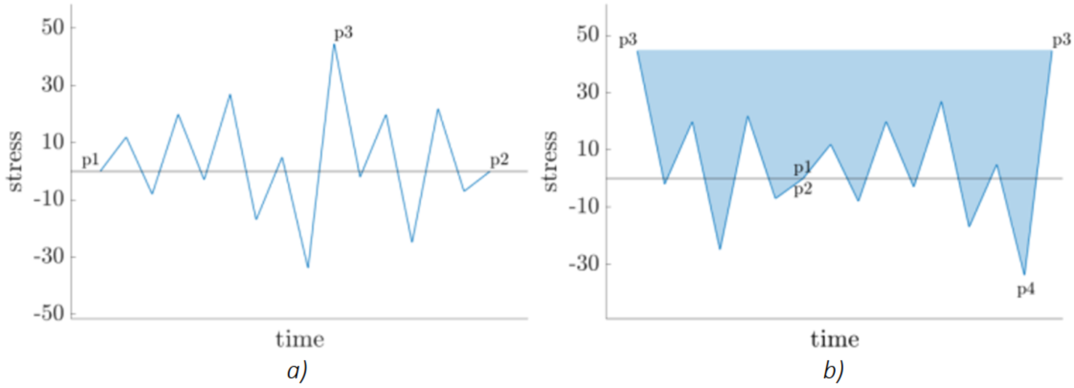

Figure 9. a) The original stress history with points p1, p2, and p3. b) The rearranged stress history acting as a reservoir. (Skoglund, 2021, modified)

In Figure 10 c) the "water" is drained from the lowest point (p4), leaving a new "water" level. Also, a new point (p5) has been introduced to the next lowest point. Figure 10 d) illustrates how the water has been drained from p5. This procedure continues until all "water" has been drained.

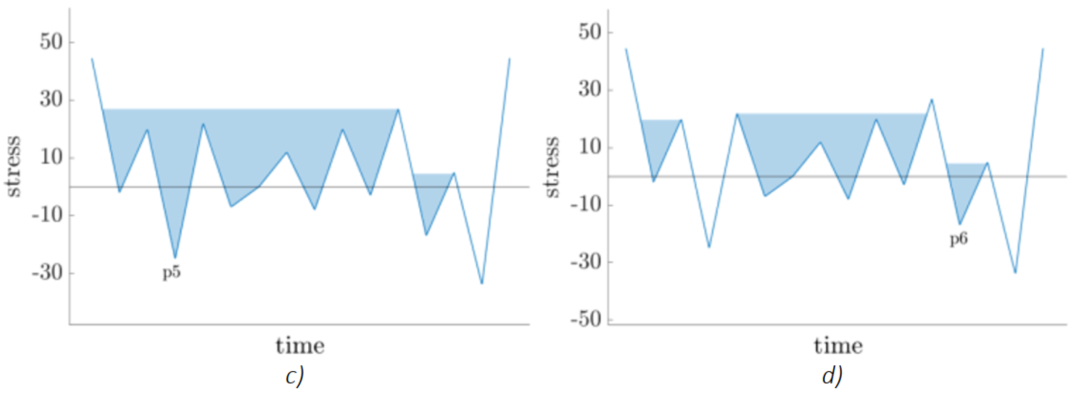

Figure 10. c) The imaginary water is drained from p4, and p5 is introduced. d) Water is drained from p5. (Skoglund, 2021, modified)

2.4 Fatigue strength and S-N curves

The S-N curve, also known as the Wöhler curve, is a method to estimate the number of load cycles a structure can resist before failure. In the S-N curve, N represents the number of cycles to failure, and S represents the stress range (Skoglund, 2021). Additionally, S can be expressed as stress amplitude (Lee, et al., 2005). Hence, the S-N curve is a tool used to express the fatigue strength of a material (Pedersen, 2018). To determine the S-N curve for a material, a specimen is applied with constant cyclic stress for a certain number of loading cycles until the specimen fails (Roylance, 2001). The data gathered from fatigue tests are usually plotted on semi-log or log-log coordinates, where the latter makes the curve linear (Lee, et al., 2005). As Figure 11 illustrates, an S-N curve can be demonstrated as a one-slope curve with a constant amplitude fatigue limit, a two-slope curve, or a two-slope curve with a cut-off limit.

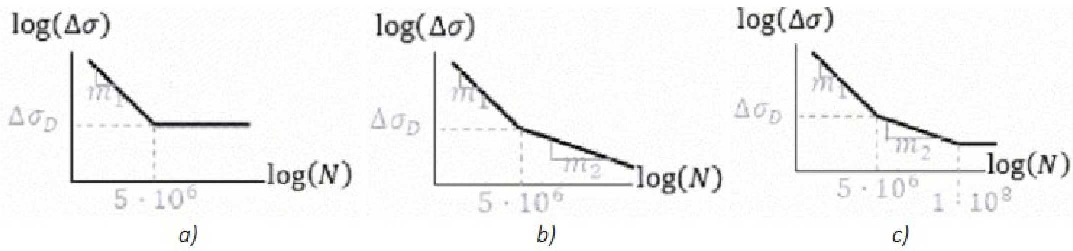

Figure 11. Illustration of three different S-N curves. a) one-slope curve with a cut-off limit, b) two-slope curve and c) two-slope curve with a cut-off limit. (Maljaars, 2020)

A typical S-N curve is presented in two parts divided by a knee-point representing a certain number of cycles, N. The primary part of the curve is located on the left side of the knee-point, while the secondary part is on the right side. In Figure 11 above, the location of the knee-point is at $5 \cdot 10^6$ cycles. The primary and secondary parts of the curve have different slope parameters, where the parameter for the primary part is lower than for the secondary part. (Pedersen, 2018)

An S-N curve can be expressed for a log-log plot with equation (5),

$$\log N = \log a - m \log \Delta\sigma \tag{5}$$

where

N	is the number of cycles to failure
Δσ	is the stress range
m	is the slope parameter
a	is the intercept value at the axis of cycles (N)

Some materials experience a flattening of the S-N curve at a very high cycle range. This flattening can be considered as an endurance limit. The material can withstand an infinite number of cycles under this limit without a failure occurring. However, materials with no endurance limit exist, like aluminium. (Roylance, 2001)

2.4.1 S-N curves in Eurocodes

The S-N curves for different structural details are presented in SFS-EN 1993-1-9 for steel structures and SFS-EN 1992-1-1 for concrete structures. Only more common details have an S-N curve in the design codes, as the curves have been constructed from several specimens, which can be both time consuming and financially expensive (Skoglund & Leander, 2022). The curves provided in the codes have a fatigue strength corresponding to a 95% survival probability (Skoglund, 2021).

Eurocodes provide different types of S-N curves depending on the material used. For fatigue assessment of steel structures according to SFS-EN 1993-1-9, the S-N curve is a two-slope curve with a cut-off limit. Meanwhile, the S-N curve in SFS-EN 1992-1-1 is a simple two-slope curve. The S-N curves provided in the design codes usually include two slope parameters m_i, one for the high cycle range and one for the low cycle range. The knee point between both slopes is usually fixed to a certain number of cycles, usually at $5 \cdot 10^6$ cycles. Additionally, depending on the detail or material, the curve will have a cut-off limit or endurance limit fixed at a certain N_i, usually at 10^8 cycles. However, these values may differ depending on the detail under consideration.

2.5 Low Cycle Fatigue and High Cycle Fatigue

Low Cycle Fatigue (LCF) involves high cyclical stresses where failure occurs after fewer cycles. As the stresses are typically above the material yield strength, plastic deformation occurs. However, for bridges, LCF is rarely the cause of failure unless earthquakes are present (Skoglund, 2021). High Cycle Fatigue (HCF) is when stresses are low, and failure occurs after a very large number of cycles. Due to low stresses, only elastic deformation occurs, and thus, verification methods using stresses can be performed (Skoglund, 2021). Fatigue failures for HCF occur above 10^5 cycles, while failures associated with LCF occur below 10^5 cycles (Li, et al., 2023). However, Lee, et al. (2005) point out that the number of cycles separating LCF and HCF cannot be specified, however, for steel components, the boundary value is 10^3 cycles, while the endurance limit is at 10^6 cycles. Figure 12 illustrates LCF, HCF, and the endurance limit.

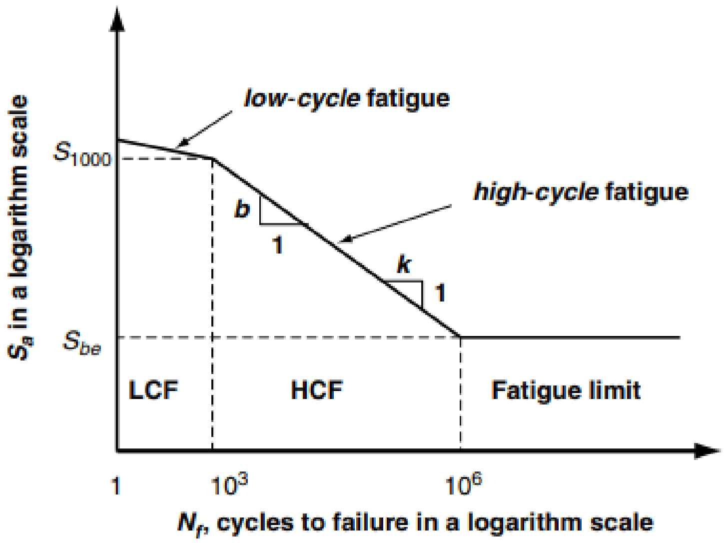

Figure 12. Illustration of LCF, HCF, and the Fatigue limit. (Lee, et al., 2005)

The fatigue life predictions for HCF and LCF are different. Current analytical approaches typically rely on multiaxial fatigue criteria, utilising stress-based approaches for HCF and strain or inelastic strain approaches for LCF (Constantinescu, et al., 2022).

2.5.1 Stress-based approach

One of the stress methods used for fatigue analysis is the stress-life method, which is primarily used for the prediction of long fatigue lives where both stresses and strains remain in the elastic region. Thus, this method is well-suited for HCF applications. Instead of differentiating between crack initiation and propagation, the stress-life method focuses on the life to failure of a structural component. With this method, a relationship is established between stress range and fatigue failure by using S-N curves, which, as stated earlier, are obtained by subjecting test specimens to constant amplitude stress cycles until visible cracks appear. (Ye, et al., 2014)

Another stress method is the nominal stress method, which is included in existing design codes, and is a widely adopted method for the fatigue assessment of steel bridges. This method involves a global assessment that focuses on the average stress within a cross-section of interest according to the theory of structural mechanics. This approach calculates the nominal stress by ignoring the local stress, but instead, it considers the large stress of the micromagnetic shape of the considered detail near welded joints. For simpler structural components, linear elastic structural mechanics can be used to determine the nominal stress, whereas, for more complicated structures finite element method is needed. While the S-N curves provided in various design codes are essential when assessing the fatigue life of steel bridges using the nominal stress method, the complexity of some details or loadings makes calculating nominal stresses highly unfeasible. Thus, for some components in steel bridges, the fatigue life prediction using the nominal stress method may lack reliability. (Ye, et al., 2014)

Another stress method given in the Eurocodes along nominal stress method is the hot spot stress method (Skoglund, 2021). This method used to analyse fatigue of more complicated welded joints has greater accuracy than the nominal stress method. Welded joints are usually common in steel bridges due to the joints existing at the intersection of longitudinal and transverse members. These welded joints often include geometrical irregularities, with weld toes being most prone to fatigue cracks due to the presence of maximum local stresses in those regions. The hot spot stress refers to the structural stress value in the hot spot located in the weld toes. This stress can be calculated by multiplying the nominal stress with a stress concentration factor, which is attained through finite element analysis or strain gauge measurements. (Ye, et al., 2014)

2.5.2 Fracture mechanics approach and strain-life method

Compared to stress-life and strain-life approaches, the fracture mechanics approach operates under the assumption that cracks already exist in a material or structure (Lee, et al., 2005). Furthermore, this approach can be used to determine the remaining life of components containing cracks or other flaws. It allows the assessment of fatigue life from an observable crack to the failure of the component. The most common approach for analysing this process is linear elastic fracture mechanics (LEFM). LEFM assumes that material conditions are primarily linear elastic. However, an elastic-plastic fracture mechanism can be applied if the crack or flaw size exceeds these assumptions. (Skoglund, 2022)

While most components are under nominal cyclic elastic stresses, some stress concentrations located in components may cause cyclic plastic deformation. Under these types of conditions, the strain-life approach, which uses local strains as the main fatigue parameter, is usually more effective. This method assumes that the time taken for crack initiation and early crack growth in a notched component can be predicted by using a smooth laboratory specimen subjected to deformation conditions at the crack initiation site. If the correlation between the localised strain and fatigue life is known, the fatigue life at a specific point in a component that is cyclically loaded can be determined with the strain-life method. (Lee, et al., 2005)

The strain-life method is applicable when the strain includes both elastic and plastic components. This can typically be observed in conditions leading to short fatigue life in LCF. However, the research on the fatigue life of steel bridges using the strain-life method is very limited due to most fatigue in steel bridges relating to HCF. (Ye, et al., 2014)

3 Fatigue verification

Fatigue assessment is performed for steel, composite steel, and concrete bridges according to SFS-EN 1993-2, SFS-EN 1994-2, and SFS-EN 1992-2, respectively. Generally, two fatigue assessment methods are presented in Eurocodes, the cumulative and the equivalent damage method. The former method attempts to determine the sufficient fatigue life using a set of equivalent lorries presented in FLM4. Furthermore, the cumulative damage method requires a cycle counting method. In the latter method, a fatigue vehicle presented in FLM3 is used to simulate the traffic. Compared to the cumulative damage method, the equivalent damage method does not require any cycle counting procedures.

In addition to Eurocodes, each country is responsible for determining design parameters that are left open in Eurocodes. These parameters are presented in National Annexes. In Finland, the Finnish Transport Infrastructure Agency (Väylävirasto, fmr. Liikennevirasto) provides NCCI codes where parameters and design guides that differ from Eurocodes concerning bridge design shall be used. The required parameters are provided in NCCI1 and NCCI4 for the fatigue assessment of steel bridges.

SFS-EN 1991-2 provides four traffic categories with yearly traffic volumes (N_{obs}) that should be utilised with both cumulative and equivalent damage methods. The traffic category should be defined by the number of slow lanes and the number of heavy vehicles observed or estimated per year and per slow lane. The GVW of the vehicles should be over 100kN. The traffic categories and their respective flow rates provided in the NCCI codes do not differ from Eurocodes. Table 1 shows the recommended traffic volumes for different traffic categories.

Table 1. Number of heavy vehicles expected per year and per slow lane according to SFS-EN 1991-2 Table 4.5(n).

Traffic categories		N_{obs} **per year and per slow lane**
1	Roads and motorways with 2 or more lanes per direction with high flow rates of lorries	$2{,}0 \times 10^6$
2	Roads and motorways with medium flow rates of lorries	$0{,}5 \times 10^6$
3	Main roads with low flow rates of lorries	$0{,}125 \times 10^6$
4	Local roads with low flow rates of lorries	$0{,}05 \times 10^6$

3.1 Fatigue Load Models

SFS-EN 1991-2 introduces five different Fatigue Load Models (FLM1-FLM5), each serving a different purpose. FLM1 and FLM2 determine if a structure has an infinite fatigue life, while FLM3 and FLM4 determine finite fatigue life. The calibration of the Fatigue Load Models was discussed in Chapter 1.3. Each Fatigue Load Model represents a different traffic situation that may occur on a bridge.

FLM1 is a modified version of Load Model 1 (LM1) presented in SFS-EN 1991-2. Both Load Models have the same characteristics. However, in FLM1, the concentrated loads (Q_{ik}) are multiplied with 0,7 x α_{Qi} and uniformly distributed loads (q_{ik}, q_{rk}) with 0,3 x α_{qi}. The adjustment factors α_{Qi} and α_{qi} are presented in the National Annexes. Figure 13 illustrates LM1.

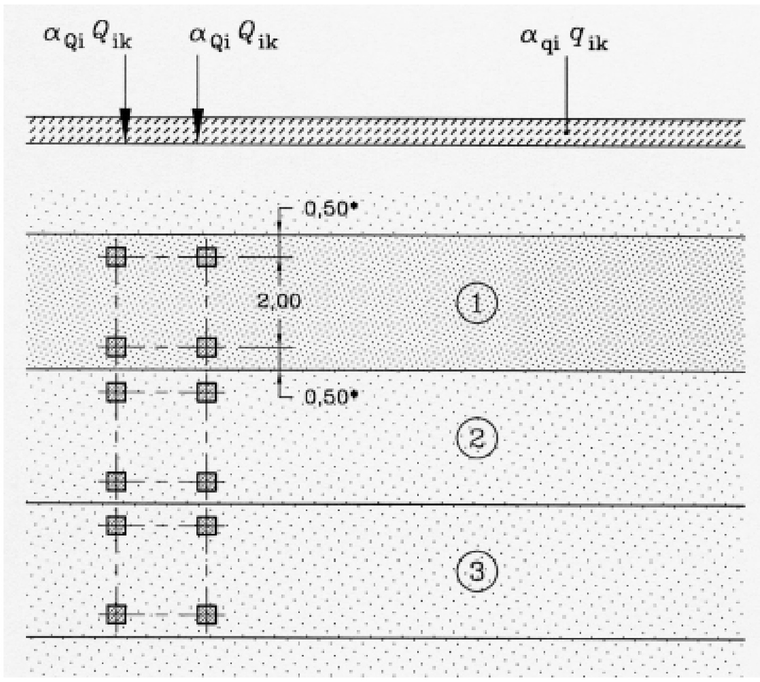

Figure 13. Load Model 1 according to SFS-EN 1991-2 Figure 4.2a.

The suggested values for the lanes may differ between Eurocodes and National Annexes. In Finland, the latter gives higher values for the UDL system and lane 2 in the Tandem system. However, the value for the 3rd lane in the Tandem system has been left empty in NCCI1. The values suggested in NCCI codes were modified following the new regulations when the maximum allowable GVW was increased (Qvisen, 2020). The corresponding values according to SFS-EN 1991-2 are presented in Table 2, and values from NCCI1 are in Table 3.

Table 2. Characteristic values for LM1 according to SFS-EN 1991-2 Table 4.2.

Location	Tandem system *TS*	*UDL* system
	Axle loads Q_{ik} (kN)	q_{ik} **(or q_{ik})** (kN/m^2)
Lane Number 1	300	9
Lane Number 2	200	2,5
Lane Number 3	100	2,5
Other lanes	0	2,5
Remaining area (q_{rk})	0	2,5

Table 3. Characteristic values for LM1 including factor α according to NCCI1 Table B.1.

Sijainti	Yleiset tiet			
	Telikuorma		UDL	
	α_{Qi}	$2\times \alpha_{Qi} \times Q_{ik}$ (kN)	α_{qi}	$\alpha_{qi} \times q_{ik}/q_{rk}$ (kN/m²)
Kaista nro 1	1,0	2×300	1,0	9
Kaista nro 2	1,5	2×300	2,4	6
Kaista nro 3	0	-	1,2	3
Muut kaistat	-	-	1,2	3
Kaistojen ulkopuolinen alue (q_{rk})	-	-	1,2	3

FLM2 consists of a set of “frequent” lorries. In FLM2, each lorry has a defined axle spacing, axle load, and wheel type. The axle spacing presented for FLM2 ranges from 1,3 to 6m, and axle loads from 80 to 190kN. The set of “frequent” lorries is presented in Table 4. With FLM2, a more precise fatigue assessment can be performed compared to FLM1. However, NCCI1 (B.4.6.3) states that FLM2 is not used. When performing the fatigue assessment according to FLM1 or FLM2, the maximum stress range $\Delta\sigma_{max}$ is determined and compared to the fatigue limit $\Delta\sigma_D$.

Table 4. Set of “frequent” lorries according to SFS-EN 1991-2 Table 4.6.

1 LORRY SILHOUETTE	2 Axle spacing (m)	3 Frequent axle loads (kN)	4 Wheel type (see Table 4.8)
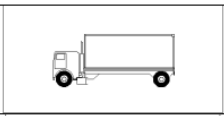	4,5	90 190	A B
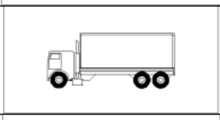	4,20 1,30	80 140 140	A B B
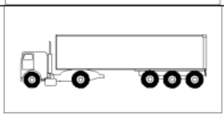	3,20 5,20 1,30 1,30	90 180 120 120 120	A B C C C
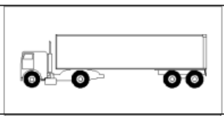	3,40 6,00 1,80	90 190 140 140	A B B B
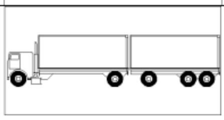	4,80 3,60 4,40 1,30	90 180 120 110 110	A B C C C

FLM3 is presented as a single fatigue vehicle with four axles, each with two identical wheels. The GVW of the vehicle is 480kN, with each axle weighing 120kN. Each axle has identical wheels with a length of 0,4m on each side. Figure 14 shows the configuration of the single fatigue vehicle. However, two vehicles should be used if relevant. These two vehicles travel in the same lane. The second vehicle has the same configuration as the single fatigue vehicle, however, with each axle weighing 36kN. Additionally, the distance between the two vehicles should not be less than 40m when measuring from centre to centre of the vehicles. When applying FLM3, the number of vehicles used in the calculations should be taken from Table 4.5(n) in SFS-EN 1991-2 or Table B.4 in NCCI1.

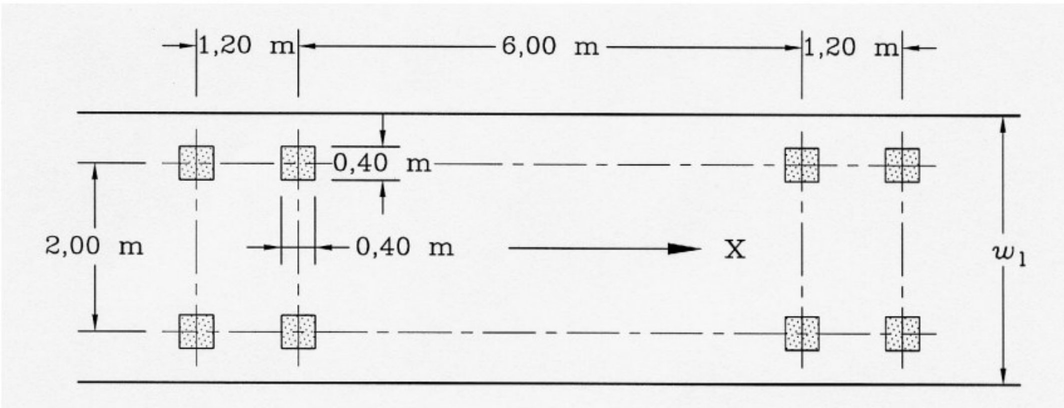

Figure 14. Configuration of the single fatigue vehicle used in FLM3 according to SFS-EN 1991-2 Figure 4.8.

FLM4 includes five different types of lorries with varying axle spacings and loads. These vehicles are called a set of “equivalent” lorries, and they are presented in Table 5. This model simulates typical European traffic with a series of equivalent trucks. Thus, the geometry and properties of lorries suggested in FLM4 are assumed to be closest to the standard and most frequent lorries on a European road. When using FLM4, each lorry shall be considered to cross the bridge separately. For the selection of traffic type, SFS-EN 1991-2 suggests “Long distance” for traffic reaching over 100 km, “Medium distance” for distances between 50 and 100 km, and “Local traffic” for distances under 50 km. The calculation process for FLM4 shall follow the damage accumulation method, where a cycle counting method like rainflow or reservoir is used to determine the fatigue life of a structure.

Table 5. Set of equivalent lorries according to SFS-EN 1991-2 Table 4.7.

VEHICLE TYPE			TRAFFIC TYPE			
1	2	3	4	5	6	7
			Long distance	Medium distance	Local traffic	
LORRY	Axle spacing (m)	Equivalent axle loads (kN)	Lorry percentage	Lorry percentage	Lorry percentage	Wheel type
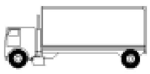	4,5	70 130	20,0	40,0	80,0	A B
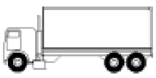	4,20 1,30	70 120 120	5,0	10,0	5,0	A B B
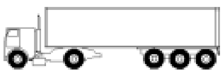	3,20 5,20 1,30 1,30	70 150 90 90 90	50,0	30,0	5,0	A B C C C
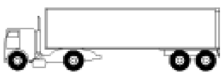	3,40 6,00 1,80	70 140 90 90	15,0	15,0	5,0	A B B B
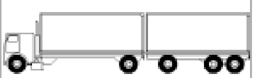	4,80 3,60 4,40 1,30	70 130 90 80 80	10,0	5,0	5,0	A B C C C

FLM5 uses recorded traffic data, allowing accurate fatigue verification due to realistic axle forces and distances. FLM5 is particularly meant for the fatigue verification of special structures like suspension bridges or cable-stayed bridges (Silvennoinen, 2007).

3.1.1 Accuracy of the Fatigue Load Models

In a background study on Fatigue Load Models and their calibration, Croce (2001) compared the FLM:s with the Auxerre reference traffic from which these models were derived. The study involved an analysis of the maximum and equivalent stress ranges between the Fatigue Load Models and the reference traffic. Four influence lines, illustrated in Figure 15, were used for the comparison. Influence line M_0 represents the bending moment at the midspan of a simply supported beam. Influence lines M_1 and M_2 correspond to the bending moment at the midspan and middle support of a two-span beam, respectively. Influence line M_3 pertains to the bending moment at the midspan of a continuous beam with three spans.

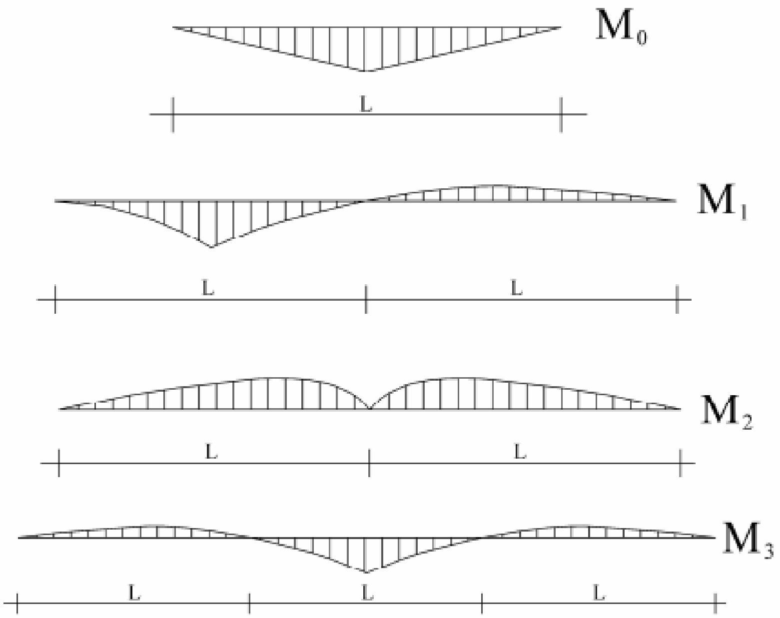

Figure 15. Influence lines used by Croce (2001).

Figure 16 illustrates the ratio between the maximum stress range of FLM1 and the reference Auxerre traffic. Similarly, Figure 17 shows the corresponding ratios for FLM2. The results indicate that FLM1 is quite conservative for short-span bridges but evens out when the span length increases. The support moment M_2, fluctuates more than other moments and shows uncertainties for multiple span lengths. Meanwhile, FLM2 generally exhibits a more consistent pattern, except for support moment M_2, which becomes slightly unconservative at a span length of 30 m.

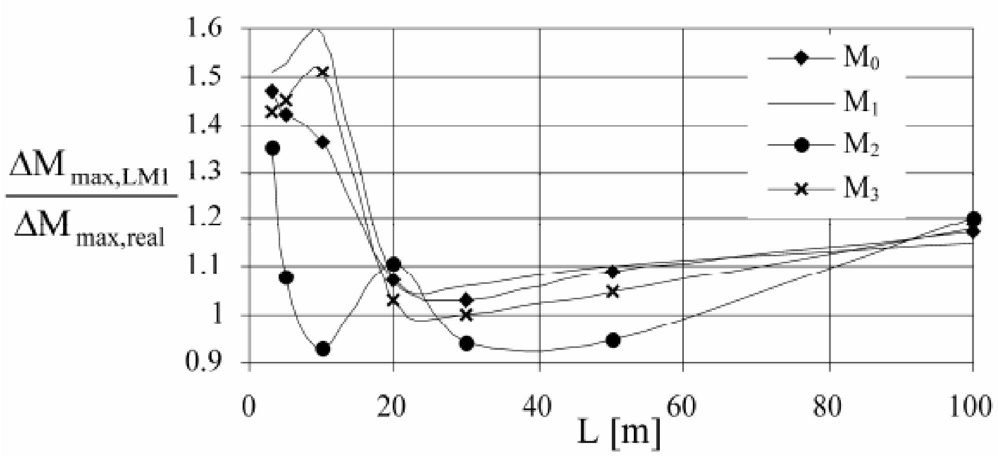

Figure 16. Accuracy of FLM1. (Croce, 2001)

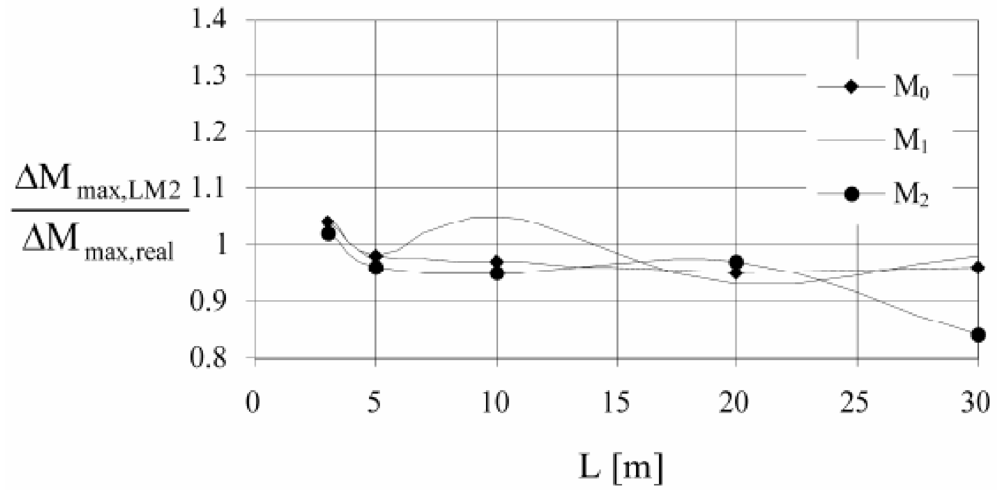

Figure 17. Accuracy of FLM2. (Croce, 2001)

Figure 18 and Figure 19 illustrate the ratios between the equivalent stress ranges for FLM3 and the reference traffic, with the slope parameter m of the S-N curve set to 3 and 5, respectively. For FLM3, the results are generally conservative, except for moments over the intermediate support of a two-span continuous beam when the span length exceeds 40m. The result for support moment M_2 becomes increasingly unconservative when both span length and slope parameter m increases. Due to the unsafe results for influence line M_2 in FLM3, an additional vehicle was proposed to the FLM. The additional vehicle with axle weights of 40kN would drive 40m behind the fatigue vehicle in the same lane. With the additional vehicle, the error would be reduced. Figure 20 shows the result obtained with the additional vehicle.

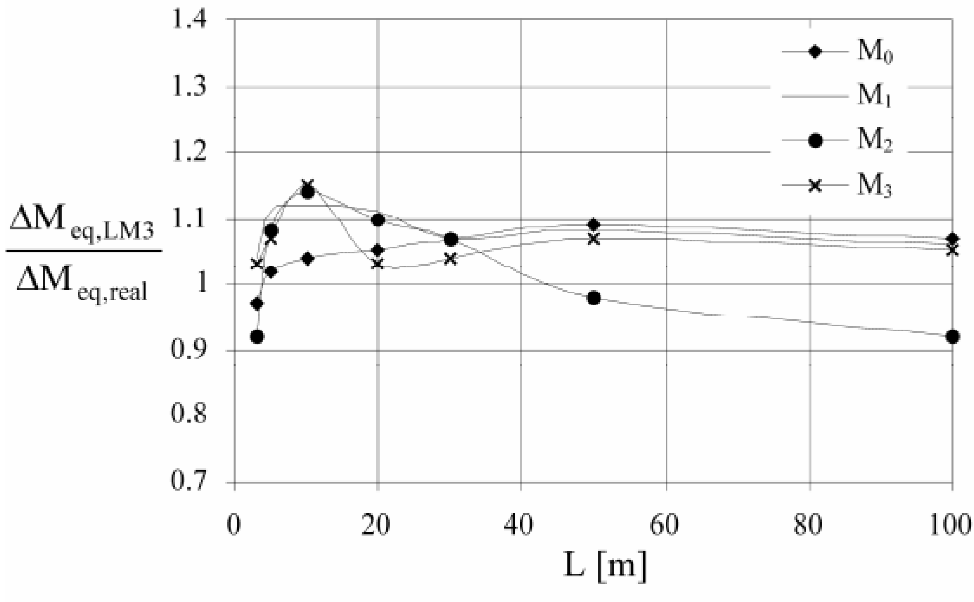

Figure 18. Accuracy of FLM3, when m=3. (Croce, 2001)

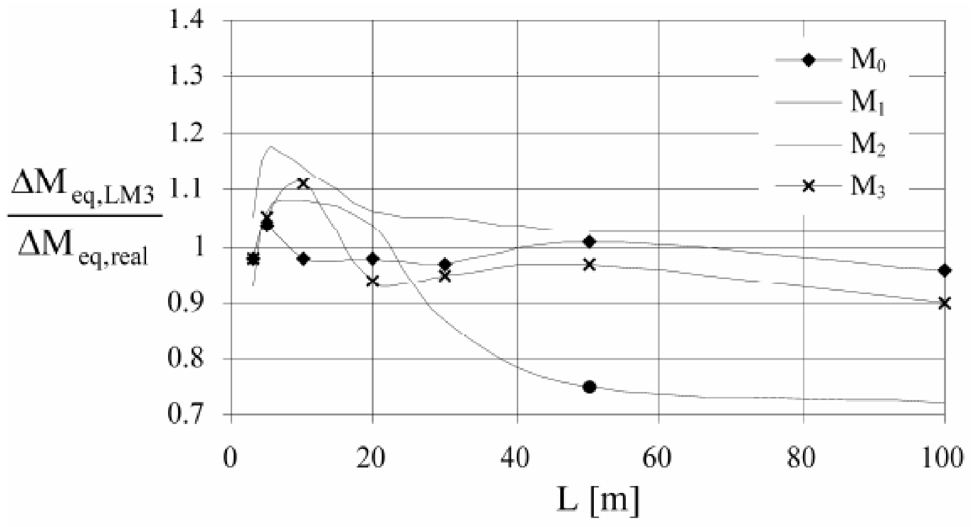

Figure 19. Accuracy of FLM3, when m=5. (Croce, 2001)

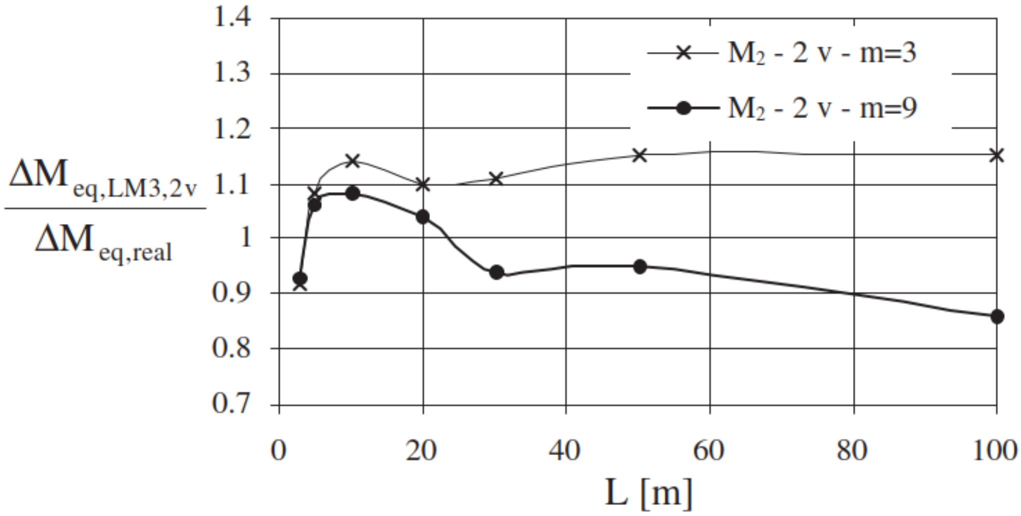

Figure 20. Accuracy of FLM3, including an additional vehicle. (Croce, 2001)

Figure 21 shows the ratio between the equivalent stress range of FLM4 and the Auxerre traffic. FLM4 shows more consistent results across all influence lines than the other Fatigue Load Models. However, slightly unsafe results can be observed for span lengths exceeding 25m.

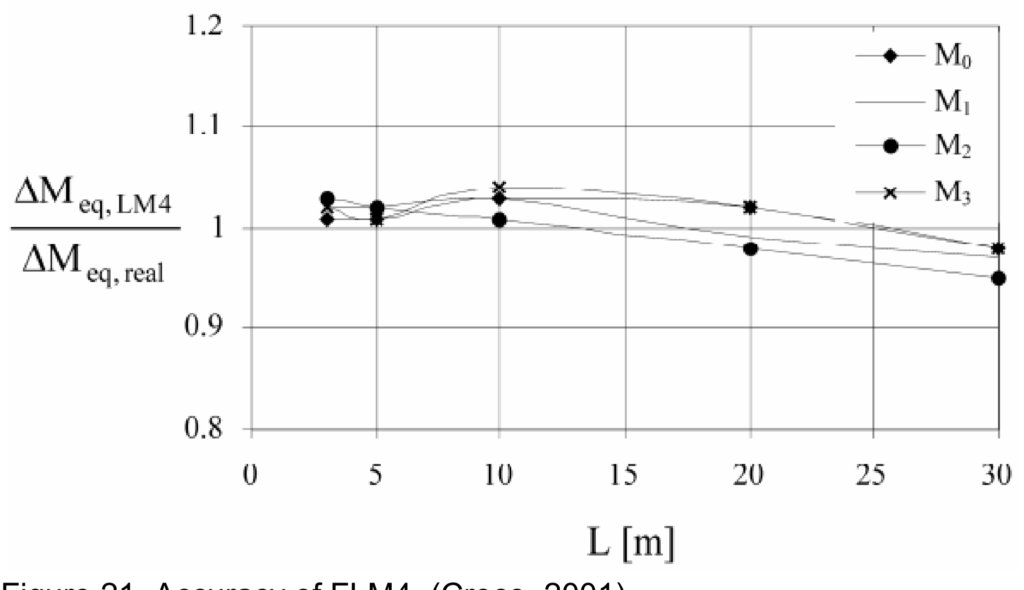

Figure 21. Accuracy of FLM4. (Croce, 2001)

3.2 Cumulative damage method

The cumulative damage method is used when fatigue assessment is performed according to FLM4 or FLM5. With this method, the stresses are determined, after which stress ranges and cycles are calculated using a cycle counting method. Different cycle counting methods were discussed in Chapters 2.3.1 and 2.3.2. The damage assessment can be performed after the stress ranges and their respective cycles have been determined. Palmgren-Miner rule is widely used in fatigue design.

The concept of cumulative fatigue damage was first proposed in the early 1920s when Palmgren (1924) published the idea of linear damage accumulation. Approximately 20 years later, Miner (1945) expressed the linear rule concept proposed by Palmgren again using a mathematical equation (Fatemi & Yang, 1998). Thus, it became the Palmgren-Miner rule, otherwise known as Linear Damage Rule (LDR) or simply Miner's rule. The rule is expressed as:

$$D = \sum \frac{n_i}{N_i} \tag{6}$$

where

D	is the cumulative damage
n_i	is the number of cycles for a given stress range
N_i	is the number of cycles to failure for a given stress range

The Palmgren-Miner damage accumulation rule linearly sums the damage caused by each stress range under variable amplitude loading (Skoglund, 2021). With this rule, the damage caused by different stress ranges are added together as each stress range contributes differently to the fatigue damage due to both low and high stresses. This means that the Palmgren-Miner rule assumes that the fatigue damage accumulates linearly and that the damage can be calculated separately for each stress range and summed up. For a studied detail to fail, the number of applied cycles n_i for a given stress range should be larger than the total number of cycles N_i suggested as the fatigue strength for that material in the S-N curve. The failure is reached when the damage D reaches the threshold value D=1. (Al-Emrani & Aygul, 2014). As Figure 22 illustrates, the rule assumes that the cycle ratio (n_i/N_i) equals the damage D.

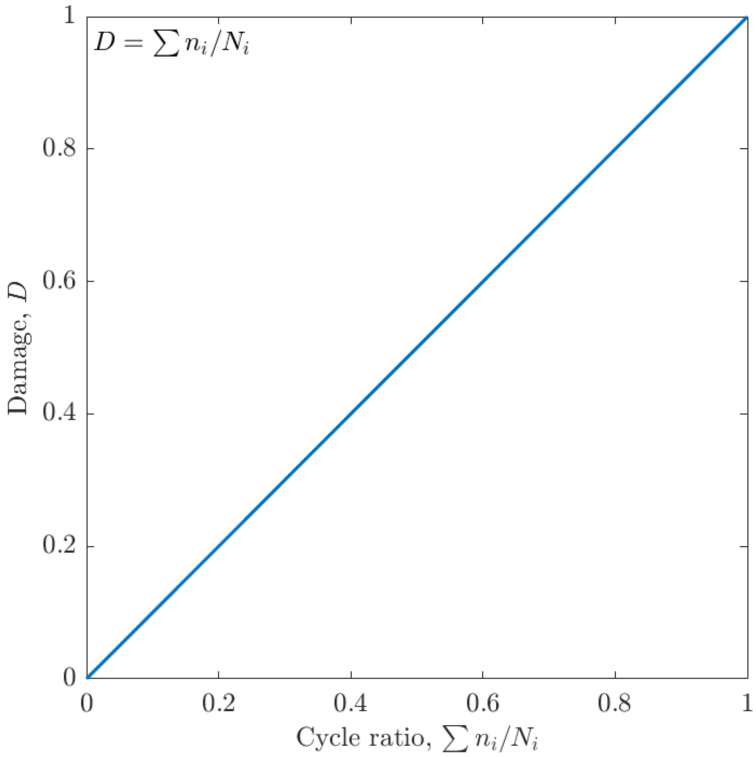

Figure 22. Illustration of the Miner's LDR.

In Miner's equation, the number of cycles for a given stress range n_i can be obtained with a cycle counting method. Meanwhile, the cycles to failure N_i are unknown and must be determined differently, like by using an S-N curve presented in Figure 23. As SFS-EN 1993-1-9 suggests, N_i is determined differently for the curve's primary and secondary parts. For the primary part, when the number of cycles to failure is less than $5 \cdot 10^6$, N_i is determined with equation (7),

$$N_i = 2 \cdot 10^6 \cdot \left(\frac{\Delta\sigma_C}{\Delta\sigma_i}\right)^3 \tag{7}$$

When the number of cycles to failure is more than $5 \cdot 10^6$ but less than 10^8, N_i is determined with equation (8),

$$N_i = 5 \cdot 10^6 \cdot \left(\frac{\Delta\sigma_D}{\Delta\sigma_i}\right)^5 \tag{8}$$

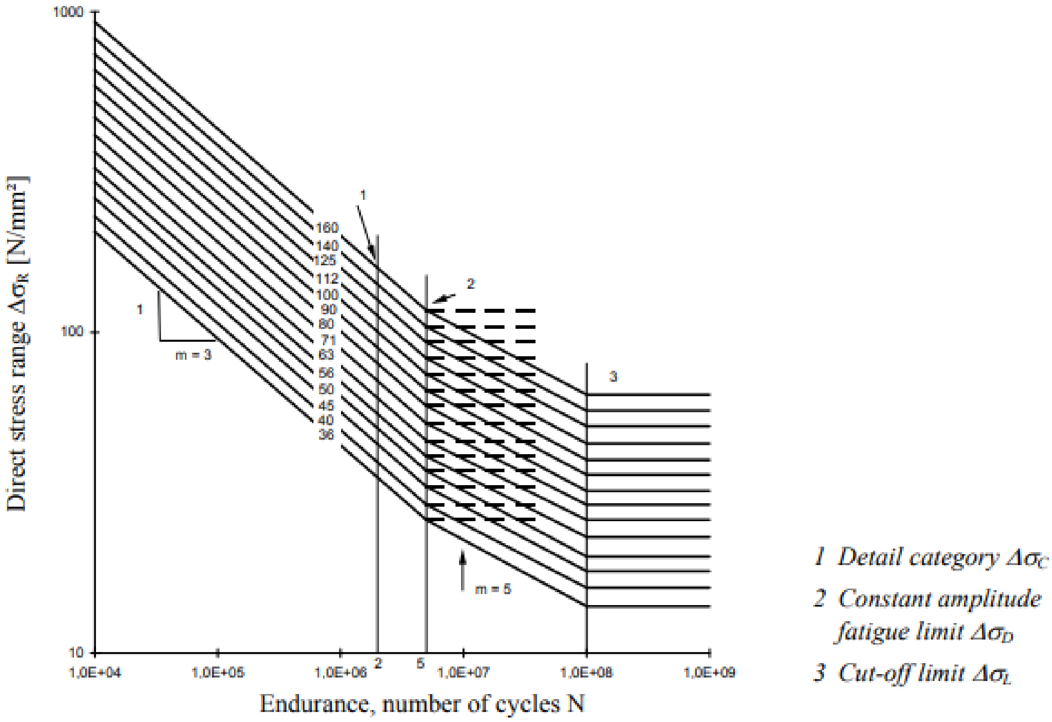

Figure 23. Fatigue strength curves according to SFS-EN 1993-1-9 Figure 7.1.

In the S-N curve, the constant amplitude fatigue limit $\Delta\sigma_D$ is obtained according to SFS-EN 1993-1-9 with equation (9),

$$\Delta\sigma_D = \left(\frac{2}{5}\right)^{\frac{1}{3}} \Delta\sigma_c \ or \ 0{,}737\Delta\sigma_c \tag{9}$$

and the cut-off limit $\Delta\sigma_L$ is obtained with equation (10),

$$\Delta\sigma_L = \left(\frac{5}{100}\right)^{\frac{1}{5}} \Delta\sigma_D \ or \ 0.549\Delta\sigma_D \tag{10}$$

3.2.1 Limitations of the Palmgren-Miner rule

While the Palmgren-Miner rule is widely used in fatigue design, it has its weaknesses. Under fluctuating mean stresses or during regular compressive overloads, the rule has been found to be somewhat inaccurate (Pedersen, 2018). As Miner's rule linearly sums the damage caused by each stress range, the order of different stress magnitudes is unimportant. However, Manson (1964) points out that the order of stresses can have great importance if the number of loading cycles is low. With low loading cycles, higher stresses are applied early in the loading history and cause more fatigue damage than if the high stresses were applied later. However, as it was implied, when the number of load cycles increases, the order of stresses is not as significant.

The accuracy of Miner's rule has also been tested throughout the years. Schütz (1996) published a critical review of fatigue history and its testing, where inaccuracies in Miner's rule were reported from different test programs. Furthermore, in a large-scale test program where hundreds of tests were collected, the rule proved to be unconservative for the most part. Hence, in the calculations performed, the testing components failed before the predicted fatigue life was reached. Usually, in fatigue predictions, the results are most likely to be conservative when low stresses are applied before high stresses and non-conservative when high stresses are applied first in a loading sequence (Hectors & De Waele, 2021).

Furthermore, as explained with the S-N curve, materials have an endurance limit under which the fatigue life is infinite regardless of the number of cycles for that stress range. Still, this usually applies only to new materials or structures, as the endurance limit may be reduced if a structure or material has already endured stresses above the endurance limit. The reduction of the endurance limit can be caused by cracks or other flaws introduced by the earlier stresses. This can lead to fatigue damage being formed even below the theoretical endurance limit. (Manson, 1964)

Several other cumulative damage rules have been constructed to overcome the defects of Miner's rule, like the Double Linear Damage Rule (DLDR) and the Nonlinear Damage Rule (NLDR). The DLDR proposed by Manson & Halford (1980) considers crack initiation and crack propagation, and therefore, both phenomena are represented with their own linear curves. Manson & Halford (1980) compared their proposed rule with Miner's rule and noticed that the LDR, on average, overestimated the fatigue damage by 37%, while the DLDR only by 12%.

The NLDR proposed by Marco & Starkey (1954) was based on the damage curve concept introduced earlier by Richart & Newmark (1975). The cumulative damage equation for NLDR resembles Miner's equation. However, it demonstrates the fatigue damage as an exponential function. Compared to the LDR, where the ratio between damage and cycle ratio is equal, as demonstrated in Figure 22, in NLDR the cycle ratio is less than one when cumulative damage D=1. (Hectors & De Waele, 2021) Nevertheless, this study applies the widely adopted Miner's rule to calculate fatigue damage accumulation.

3.3 The damage equivalent method

The damage equivalent method, or simpler the λ-coefficient method, is a simplified method for fatigue assessment. In this method, equivalent stress ranges are compared with the detail category that is studied (Al-Emrani & Aygul, 2014). This method is derived for vehicles from the procedure utilised for railway bridges (Croce, 2001). Compared to the cumulative damage method, the damage equivalent method does not require a direct analysis of variable amplitude loadings (Skoglund, 2021).

The λ-coefficient method converts the fatigue verification into conventional resistance checks, where a conventional equivalent stress range $\Delta\sigma_{E2}$ is compared with a detail category $\Delta\sigma_C$ (Croce, 2001). The stress range is modified with λ-coefficients to consider different effects such as the shape and length of the influence line, traffic volume, design life of the bridge, and the influence of multiple vehicles on the bridge simultaneously (Skoglund, 2021). The stress range is produced by a fatigue vehicle given in the Eurocode, which is also presented in Figure 14. The fatigue assessment should be performed according to SFS-EN 1993-2 as follows:

$$\gamma_{Ff}\,\Delta\sigma_{E2} \leq \frac{\Delta\sigma_c}{\gamma_{Mf}} \tag{11}$$

Where the damage equivalent stress range $\Delta\sigma_{E2}$ at $2 \cdot 10^6$ cycles shall be obtained with equation (12),

$$\Delta\sigma_{E2} = \lambda\phi_2\,\Delta\sigma_p \tag{12}$$

where

λ	is the damage equivalent factor
ϕ_2	is the damage equivalent impact factor
$\Delta\sigma_p$	is the stress range

and the damage equivalent factor λ is determined by considering four different sub-factors:

$$\lambda = \lambda_1\,\lambda_2\,\lambda_3\,\lambda_4 \leq \lambda_{max} \tag{13}$$

λ_1	factor considering the length of the influence line
λ_2	factor considering traffic volume
λ_3	factor considering the design life of the bridge
λ_4	factor considering the traffic on other lanes
λ_{max}	factor considering the fatigue limit

The λ_1 sub-factor takes the span length into consideration with the location of the loads. Figure 24, gives the recommended values for λ_1 for both midspan and support section. Hence, two different curves are given for determining λ_1 depending on the location of the detail that is studied.

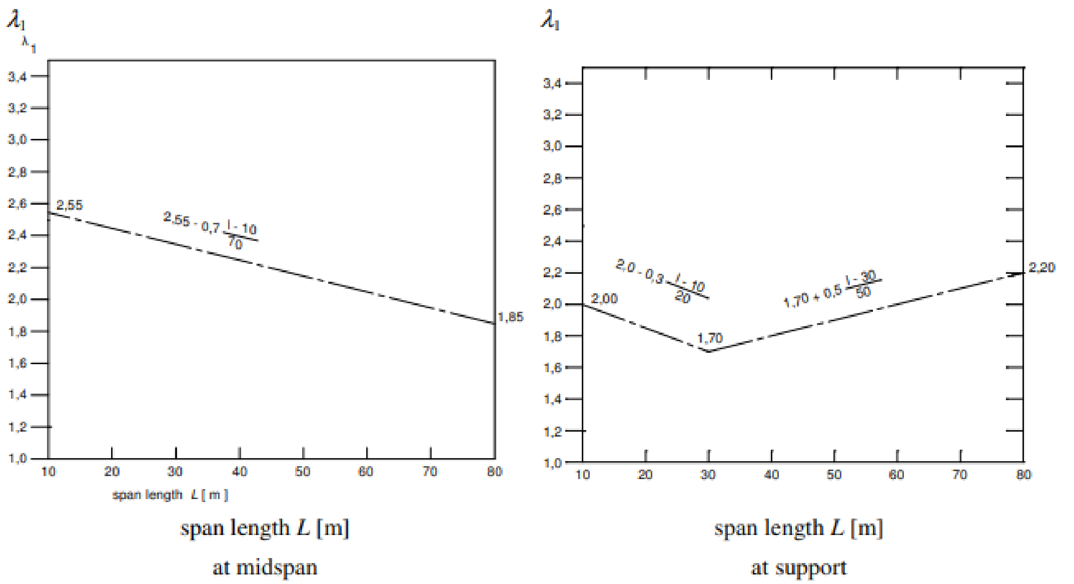

Figure 24. Sub-factor λ_1 for moments for road bridges according to SFS-EN 1993-2 Figure 9.5.

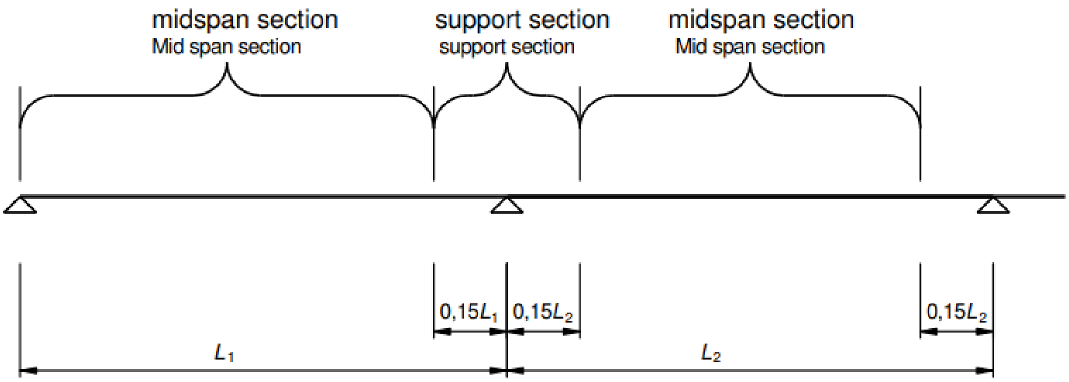

Figure 25. Location of midspan and support section according to SFS-EN 1993-2 Figure 9.7.

The critical span length when determining λ_1 should be defined according to SFS-EN 1993-2. Depending on the case, the critical span length is defined differently for both the midspan and support sections. As only moments are concerned in this analysis, the critical lengths for moments are:

- For simply supported bridges, the critical length is the same as the span length.

- In the midspan section (Figure 25), for a continuous-span bridge, length is the span length under consideration.

- In the support section (Figure 25), for a continuous-span bridge, the length is the mean of the two spans next to the support.

However, sub-factor λ_1 has some weaknesses. Maddah (2013) points out that the traffic flow is simplified in the determination of λ_1. This is because multi-vehicle presence is neglected, and λ_1 only considers one-by-one vehicle crossing. Additionally, the influence of the span length is not considered realistically in the calculation of λ_1 (Maljaars, 2020).

The λ_2 coefficient considers the annual traffic flow and composition derived from the Auxerre traffic. As the Auxerre traffic is used as reference traffic, values for N_0 and Q_0 are already determined. The λ_2 sub-factor, according to SFS-EN 1993-2, is obtained with equations (14) and (15),

$$\lambda_2 = \frac{Q_{m1}}{Q_0}\left(\frac{N_{Obs}}{N_0}\right)^{\frac{1}{5}} \tag{14}$$

where

$$Q_{m1} = \left(\frac{\sum n_i Q_i^5}{\sum n_i}\right)^{\frac{1}{5}} \tag{15}$$

Q_0	480kN
N_0	$0{,}5 \cdot 10^6$
N_{Obs}	is the number of lorries per year determined from Table 1
Q_i	is the gross weight of the i:th lorry in the slow lane
n_i	is the number of lorries with a gross weight Q_i in the slow lane

From SFS-EN 1993-2 table 9.1, λ_2 can be taken for given values Q_{m1} and N_{Obs}. However, National Annexes may provide values that shall be used. NCCI4 table 6.23 gives values for Finnish structural steel depending on the traffic type and traffic category. The values provided in the NCCI codes are explained later in Chapter 4.5.1.

The λ_3 coefficient presented in SFS-EN 1993-2 considers the design life of the bridge. Eurocodes recommend the design life to be 100 years, as the Fatigue Load Models were calibrated with a reference design life of 100 years (Al-Emrani & Aygul, 2014). However, National Annexes may give different values and recommended design life. Nevertheless, λ_3 is obtained with equation (16),

$$\lambda_3 = \left(\frac{t_{Ld}}{100}\right)^{\frac{1}{5}} \tag{16}$$

where

t_{Ld} is the design life of the bridge.

The effect of multiple vehicles occurring on several lanes is considered in the calculation of λ_4. According to SFS-EN 1993-2, sub-factor λ_4 shall be determined with equation (17),

$$\lambda_4 = \left[1 + \frac{N_2}{N_1}\left(\frac{\eta_2 Q_{m2}}{\eta_1 Q_{m1}}\right)^5 + \frac{N_3}{N_1}\left(\frac{\eta_3 Q_{m3}}{\eta_1 Q_{m1}}\right)^5 + \cdots + \frac{N_k}{N_1}\left(\frac{\eta_k Q_{mk}}{\eta_1 Q_{m1}}\right)^5\right]^{\frac{1}{5}} \tag{17}$$

where

k is the number of lanes with heavy traffic
N_j is the number of vehicles per year in lane j
Q_{mj} is the average weight of vehicles in lane j
η_j is the influence line value of internal force that produces the stress range

After the λ-coefficients have been determined, the damage equivalent factor shall be calculated by multiplying the coefficients. However, an upper limit needs to be defined, which considers the fatigue limit of the detail under consideration. This upper limit is λ_{max} and it is defined similarly to λ_1 for details considering the moment at midspan and the support section. The value of λ_{max} for a given span length shall be determined as presented in Figure 26.

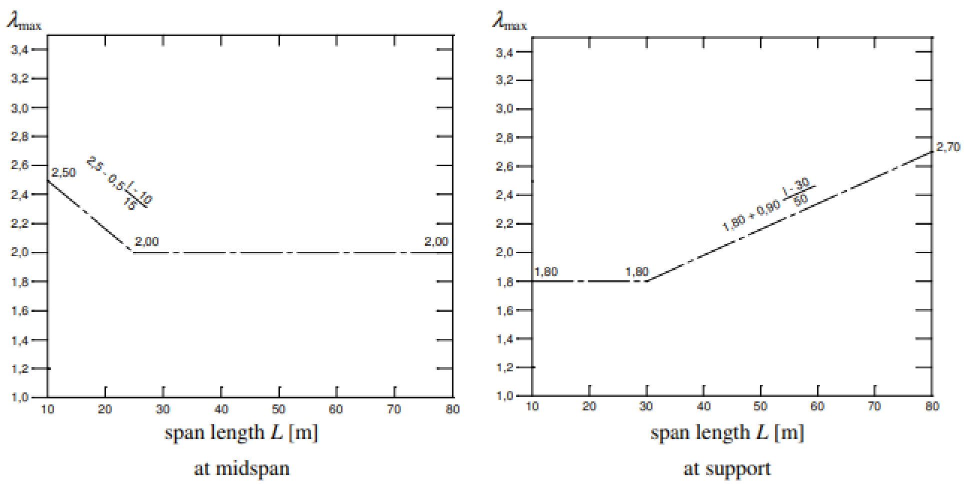

Figure 26. λ_{max} for moments for road bridges according to SFS-EN 1993-2 Figure 9.6.

3.4 Summary of the literature review

The increase in vehicle weights, particularly in Finland, has been somewhat significant through the years, as illustrated in Figure 1. Today, the largest allowable GVW of a vehicle on the Finnish road network has been regulated to 76 tonnes, adding pressure on the Finnish infrastructure, including bridges. This has affected somewhat the fatigue design as measures have been taken to update the NCCI codes to comply with the new regulations.

Due to the evolution of vehicle weights, the importance of traffic measurement increases. The measurement of traffic enhances the accuracy of the fatigue assessment of future bridges and the examination of existing bridge stock. The technologies used for measuring traffic have improved significantly through the years, from static weighing to WIM and B-WIM. However, each of these has its benefits. Static weighing is the most accurate weighing technology, yet still time consuming compared to other technologies. WIM systems enable vehicle measurements during motion and thus require a shorter measurement time for individual vehicles. Similarly to WIM, B-WIM technologies record vehicles during motion. However, B-WIM measurements disturb less traffic as B-WIM technologies are installed at the soffit of a bridge. These technologies have enabled faster and more precise traffic recording. In addition to weight, measurement technologies can record other vehicle parameters, such as axle spacings and velocities, which are crucial in fatigue assessment.

As mentioned earlier, the fatigue design can be more precise with recorded traffic and vehicle data. A vehicle crossing a bridge causes moments and stresses. With recorded data, more realistic stress ranges and other stress parameters are obtained than when fatigue vehicles provided in Eurocodes are used. This is due to the larger variety of vehicle weights, axle weights, vehicle configurations, and vehicle velocities present in WIM databases. Additionally, as already has been done, recorded data can be useful for developing and reviewing Fatigue Load Models provided in the Eurocodes.

Eurocodes provide five Fatigue Load Models for fatigue verification. However, only two are used in this thesis, FLM3 and FLM4. A single fatigue vehicle with a GVW of 480kN is used with FLM3. Whereas a set of “equivalent” lorries are provided in the Eurocodes when fatigue verification is performed according to FLM4. Additionally, two damage methods presented in Eurocodes are widely used in fatigue assessment. That is the cumulative damage method and the damage equivalent method. While several cumulative damage rules have been proposed, Miner’s LDR has remained the most used due to its simplicity. The LDR assumes that the damage accumulates linearly. This means that the damage for each stress range can be summed to obtain the total damage. In this thesis, the LDR is used in the following chapters in the analysis of the recorded traffic and FLM4. The damage equivalent method is used with FLM3 in this thesis. In this method, the stress range caused by the single fatigue vehicle is modified with a damage equivalent factor. This factor considers the critical length of the influence line, the traffic volume and weight of the traffic, the design life, and the traffic on other lanes.

The following chapters study the effect of the regulation change implemented in 2013 and compare actual traffic to FLM3 and FLM4. Furthermore, a new Fatigue Load Model is calibrated from actual traffic. The calibration follows the method introduced by Maljaars (2020). The method and calculation process are explained step by step. The obtained results are presented immediately after the calculations to ensure a smoother flow and prevent the need for the reader to jump between chapters.

4 Method

As stated in Chapter 1.4, this thesis has three primary goals. The first is to analyse the effect of the increased vehicle weights, the second is to compare the Fatigue Load Models to actual traffic, and the third goal is to calibrate a new FLM from recorded traffic data. The analysis of the regulation change will be done by comparing the required elastic section modulus ($W_{,el}$) obtained between two different measurement years. Meanwhile, the Fatigue Load Models will be compared by comparing the $W_{,el}$ required for the recorded traffic with that required for FLM3 and FLM4. A cumulative damage method, in this case, Miner's LDR, will be utilised for the fatigue assessment of the recorded traffic and for the analysis of FLM4, whereas the fatigue assessment of FLM3 will be done with the damage equivalent method.

As explained earlier the analysis aims not to inspect the fatigue life of an existing bridge or to determine the accumulated fatigue damage caused by the recorded traffic data for a certain detail. The analysis is done by calculating the required elastic section modulus for a 100-year design life. This means that each case bridge and span length that is used will give a different elastic section modulus. The differences between FLM and B-WIM are reviewed by calculating the ratio between $W_{,el}$ obtained for the Fatigue Load Models and the real traffic data. The differences between 2014 and 2016 B-WIM data are equally determined by calculating the ratio. A ratio of R=1 would indicate an equal contribution to the fatigue damage. These calculations are done for the B-WIM databases, FLM3 and FLM4. Therefore, the effect from the increased vehicle weights is studied by:

- Calculating the elastic section modulus for the 2014 and 2016 B-WIM databases. The elastic section modulus obtained for all influence lines and span lengths for 2016 are compared with the ones obtained for 2014. This means that $W_{,el}$ obtained for the 2016 database is divided by the $W_{,el}$ obtained for the 2014 database. This gives a ratio between the two years. If the ratio is over R=1, the 2016 traffic requires a larger section modulus for the fatigue damage to be D=1 after 100 years. If the ratio is under R=1, the 2014 traffic requires a larger section modulus. Hence, the ratio between the 2016 B-WIM database and the 2014 B-WIM database for a given span length is obtained with equation (18),

$$R_{WIM} = \frac{W_{,el.2016}}{W_{,el.2014}} \tag{18}$$

The difference between FLM and B-WIM is studied by:

- Calculating the elastic section modulus for FLM3 and FLM4 required for all span lengths and influence lines. The elastic section modulus obtained for all influence lines and span lengths for FLM3 and FLM4 are compared with those obtained for the 2016 B-WIM database. The 2016 B-WIM data is used as it is closer to today's traffic. Hence, $W_{,el}$ obtained for FLM3 is divided by the $W_{,el}$ obtained for the 2016 database and $W_{,el}$ obtained for FLM4 is divided by the $W_{,el}$ obtained for the 2016 B-WIM database. This gives a ratio between FLM3 and the recorded traffic and FLM4 and the recorded traffic. If the ratio exceeds R=1, the Fatigue Load Models are conservative. Whereas if the ratio is under R=1, the Fatigue Load Models give unsafe results. Hence, the ratios between FLM3 and 2016 B-WIM data and FLM4 and 2016 B-WIM data for a given span length are obtained with equations (19) and (20),

$$R_{FLM3/WIM} = \frac{W_{,el.FLM3}}{W_{,el.2016}} \tag{19}$$

$$R_{FLM4/WIM} = \frac{W_{,el.FLM4}}{W_{,el.2016}} \tag{20}$$

Additionally, a new Fatigue Load Model will be calibrated that represents the traffic measured in Kaarina. The new fatigue vehicle and FLM calibration are done according to the principle introduced by Maljaars (2020). The derivation process of the new fatigue vehicle and FLM is explained from Chapter 5 onwards. The elastic section modulus obtained from the new Fatigue Load Model is compared with the one obtained for the 2016 recorded traffic. This is as the calibration is done with the 2016 B-WIM data. The aim is to get the ratio as close to R=1 as possible. This means that the fatigue damage caused by the new FLM should equal the damage caused by the 2016 traffic.

4.1 Recorded traffic used in the analysis

Traffic and vehicle parameters of the recorded traffic used in this analysis were gathered during a larger measurement campaign conducted by the Finnish Transport Agency (2018), in which traffic data was collected from multiple sites between the years 2013 and 2017. The measurement was executed with a SiWIM system. More specifically, the measured traffic data used in this analysis was gathered south of Kaarina, located in Southwest Finland, in the years 2014 and 2016. The measurement period was one week for both years. SFS-EN 1991-2 Annex B (11) states that some form of adjustment is needed if the measurement period is less than one week. Thus, in this case, any adjustments can be excluded. The measurement site has two lanes, and thus the measurement was done in both directions. Because of the new regulation implemented in 2013, the vehicle data of the 2016 measurement year contains heavier vehicles than in 2014 as was illustrated in Figure 2. However, while the data shows a larger number of heavier vehicles for the latter year, the average GVW still remains similar. Nevertheless, the recorded data gathered during 2016 will be used for the FLM analysis and calibration of the new FLM as it closer represents today's traffic. However, the difference between the years 2014 and 2016 will be analysed and presented.

Furthermore, the data gathered in the year 2016 showed an increase in the number of vehicles during the one-week measurement period, with 3730 vehicles recorded in 2016 and 3366 vehicles in 2014. Hence, the latter year will contribute more to fatigue damage due to a larger number of cycles. The regulation changes presented in 2013 were expected to decrease the number of vehicles. However, the number of vehicles increased from 2014 to 2016, as can be observed from the B-WIM databases. Naturally, a one-week measurement period does not show if this is true for longer measurement periods. Nevertheless, for these measurement weeks, the traffic volumes have not decreased but rather increased. Furthermore, the traffic data presented by the Finnish Transport Agency (2018) includes only vehicles that are equal to or heavier than 10 tons. This is due to the small effect on fatigue damage caused by lighter vehicles. This was also demonstrated by Qvisen (2020), where it was concluded that axle weights below 50kN caused insignificant damage.

4.2 Case

The fatigue assessment of B-WIM data can be divided into four steps, as presented by Maljaars (2020). Firstly, the measured axle weights and axle distances are transformed into a long array. Secondly, the array will be run over different influence lines for the calculation of moment and stress history. In this thesis, the traffic array will be run in one direction. Thirdly, a stress range histogram will be created with a cycle counting method. The rainflow method will be utilised in this thesis. Fourthly, the fatigue damage will be calculated with the Miner's LDR by using a two-slope S-N curve.

This analysis considers four cases. That is, four different moment influence lines, illustrated in Figure 27, are used in this analysis for various numbers of spans and span lengths. The span lengths (L) that will be used are 10, 20, 30, 40, 50, 60, 70, and 80 meters. Therefore, the shortest case bridge will be 10m (IL_1), and the longest will be 280m (IL_4).

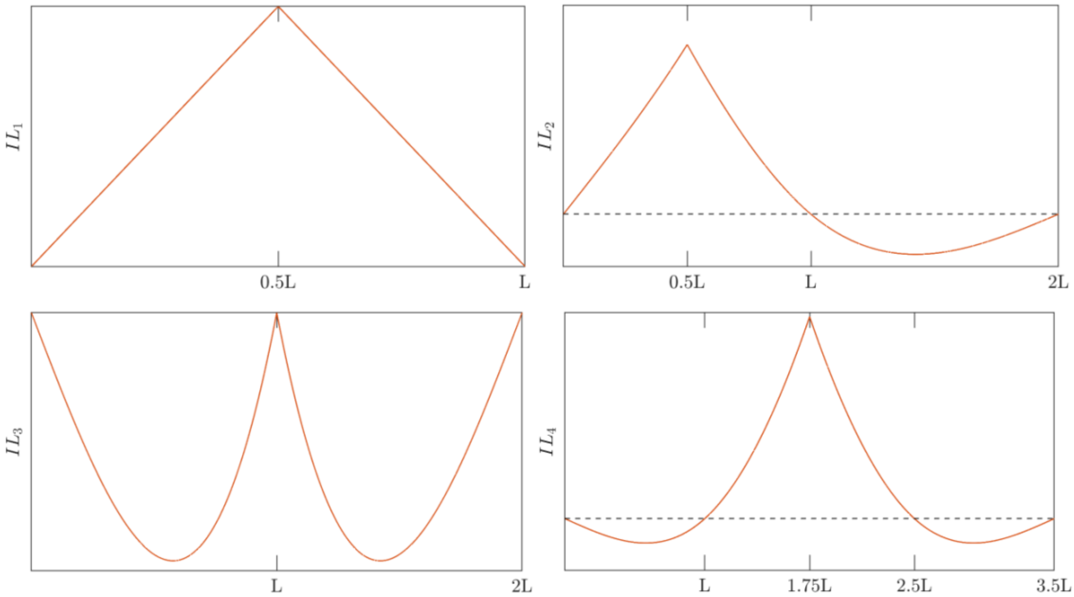

Figure 27. Illustration of the influence lines used in the analysis.

The first influence line (IL_1) represents the bending moment at the midspan of a simply supported bridge, and it is expressed as:

$$IL_1(x) = \begin{cases} \frac{x}{2} & 0 \leq x \leq \frac{L}{2} \\ \frac{L}{2} - \frac{x}{2} & \frac{L}{2} \leq x \leq L \end{cases} \tag{21}$$

The second influence line (IL_2) corresponds to the bending moment at the midspan of a two-span continuous bridge, and it is expressed as:

$$IL_2(x) = \begin{cases} \frac{x^3}{8L^2} + \frac{3x}{8} & 0 \leq x \leq \frac{L}{2} \\ \frac{x^3}{8L^2} - \frac{5x}{8} + \frac{L}{2} & \frac{L}{2} \leq x \leq L \\ -\frac{x^3}{8L^2} + \frac{3x^2}{4L} - \frac{11x}{8} + \frac{3L}{2} & L \leq x \leq 2L \end{cases} \tag{22}$$

The third influence line (IL_3) represents the bending moment at the mid-support of a two-span continuous bridge, and it is expressed as:

$$IL_3(x) = \begin{cases} \frac{x^3}{4L^2} - \frac{x}{4} & 0 \leq x \leq L \\ -\frac{x^3}{4L^2} + \frac{3x^2}{2L} - \frac{11x}{4} + \frac{3L}{2} & L \leq x \leq 2L \end{cases} \tag{23}$$

The fourth influence line (IL_4) represents the bending moment at midspan of a continuous bridge with three spans, and it is expressed as:

$$IL_4(x) = \begin{cases} \frac{1}{13} \cdot \left(-x + \frac{x^3}{L^2}\right) & 0 \leq x \leq L \\ \frac{1}{13} \cdot \left(-x + \frac{x^3}{L^2} - \frac{(x-2)^3}{L^2}\right) & L \leq x \leq 1.75L \end{cases} \tag{24}$$

These influence lines are used to describe how each case is influenced by the moving vehicles. Additionally, the most critical loading configurations and loading points that create the greatest effects can be identified with influence lines. An influence line represents how load effects, like moments, at a particular bridge location vary as a load moves across it. The influence line concept can also be represented in two dimensions, where instead of an influence line, the analysis is based on the influence surface. These influence lines are calculated for various sections and components of a structure to identify the most critical areas and to determine the load positions that produce the most significant effect for each load. (Fiorillo & Ghosn, 2015)

In this analysis, the traffic data will be considered as previously explained. The recorded traffic is analysed as if moving in a single direction over a slow lane, even if the B-WIM data was originally collected for two-way traffic. Additionally, each vehicle is assumed to cross the case bridges separately. However, as the span length increases, so does the probability of multiple vehicles crossing a bridge simultaneously. This can occur due to vehicles travelling close together or by moving in opposite directions on the bridge. Evidence of this can be observed in the measured traffic from Kaarina. For the shortest case bridge with a length of 10 meters, the 2016 data show 16 instances where more than one vehicle would be on the bridge simultaneously, accounting for 0,43% of the total. For the year 2014, the corresponding numbers are 12, or 0,36%. If the length of the bridge increases to 280 meters, representing the longest case bridge, the instances when more than one vehicle is on the bridge at the same time also increase significantly. For 2016 there would be 690 instances (18,5%), and for 2014, 612 instances (18,18%).

As this analysis is performed as mentioned above, it does not perfectly simulate actual traffic. Simultaneous crossing of heavy vehicles can cause more fatigue damage due to increased stress ranges compared to scenarios where vehicles cross the bridge separately. This means that the accuracy of the results obtained from the measured traffic may be underestimated when calculations are done for longer span lengths. However, as this analysis is done with only one lane considered, the accuracy is not affected that much. This is because the vehicles would cross the bridges in a queue, and therefore, the increase in stress ranges would not be as significant. In an analysis with multiple lanes, the stress ranges could theoretically get larger if two or more vehicles were travelling alongside in different lanes.

4.2.1 Multi-vehicle effect

Sivakumar, et al. (2011) studied the occurrence of multiple vehicles on different span lengths. The studied data was collected from various WIM measurement sites in New Jersey during an 11-year measurement period. The study indicated that the simultaneous crossing of vehicles on a given bridge depends on traffic volume and span length. Figure 28 shows the results obtained by Sivakumar, et al. (2011) for four loading patterns, including single, following, side by side, and staggered. The simultaneous crossing clearly increases with the span length. However, the percentage of vehicles travelling side by side remains even for all span lengths. The results were obtained with daily measurements. Each day simultaneous events were recorded and compared to the total traffic of that day, and thus, the percent of occurrence was obtained.

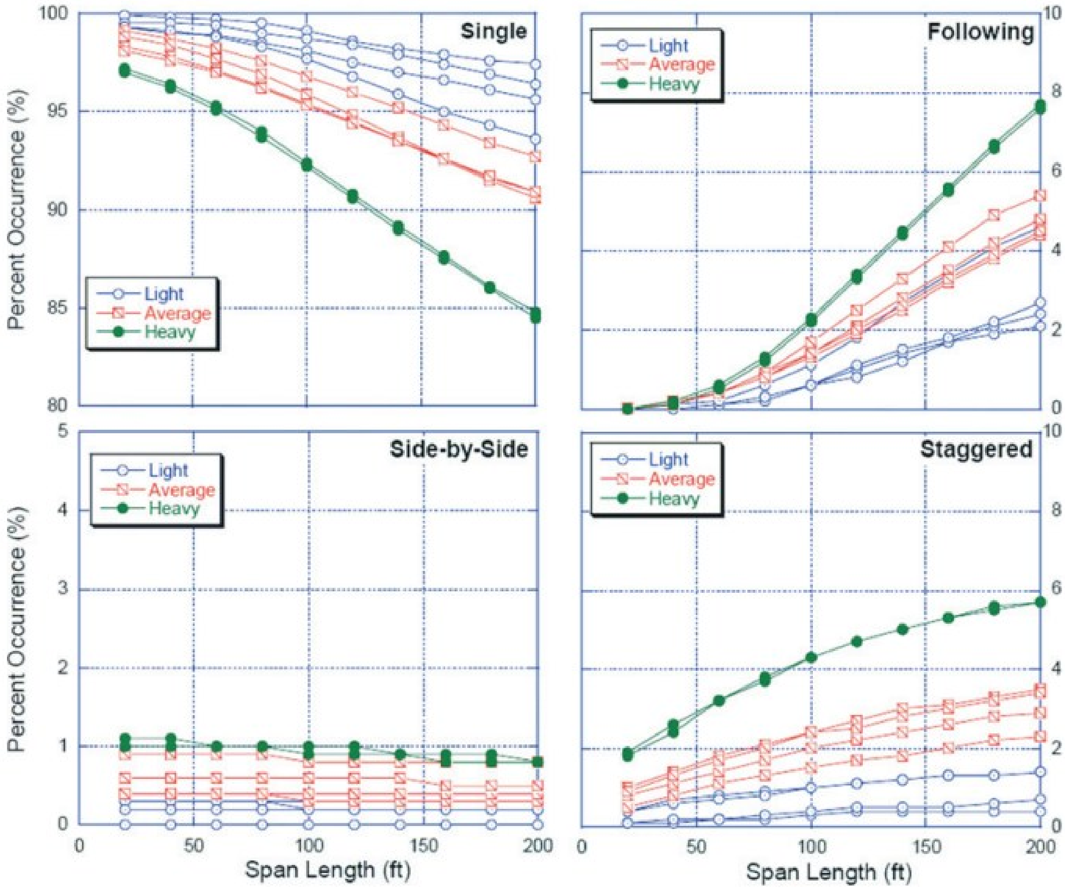

Figure 28. Percentages for multiple-presence vehicles for different span lengths. (Sivakumar, et al., 2011)

Lee, et al. (2022) studied the multi-vehicle effect on bridge fatigue. For medium-span bridges with no loading parameters (only GVW), the effect on the fatigue life of simultaneous crossing was minimal compared to one-by-one crossing. This was due to the small occurrence of multiple vehicles crossing the bridge simultaneously due to the short span length of the studied bridge. Additionally, the results obtained without loading parameters showed a clear underestimation of fatigue life. In cases where loading parameters were considered (axle loads and axle spacings), the fatigue life shortened slightly due to simultaneous crossing. However, the one-by-one crossing provided similar results as the measured strain data.

However, there are multiple ways vehicles can simultaneously cross a bridge, as shown in Figure 28. The crossing can occur side by side on different lanes, one vehicle following another on the same lane, or staggered on different lanes. Walbridge, et al. (2013) studied the multi-vehicle effect on the North American damage equivalent factor. The analysis was done for two different influence lines with varying span lengths. For a simple span bridge with an influence line resembling IL_1 in this thesis, the damage equivalent factor decreased when the vehicle flow rate increased with two vehicles simultaneously in the same lane. This is because two vehicles crossing the bridge simultaneously on the same lane can increase the maximum stress but, at the same time, decrease the minimum stress. However, the damage equivalent factor increased with the span length when simultaneous crossing on multiple lanes was considered. This is due to the possibility of more than one vehicle occurring simultaneously near the midspan or other critical locations along the bridge. The damage equivalent factor increased further for a two-span bridge, with the bending moment considered at the mid-support, resembling IL_3 in this thesis. Nevertheless, while bidirectional crossing can greatly affect stress ranges due to multiple vehicles occurring simultaneously on unfavourable locations along the span length, this analysis is performed with a one-by-one crossing of vehicles.

4.2.2 Analysis setting

SFS-EN 1993-1-9 gives reference design values of the fatigue strength ($\Delta\sigma_C$) for different members and joints. However, as this analysis uses example cases and no real bridge is being investigated, the reference design value is chosen freely. Therefore, in this analysis $\Delta\sigma_C$=66 MPa, which represents the fatigue strength. The stress range at the knee-point $\Delta\sigma_D$ of the S-N curve is obtained with equation (9). As a two-slope S-N curve is utilised in the fatigue calculation, the curve does not include an endurance limit. However, a limit under which stresses do not cause any fatigue damage will be determined. This limit is obtained with equation (10). The endurance limit is further multiplied by 0,1 to make the analysis more unfavourable. Hence, in this analysis, smaller stress ranges will influence the fatigue damage than if the equation provided in the Eurocode was solely used. To accurately compare the results, the same design values will be applied to analyse B-WIM data, FLM3 and FLM4. Furthermore, the partial factor for fatigue strength γ_{Mf} and for loading γ_{Ff} given in SFS-EN 1993-1-9 will be used in the FLM3 and FLM4 calculations. These factors are 1,0 and 1,35, respectively.

SFS-EN 1991-2 Annex B provides a dynamic amplification factor (DAF) that should be multiplied with the recorded axle loads unless otherwise specified. The amplitude of the factor depends on the quality of the road surface. Hence, for a road with a good surface roughness, φ_{fat}=1,2 shall be used, and with a medium surface roughness, φ_{fat}=1,4 shall be used. In this thesis, the DAF is set to φ_{fat}=1,2. However, calibration results obtained with a φ_{fat}=1,0 are presented in Appendix A. For the calibration of the new FLM, no amplification factor is used. This means the new fatigue vehicle will have true axle weights and true GVW.

The DAF of a bridge is obtained by dividing the maximum total load by the maximum static load (Brady, et al., 2006). These factors are usually determined with field tests where the effect of moving vehicles on a rough road surface is measured. However, in addition to the condition of the road surface, several other factors affect the DAF, like wind, the inclination of the road surface, acceleration, and braking, the balance of axle groups and loads, and the condition of wheels (Ludescher & Bruhwiler, 2009). DAFs given in design codes, like in SFS-EN 1991-2, are constant values and can overestimate the dynamic effect of heavy vehicles, whereas they can underestimate that for lighter vehicles (Qvisen, 2020).

4.3 B-WIM analysis

The fatigue analysis and traffic simulations are performed with the MATLAB programming platform. Three different codes are constructed for each analysis. Each code computes the required $W_{,el}$ for a 100-year design life. MATLAB is used due to its many inbuilt functions that simplify the coding process.

4.3.1 B-WIM data presentation

Over the years, the presentation of B-WIM data has lacked standardisation. Using B-WIM data has been difficult, as the measured data has been presented in multiple formats. As of this, no software utilising the B-WIM data has been developed due to the lack of efficiency in non-standardised data formatting. Also, measurements are expensive and due to this, the data is not shared a lot. However, there have been developments regarding the standardisation in recent years. Qvisen (2020) proposed a new standardised presentation of B-WIM data based on the earlier presentation of SiWIM systems. (Qvisen, 2020)

The B-WIM data used in this analysis is presented according to the format proposed by Qvisen (2020). The standardised format is presented in Table 6. The data is provided in an Excel file, which means that the data is imported into MATLAB. However, the original information is modified to import only relative parameters. Furthermore, the data is rearranged to make the coding process less tedious. The rearrangement is done as information in the provided file overlaps each other, as columns contain, for example, both axle loads and axle distances. As previously mentioned, only relevant parameters are utilised in the fatigue analysis. The relevant parameters are axle loads, axle spacings, and velocities of vehicles. As each vehicle is considered to cross the case bridge separately, the arrival time is unnecessary.

Table 6. Standardised presentation of B-WIM data. (Qvisen, 2020)

Column	Data	Unit	Note
1	Vehicle ID		
2	Timestamp		Format: YYYY-MM-DD-HH-MM-SS-mmm
3	Error code		Specified by measurement software. Default is 0
4	T	[°C]	Temperature
5	Lane		Marked as A1, A2, B1, B2, and so on. A for the northbound lanes and B for the southbound.
6	DAF		Dynamic Amplification Factor
7	v	[m/s]	Vehicle speed
8	Lateral offset	[m]	Lateral offset of the vehicle
9	Vehicle class		
10	N		Number of axles in the vehicle
11	Axle composition		Shows bogie types, e.g. semitrailer would be 113
12	Wheel types		Wheel types A, B, C according to SFS-EN 1991-2. D for other wheel types.
13	A_{GVW}	[kN]	Gross Vehicle Weight
13+1	A_1	[kN]	Axle 1 weight
⋮	⋮	⋮	⋮
13+N	A_N	[kN]	Axle N weight
14+N	D_{TOT}	[m]	Total axle spacing from first axle to the last
15+N	D_1	[m]	Distance/spacing between axle 1 and 2
⋮	⋮	⋮	⋮
13+2N	D_{N-1}	[m]	Distance/spacing between axle N-1 and N
14+2N	Reserve for future		If needed, additional values can be added here

4.3.2 Calculation procedure for the B-WIM analysis

The imported parameters are extracted from the database to calculate the moments. Also, the time for each vehicle to cross the bridge (t_r) is computed. For the moments to be captured correctly and for all axles of each vehicle to contribute to the moments, the vehicle length is included in the computation of crossing time. This also ensures that the effect of multi-axle vehicles is captured realistically. Therefore, the crossing time is determined with equation (25),

$$t_r = \frac{L_{span} + L_{vehicle}}{v} \tag{25}$$

Where L_{span} is the span length of the bridge, $L_{vehicle}$ is the length of the vehicle, and v is the vehicle speed.

As time-dependent bending moment is computed, the implementation of a time step is necessary, where each axle position is calculated at each time step. To capture a detailed moment history, the simulation should progress in small increments, hence the time step should be small. In this thesis, the time step is set to 0,01. This means that the axle positions are updated, and the bending moment is recalculated every 0,01 seconds. With a small time step, the real movement of the vehicles is captured correctly. Additionally, a smaller time step provides a smoother and more continuous bending moment curve as sudden changes in the curve due to axles leaving the bridge are minimised. This is important for the rainflow calculation as the stress curve and stress ranges are the direct product of the moment history. This leads to a smoother stress history, creating a more precise identification of stress ranges. During each time step, the moment is calculated by multiplying the axle force present on the influence line with the influence line value itself. Therefore, the bending moment at a specific time step is obtained with equation (26),

$$M(t) = \sum_{axles} F_{axle} \cdot IL_{value} \tag{26}$$

Where F_{axle} is the axle force, and IL_{value} is the influence line value.

As mentioned earlier, the moment-time history is converted into a stress-time history. This is done by dividing the moment with the structure's elastic section modulus. However, as the unit of stress is presented as Pa or MPa, either bending moment (kNm) or elastic section modulus (m^3) needs to be converted. Therefore, stress at a given time step can be expressed with equation (27),

$$\sigma(t) = \frac{M(t)}{W} \cdot 10^{-3} \tag{27}$$

Where M(t) is the moment at a specific time step, and W is the elastic section modulus.

The stress ranges needed for cumulative damage computation are then obtained with cycle counting. MATLAB provides a default rainflow cycle counting function which is utilised in this analysis. This in-built function returns the cycle counts for the stress-time history according to the ASTM E 1049 standard (American Society for Testing and Materials). Rainflow counting was explained in more detail in Chapter 2.3.1. MATLAB provides a histogram of the stress ranges and their cycles, which is later used in the fatigue assessment. When the stress ranges and their cycle counts have been extracted, the fatigue analysis itself can be performed. In this thesis, the cumulative fatigue analysis is performed according to Miner's LDR, which was discussed in more detail in Chapter 3.2.

For simplification, the stress ranges for a given bin in the histogram are the mean stress of that bin. This means that the code assumes that all cycles in a bin have the same average stress range. As the bin widths are relatively low, the accuracy of the cumulative damage analysis is not affected. When the stress range is determined, the code computes the allowable number of cycles N_i based on the material limits. The stress range $\Delta\sigma_{(i)}$ for a bin can be expressed as:

$$\Delta\sigma_{(i,WIM)} = \frac{edges_{(i)} + edges_{(i+1)}}{2} \tag{28}$$

where $edges_{(i)}$ and $edges_{(i+1)}$ are the stress values at the i:th and (i+1):th of the bin edges, respectively.

To make the computation faster, an iterative loop is created for the determination of the required elastic section modulus. The code starts the computation with an initial W (0,01), which increases gradually in small steps (W_{step} = 0,0001). This can be done because fatigue damage decreases when the elastic section modulus increases. For each increment of W, the code performs the moment calculation and converts the moments into stresses. After stresses are obtained, the code performs the rainflow counting procedure and, finally, the cumulative fatigue calculation. The loop ends when the cumulative fatigue damage gets below its threshold value (D=1). As the analysis is done for 100 years and the B-WIM dataset includes vehicle data for a one-week period, the final damage needs to be scaled. Hence, the damage is multiplied by 5200 to represent 100 years. Therefore, the final damage is expressed as:

$$D_{WIM} = \sum \frac{n_i}{N_i} \cdot 5200 \tag{29}$$

4.3.3 Results from the B-WIM analysis

As has been explained earlier, in 2013 the vehicle regulations changed and thus allowed heavier vehicles on the Finnish road network. As the first year is so close to 2013, it can be considered as a transition phase compared to the latter year. Moments obtained from the 2016 database are clearly higher compared to the 2014 database, which leads to higher stresses and stress ranges. Furthermore, the moment-time curve for the 2016 database shows a longer crossing time for the entire database, showing the increase in the number of vehicles from 2014 to 2016. As an example illustration, moment-time curves obtained for IL_4 with a 40m span length for both 2014 and 2016 databases are shown in Figure 29. The corresponding stress-time curves obtained for the years 2014 and 2016 are presented in Figure 30. The stress-time curves are obtained by applying the correct elastic section modulus representing a design life of 100 years.

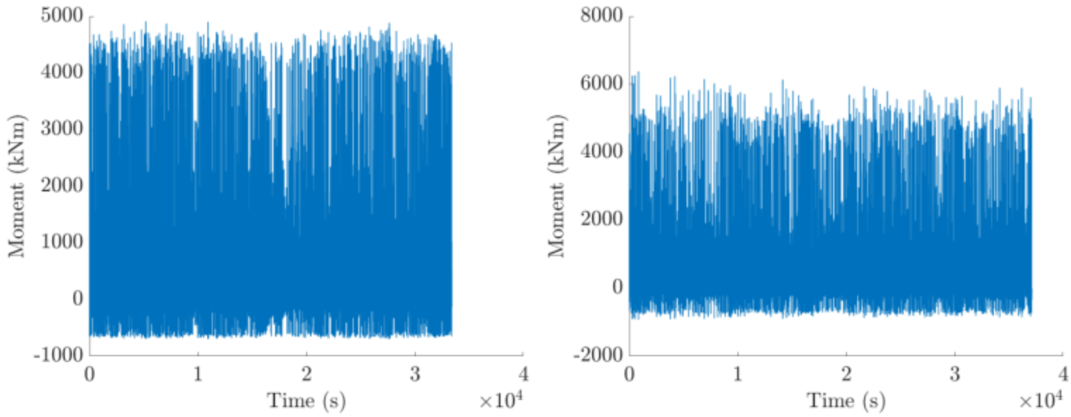

a) *b)*

Figure 29. Moment-time curve for IL_4 (40m). a) 2014, b) 2016.

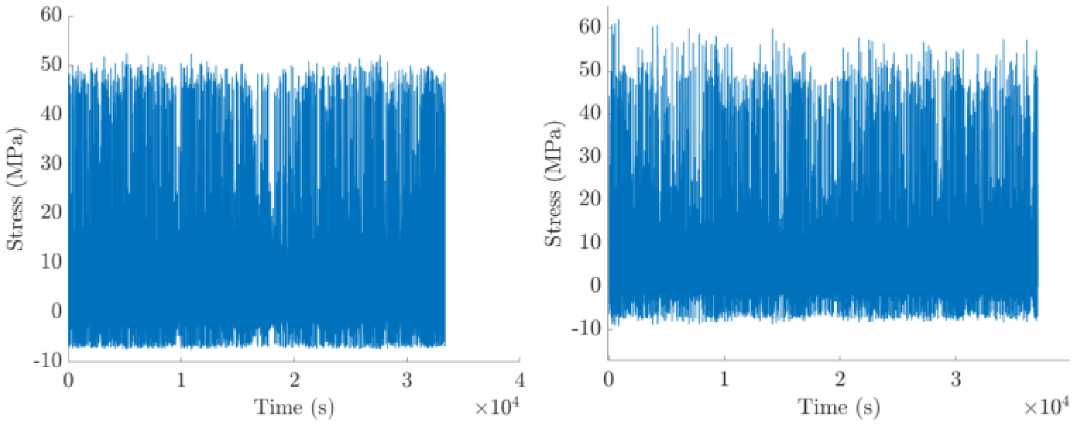

a) *b)*

Figure 30. Stress-time curve for IL_4 (40m). a) 2014, b) 2016.

Figure 31 shows the stress ranges and their corresponding cycles, with the accumulated damage for each stress range obtained for IL_4 with a 40m span length. These results are presented to show the distribution of stress ranges and how the damage accumulates. The left vertical axis in Figure 31 shows the number of cycles for each stress range, the horizontal axis shows the stress ranges in the form of bins, whereas the right vertical axis shows how the damage accumulates for each stress range. The bins are obtained with the rainflow cycle counting method and each bin represents a certain stress range. As mentioned earlier, the latter year is subjected to higher stress ranges and more cycles. This is due to the heavier and larger number of vehicles observed in 2016. As expected, the stress ranges are primarily concentrated in the lower ranges for both years. Additionally, the latter year appears to be influenced by more cycles for stress ranges under 10MPa. However, the contribution to the fatigue damage for these stress ranges is almost insignificant due to the implemented endurance limit. The endurance limit $\Delta\sigma_L$=2,6MPa is obtained from the chosen fatigue strength of $\Delta\sigma_C$=66MPa. The damage accumulation is relatively slow for both years, up to 50MPa. The constant amplitude fatigue limit obtained from the chosen fatigue strength is $\Delta\sigma_D$=48,6MPa. This means that for stress ranges lower than that, the total number of cycles is calculated with equation (7). Whereas for stress ranges over 48,6MPa, N_i is obtained according to equation (8). Hence, the fatigue damage accumulates faster for higher stress ranges. The damage accumulation appears to be more rapid for the year 2014 compared to 2016. This is due to a higher concentration of high stress ranges at 50-60MPa.

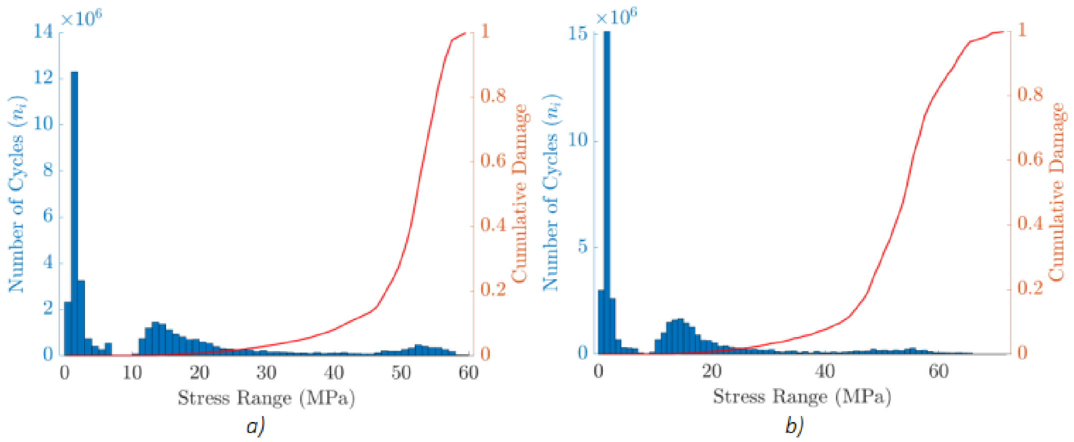

Figure 31. Stress range and cumulative damage histogram for IL_4 (40m) (Bin width=1MPa). a) 2014, b) 2016.

Table 7 shows the required $W_{,el}$ obtained for the 2014 database, and Table 8 shows the required $W_{,el}$ obtained for the 2016 database. The values are presented in m^3. The calculated values for the required $W_{,el}$ saw an 8-11% increase from the year 2014 to 2016, depending on the span length and influence line. This was expected due to the increase in GVW and number of vehicles during the same years. Furthermore, the corresponding damage is

D=1 for each $W_{,el}$. The higher $W_{,el}$ required for the latter year indicates that the 2016 traffic induces higher stress levels and, therefore, is more unfavourable in terms of fatigue compared to the 2014 traffic. Furthermore, the elastic section modulus obtained for 2014 would lead to a shorter fatigue life if used with the 2016 recorded traffic. For IL_4 with a span length of 40m, the accumulated damage with the 2016 traffic is D=1,35 when calculated with the $W_{,el}$=0.0937 obtained for the 2014 database.

Table 7. Required $W_{,el}$ for the 2014 B-WIM database for different span lengths and influence lines (unit: m^3).

2014	10m	20m	30m	40m	50m	60m	70m	80m
IL1	0.0092	0.0274	0.0531	0.0805	0.108	0.1355	0.163	0.1907
IL2	0.0089	0.0274	0.0534	0.081	0.1086	0.1364	0.164	0.1917
IL3	0.0072	0.017	0.026	0.038	0.0501	0.0621	0.0744	0.0866
IL4	0.0107	0.0344	0.0636	0.0937	0.124	0.1545	0.185	0.2156

Table 8. Required $W_{,el}$ for the 2016 B-WIM database for different span lengths and influence lines (unit: m^3).

2016	10m	20m	30m	40m	50m	60m	70m	80m
IL_1	0.0123	0.0362	0.0697	0.1057	0.1419	0.1781	0.2145	0.2507
IL_2	0.0118	0.0362	0.0701	0.1063	0.1428	0.1793	0.2157	0.2521
IL_3	0.0094	0.0224	0.0344	0.05	0.0658	0.0818	0.0978	0.1141
IL_4	0.0143	0.0452	0.0836	0.1232	0.1632	0.2033	0.2436	0.2839

The ratio between required $W_{,el}$ for the years 2016 and 2014 is also illustrated in Figure 32, where the vertical axis shows the ratio between the required elastic section modulus for the years 2016 and 2014, and the horizontal axis shows the span lengths. The ratios for each span length are obtained with equation (18). Similarly to the values presented in the tables above, the difference remains consistent along all influence lines and span lengths. As can be observed from the graph, the increase in vehicle weight has a similar effect on the required $W_{,el}$, regardless of the influence line or span length.

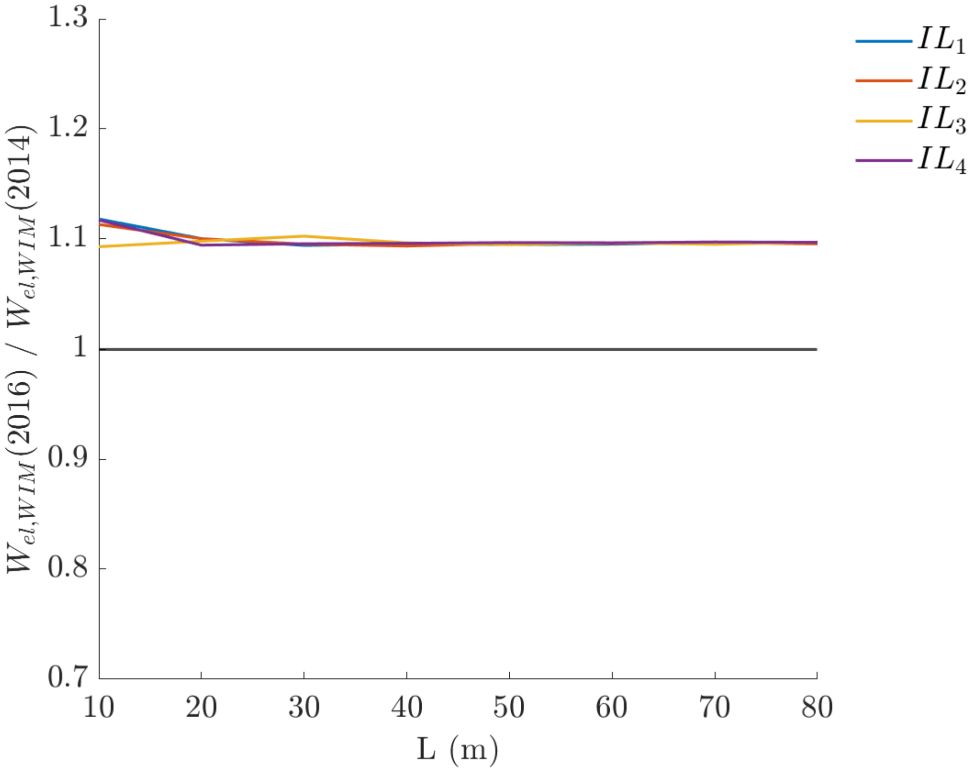

Figure 32. The ratio of the required $W_{,el}$ between the 2014 B-WIM database and the 2016 B-WIM database.

4.4 Fatigue Load Model 4 analysis setting

For the fatigue assessment of FLM4, SFS-EN 1991-2 provides a set of equivalent lorries, including five different vehicles. Three different traffic types and four yearly traffic flows (N_{obs}) are also provided. The traffic types give different percentages for each of the five lorries used with FLM4. FLM4 was discussed in more detail in Chapter 3.1. The focus will be on medium traffic type as both Qvisen (2020) and Hirvonen (2022) classified the traffic measured in Kaarina as medium-distance traffic. However, all traffic types will be calculated, and the results will be presented. The yearly traffic volume $N_{obs}=0{,}5\cdot10^6$ is used in this analysis. This traffic volume represents the closest to the theoretical yearly traffic volume of the 2016 B-WIM data, as NCCI1 specifies that $N_{obs}=0{,}5\cdot10^6$ shall be used when daily traffic per direction is between 200 and 1200 vehicles. For the 2016 recorded traffic, the daily traffic volume is 266 vehicles per direction. Additionally, while the B-WIM flow rate is between the $0{,}125\cdot10^6$ and $0{,}5\cdot10^6$ N_{obs} provided in Eurocodes, the latter is more unfavourable and therefore used. As either Eurocode or the Finnish National Annex provides any information about the velocities of the vehicles, the speed is determined according to B-WIM data. That is, the average vehicle speed of all vehicles in the 2016 B-WIM database is used in the simulation. Therefore, the speed of the set of equivalent lorries is set to 15,5 m/s.

4.4.1 Fatigue Load Model 4 calculation procedure

The construction of the code for the analysis of FLM4 is like that for the B-WIM analysis. Hence, Miner's LDR and the same time step are utilised in the analysis. However, small changes are made due to differences in output data. B-WIM databases usually include thousands of vehicles with different parameters for a shorter time, like for one week or one month. However, the vehicle information provided in SFS-EN 1991-2 includes only five different vehicles. Additionally, the traffic volumes given in Eurocodes are for a one-year period. This means that the modification made compared to the first code includes the change of the scaling factor. As the fatigue analysis is performed for a one-year period due to the traffic flow provided in Eurocodes, the final damage is multiplied by 100 to represent a 100-year fatigue analysis.

Furthermore, rainflow counting is performed for bending moment instead of stress, as the low number of vehicles causes small variations in stress curves and, therefore, can oversimplify the fatigue analysis. As moments are larger than stresses, the moment curves provide a larger variety for a small set of vehicles. While the moment curve provides a greater variation, the in-built rainflow function returns to large ranges. Therefore, the bin width of each bin will be manually decided. Hence, the bin width is set to 1. The moment calculation follows the same principle as the analysis of B-WIM data. This means that the stress ranges are converted from the cycles and ranges returned from the bending moment diagram. Therefore, the i:th stress range in the analysis of FLM4 is obtained with equations (30) and (31),

$$\Delta M_{(i)} = \frac{edges_{(i)} + edges_{(i+1)}}{2} \tag{30}$$

$$\Delta\sigma_{(i,FLM4)} = \frac{\Delta M_{(i)}}{W} \cdot 10^{-3} \tag{31}$$

Where the rainflow has been applied to the moment calculation and therefore, equation (30) computes the moment ranges, with $edges_{(i)}$ and $edges_{(i+1)}$ being the moment values of i:th and (i+1):th bin edge, respectively. The stress range for each bin is then obtained with equation (31), where "moment range" values are converted into stress ranges.

As each vehicle is considered to cross the influence line in the absence of other vehicles, the code performs the moment calculation separately for each vehicle. This is stated in SFS-EN 1991-2 (4.6.5). The same principle was followed in the analysis of B-WIM data. The percentages provided for the traffic types and the flow rate (N_{obs}) are multiplied by the damage of their representative vehicle, creating the total damage of each vehicle. The combined damage is then obtained by summing the total damage of each vehicle. Hence, the fatigue damage caused by the vehicles is obtained with equation (32),

$$D_{FLM4} = D_{V1} \cdot N_{obs} \cdot L_{P1} + \ldots + D_{V5} \cdot N_{obs} \cdot L_{P5} \tag{32}$$

Where D_{V1} is the damage of the first vehicle, N_{obs} is the traffic volume, and L_{P1} is the lorry percentage of the first vehicle obtained from Table 5.

Finally, an inductive loop calculates the elastic section modulus needed for the fatigue damage representing 100 years to be D=1. As the N_{obs} given in SFS-EN 1991-2 represent a traffic volume of one year, the combined damage obtained from the equivalent vehicles is multiplied by a scaling factor of 100. Hence, the final damage representing 100 years is obtained with equation (33),

$$D_{Final,FLM4} = D_{FLM4} \cdot 100 \tag{33}$$

4.4.2 Results from Fatigue Load Model 4 analysis

Table 9 shows the required $W_{,el}$ obtained for local traffic type. Table 10 presents the required $W_{,el}$ obtained for medium distance traffic type, and Table 11 shows $W_{,el}$ obtained for long-distance traffic type. The difference between traffic types can clearly be observed from the obtained $W_{,el}$. The difference between local traffic type and medium distance type is notably larger than the difference between medium distance type and long-distance traffic type. The required $W_{,el}$ increases between 1-10% when applying long-distance type instead of medium distance type, depending on the span length and influence line. Meanwhile, the required $W_{,el}$ increases by 13-35% when applying the medium distance type instead of the local traffic type.

Table 9. Required $W_{,el}$ for FLM4 Local traffic for a corresponding fatigue damage of D=1 (unit: m^3).

FLM4	10m	20m	30m	40m	50m	60m	70m	80m
IL_1	0.0174	0.0453	0.0802	0.1155	0.148	0.173	0.2197	0.2514
IL_2	0.0158	0.0431	0.0744	0.1063	0.1383	0.1706	0.2028	0.235
IL_3	0.0117	0.0225	0.0375	0.0524	0.0672	0.0822	0.0971	0.1122
IL_4	0.0206	0.055	0.0924	0.1301	0.1681	0.2063	0.2444	0.2826

Table 10. Required $W_{,el}$ for FLM4 Medium distance for a corresponding fatigue damage of D=1 (unit: m^3).

FLM4	10m	20m	30m	40m	50m	60m	70m	80m
IL_1	0.0211	0.0574	0.1025	0.1477	0.1907	0.2326	0.2819	0.3243
IL_2	0.0179	0.0539	0.0945	0.1356	0.1769	0.2184	0.2598	0.3012
IL_3	0.0156	0.0288	0.0481	0.0671	0.0862	0.1054	0.1246	0.144
IL_4	0.0243	0.0696	0.1179	0.1665	0.2155	0.2646	0.3135	0.3627

Table 11. Required $W_{,el}$ for FLM4 Long distance for a corresponding fatigue damage of D=1 (unit: m^3).

FLM4	10m	20m	30m	40m	50m	60m	70m	80m
IL_1	0.0223	0.0627	0.1119	0.161	0.2093	0.2535	0.3079	0.356
IL_2	0.0182	0.0581	0.1027	0.1477	0.1929	0.2383	0.2836	0.329
IL_3	0.017	0.0313	0.0525	0.0732	0.0941	0.1151	0.1361	0.1574
IL_4	0.0255	0.0754	0.1284	0.1816	0.2352	0.289	0.3426	0.3964

The general trend between all traffic types (Long-distance, Medium distance, and Local traffic) has clear similarities, as shown in Figure 33. All traffic types are plotted on the same graph to illustrate the differences better. FLM4 gives conservative results for the required elastic section modulus for all traffic types and influence lines, especially for shorter span lengths. Whereas, for longer spans, the ratios between FLM4 and B-WIM stabilises. IL_1, IL_2, and IL_4 have a smoother and more consistent decrease compared to IL_3, which shows a more erratic pattern. The local traffic type becomes unsafe for longer span lengths, especially for IL_1 and IL_2. These results shows that the Kaarina traffic was classified correctly by Qvisen (2020) and Hirvonen (2022), as the medium distance traffic type gives overall best results.

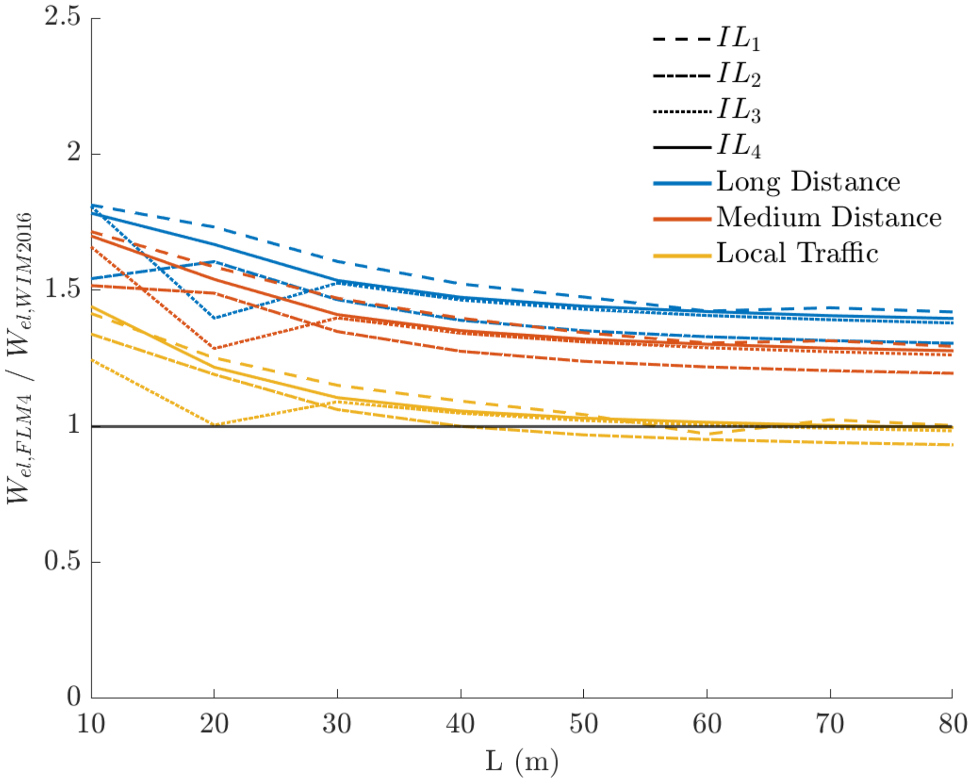

Figure 33. The ratio of the required $W_{,el}$ between FLM4 and the 2016 B-WIM database.

Maljaars (2020) obtained similar results in comparing the required elastic section modulus needed for FLM4 and WIM data. The WIM data was collected in three separate years at the A16 motorway in the Netherlands. Even there, FLM4 clearly overestimated the required elastic section modulus for shorter spans, and the ratio decreased when span length increased. Furthermore, based on the results from FLM4, the traffic in Kaarina differs clearly from the Auxerre traffic, from which the Fatigue Load Models were derived, as can be seen when compared to Figure 21.

4.4.3 Discussion

The very conservative results obtained from FLM4 calculations are mainly due to the high traffic volume of $0{,}5 \cdot 10^6$ lorries per year used in the analysis. However, FLM4 would underestimate the required $W_{,el}$ for longer span lengths if a lower traffic volume of $0{,}125 \cdot 10^6$ was used. This can be observed in Figure 34 a), where the ratio of the required $W_{,el}$ between FLM4 Medium distance traffic type and the B-WIM data for the year 2016 is plotted. Meanwhile, if a traffic volume that more closely represents the Kaarina traffic was used, the accuracy of FLM4 would improve substantially. Figure 34 b) shows the ratio of the required $W_{,el}$ between FLM4 medium distance traffic with a flow rate of $0{,}195 \cdot 10^6$ and the 2016 B-WIM data. Only IL_2 shows unsafe results when span length increases to above 60m. With a traffic volume close to the theoretical yearly traffic volume of the B-WIM data, FLM4 appears to be accurate for longer span lengths, with a slight overestimation for shorter spans. Hence, the equivalent fatigue vehicles provided in the Eurocodes appear to align well with the 2016 B-WIM database.

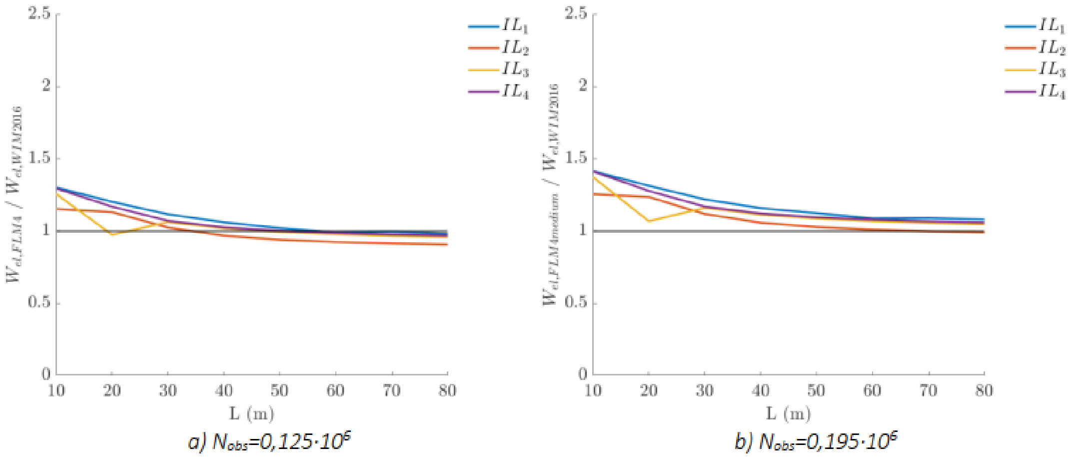

Figure 34. The ratio of the required $W_{,el}$ for FLM4 medium distance traffic and 2016 B-WIM data, with different yearly traffic volumes.

The overall overestimation of the required $W_{,el}$ for short span lengths can be explained by the difference between the equivalent vehicles and the vehicles in the B-WIM database. Longer vehicles with more axles can be found in the database compared to the equivalent fatigue vehicles. Additionally, the B-WIM database includes vehicles with higher GVW. However, the axle weights of the equivalent fatigue vehicles are generally higher than those with similar configurations found in the B-WIM database. This leads to higher required $W_{,el}$ for shorter span lengths, as seen from the above figures. The reason is that bridges with shorter span lengths are rarely sensitive to GVW but rather to axle and axle group weights (De Ceuster, et al., 2008). This is because vehicles with larger GVW usually exceed the span length. When the span length increases, so does the effect of GVW, which can be seen in the decrease in the ratio between the required $W_{,el}$ in the FLM4 and B-WIM database as the heavier vehicles in the database start to affect the results more.

Furthermore, Maddah (2013) concluded that for extremely short bridges where the span length approaches zero, each axle causes one cycle that is equal to the axle force. Meanwhile, for extremely long bridges where the span length approaches infinity, a cycle is caused by each vehicle where the cycle equals the GVW. Naturally, these are extreme cases as the span lengths approach zero and infinity. Nevertheless, they show how axle loads govern shorter span lengths and GVW longer span lengths.

The effect of axle and axle group weights on short span lengths is illustrated in Figure 35, where a) shows the moment-time curve for two vehicles on a simply supported bridge with a span length of 10m and b) with a span length of 50m. Vehicle parameters used in the example are presented in Table 12. Note that the parameters were obtained from the 2016 B-WIM database and, therefore, represent realistic vehicle configurations. Due to the higher axle loads relatively close to each other, vehicle 1 produces a larger maximum moment when the span length is 10m. Meanwhile, when the span length increases to 50m, the GVW and distribution of loads to a larger area create higher maximum moments, leading to vehicle 2 producing a higher maximum moment.

Table 12. Vehicle parameters for the example case.

Vehicle	GVW (kN)	Axle Loads (kN)	Axle Spacings (m)
1	310	80, 115, 115	4.6, 1.4
2	550	65, 70, 70, 70, 80, 100, 95	3, 1.2, 1.2, 4.5, 2.7, 2.4

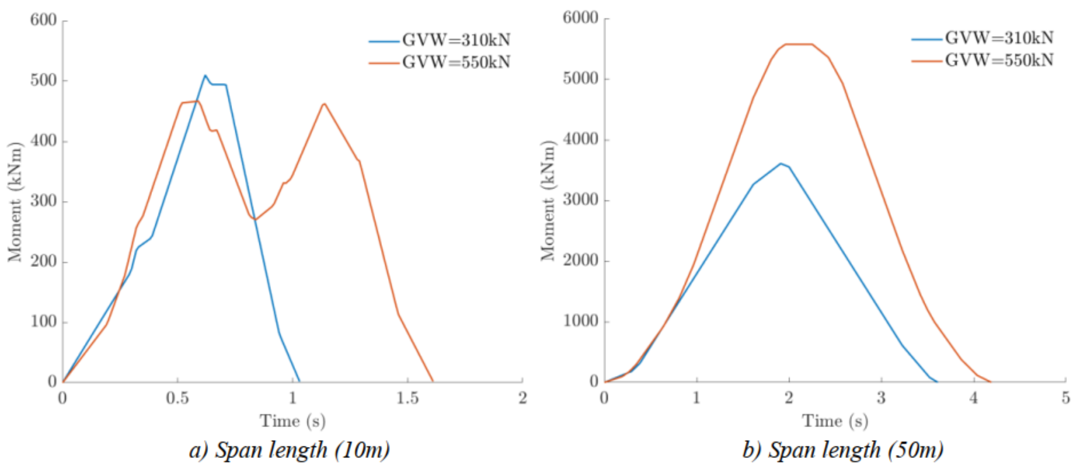

Figure 35. Moment-time curves for the example illustration.

4.5 Fatigue Load Model 3 analysis setting

The fatigue assessment of FLM3 follows the principle presented in SFS-EN 1991-2 and Chapter 3.3 in this thesis. However, due to different parameters provided in the Finnish NA compared to Eurocodes, the calculation will be done according to both codes, and the differences will be presented. FLM3 consists of a single fatigue vehicle with a GVW of 480kN and four sets of axles, each weighing 120kN.

Compared to the analysis of B-WIM data and FLM4, where the codes were almost identical, the code constructed for the analysis of FLM3 differs completely. This is because no cycle counting, or cumulative damage method is needed. However, the main principle is similar. That is, the required elastic section modulus is determined.

4.5.1 Sub-factor λ_2 in the Finnish National Annex

The Eurocode and Finnish National Annex give different guides for calculating the damage equivalent factor λ. The sub-factors λ_1, λ_3, and λ_4 remain similar in both design codes. However, the procedure for obtaining λ_2 differs. To obtain λ_2 according to SFS-EN 1993-2, see equations (14) and (15). NCCI4 Table 6.23 (presented in Table 13) provides ready-made values depending on the traffic type and traffic category. NCCI1 further specifies that λ_2 should be obtained by using medium distance if the span length is less than 40m and long distance if the span length is longer than 60m. If the span length is 40-60m, the λ_2 value shall be obtained with some form of interpolation.

Table 13. Values given for λ_2 in NCCI. (Modified from NCCI4 Table 6.23)

λ_2	Traffic Type		
Traffic Category	Long Distance	Medium Distance	Local Traffic
1	1,22	1,12	0,87
2	0,93	0,85	0,66
3	0,70	0,64	0,50
4	0,59	0,54	0,42

The values for the sub-factor λ_2 presented in the NCCI codes were calibrated using traffic data measured in Finland. These calibrations were made for tables 4.5 and 4.7 presented in SFS-EN 1991-2 to maintain the wanted safety level, as these tables underestimated the vehicle weights and overestimated the traffic volumes. The traffic measurements were conducted with an automatic traffic count system developed by the Finnish Road Administration (now named Finnish Transport Infrastructure Agency), with 473 automatic counting stations measuring the traffic. The goal was to find limit values between different traffic categories and to define the flow rates for each value. The vehicle data used in the calibration was recorded in the year 2007. (Chatzis & Lilja, 2012)

4.5.2 Fatigue Load Model 3 calculation procedure

The code itself computes the moments caused by the single fatigue vehicle when it crosses the influence lines, after which the moments are converted into stresses. The same vehicle speed is assumed as in FLM4, ensuring consistency with both calculations. The code extracts the maximum and minimum stresses from the resulting stress-time curve and calculates the stress ranges produced by the fatigue vehicle. The sub-factors required for calculating the damage equivalent factor (λ) are defined according to span length. The damage equivalent factor is then compared against the allowable maximum value λ_{max}. If the damage equivalent factor exceeds λ_{max}, the code issues an error message, highlighting the need for adjustments in the parameters. The damage equivalent factor is calculated separately for the midspan and support section, after which the code implements the correct λ according to the influence line. The code compares the damage equivalent stress range $\Delta\sigma_{E2}$ with the detail category $\Delta\sigma_C$ according to equation (11). The damage equivalent impact factor in equation (12) is $\phi_2=1$, as specified in SFS-EN 1993-2. An iterative loop determines the required $W_{,el}$ by calculating the ratio between the equivalent stress range and the detail category. $W_{,el}$ is obtained when the ratio drops to under one.

Table 14. Calculated values for different sub-factors according to the NCCI codes. λ_1 values are shown for midspan / support section.

Sub factors	10m	20m	30m	40m	50m	60m	70m	80m
λ_1	2.55 / 2.0	2.45 / 1.85	2.35 / 1.7	2.25 / 1.8	2.15 / 1.9	2.05 / 2.0	1.95 / 2.1	1.85 / 2.2
λ_2	0.85	0.85	0.85	0.87	0.89	0.91	0.93	0.93
λ_3	1	1	1	1	1	1	1	1
λ_4	1	1	1	1	1	1	1	1

The sub-factors obtained for the calculation of the damage equivalent factor according to NCCI codes are presented in Table 14 above. Sub-factors λ_1 and λ_2 are both dependent on the span length while $\lambda_3=\lambda_4=1$ due to the use of a 100-year design life and as no other lanes are considered. For the calculation of λ_2 according to NCCI, see Chapter 4.5.1.

Sub-factor λ_2 for the calculation according to Eurocode gives the same value for all span lengths, and the value obtained according to equation (14) is $\lambda_2=0{,}8277$. As recorded traffic can be utilised when calculating λ_2, the average GVW (Q_{m1}) and the number of heavy vehicles (N_{obs}) are determined with the recorded 2016 Kaarina traffic. The obtained values for these parameters are 480,12kN and 193960, respectively. The high average GVW clearly inflates λ_2 as Q_{m1} is almost identical to the GVW of the fatigue vehicle, by which it is divided.

4.5.3 Results from Fatigue Load Model 3 analysis

The required $W_{,el}$ for all span lengths and influence lines representing a 100-year design life are presented in Table 15. These values are calculated according to the NCCI codes. Hence, for the calculation of sub-factor λ_2, NCCI1 and NCCI4 were followed.

Table 15. Required $W_{,el}$ for FLM3 calculated according to NCCI codes. The values correspond to a design life of 100 years (unit: m^3).

FLM3 NCCI	10m	20m	30m	40m	50m	60m	70m	80m
IL_1	0.0235	0.0655	0.1118	0.1576	0.2011	0.2418	0.2796	0.3075
IL_2	0.0238	0.0682	0.1148	0.1608	0.2043	0.2451	0.283	0.3109
IL_3	0.0155	0.0254	0.0383	0.057	0.078	0.1015	0.1276	0.1532
IL_4	0.0278	0.0791	0.1286	0.1783	0.2256	0.2701	0.3113	0.3417

The ratio between $W_{,el}$ designed with FLM3 according to NCCI codes, and $W_{,el}$ required for the 2016 B-WIM database is shown in Figure 36. Overall, FLM3 gives very conservative results. However, the ratio decreases for influence lines IL_1, IL_2, and IL_4 when span length increases. This resembles the results obtained for FLM4. However, unlike FLM4, FLM3 overestimates the required $W_{,el}$ more. The results for IL_3 are less conservative but fluctuate more than IL_1, IL_2, and Il_4. This is due to the different equations used to calculate sub-factor λ_1, as IL_3 concerns the bending moment at the support. Additionally, between influence lines, the difference for the required $W_{,el}$ is larger for shorter spans, whereas when span length increases, the difference decreases. Additionally, the scatter between the moment influence lines for the midspan section is smaller than that of FLM4.

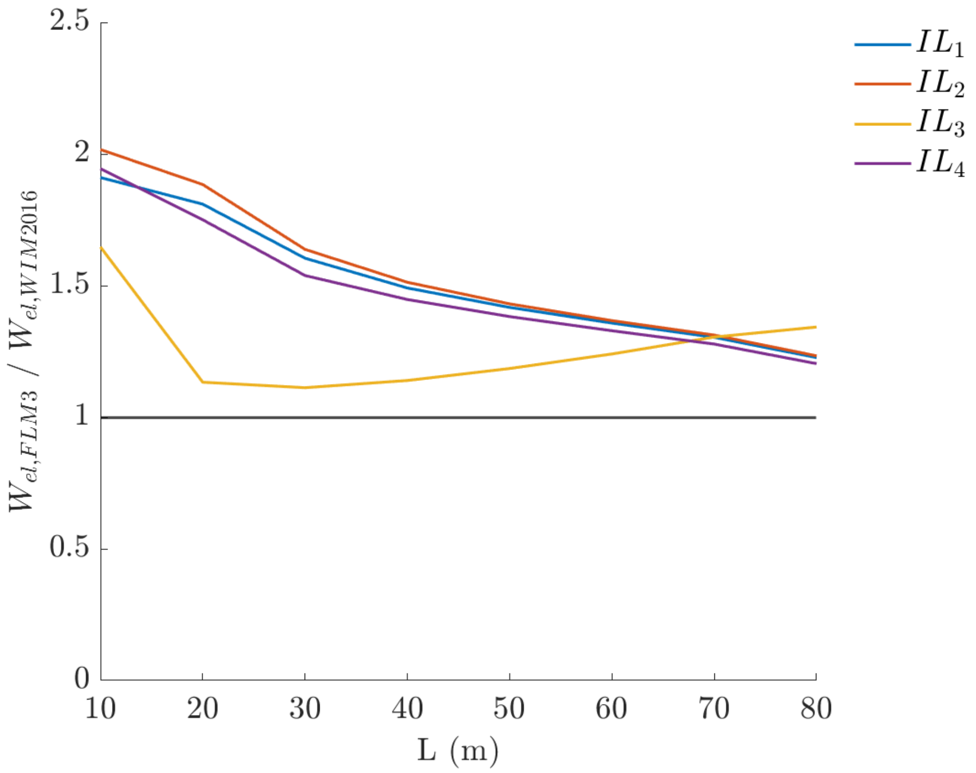

Figure 36. The ratio of the required $W_{,el}$ between FLM3 (NCCI) and the 2016 B-WIM database.

The ratio between $W_{,el}$ for FLM3 according to Eurocode and the 2016 B-WIM database is illustrated in Figure 37. Furthermore, the $W_{,el}$ that corresponds to a design life of 100 years are presented in Table 16. The results show clear similarities to those obtained according to the NCCI codes. However, the results are slightly less conservative, although the slopes for IL_1, IL_2, and IL_4 are steeper. This means that the ratio decreases more rapidly. Ratios for IL_3 show more consistent results for span lengths 20-80m while still showing very conservative results for shorter span lengths.

Table 16. Required $W_{,el}$ for FLM3 calculated according to Eurocodes. The values correspond to a design life of 100 years (unit: m^3).

FLM3 SFS-EN	10m	20m	30m	40m	50m	60m	70m	80m
IL_1	0.0228	0.0638	0.1089	0.15	0.187	0.22	0.2488	0.2737
IL_2	0.0232	0.0664	0.1118	0.153	0.19	0.2229	0.2519	0.2767
IL_3	0.0151	0.0247	0.0373	0.0542	0.0725	0.0923	0.1135	0.1364
IL_4	0.0271	0.077	0.1253	0.1697	0.2098	0.2456	0.2771	0.3041

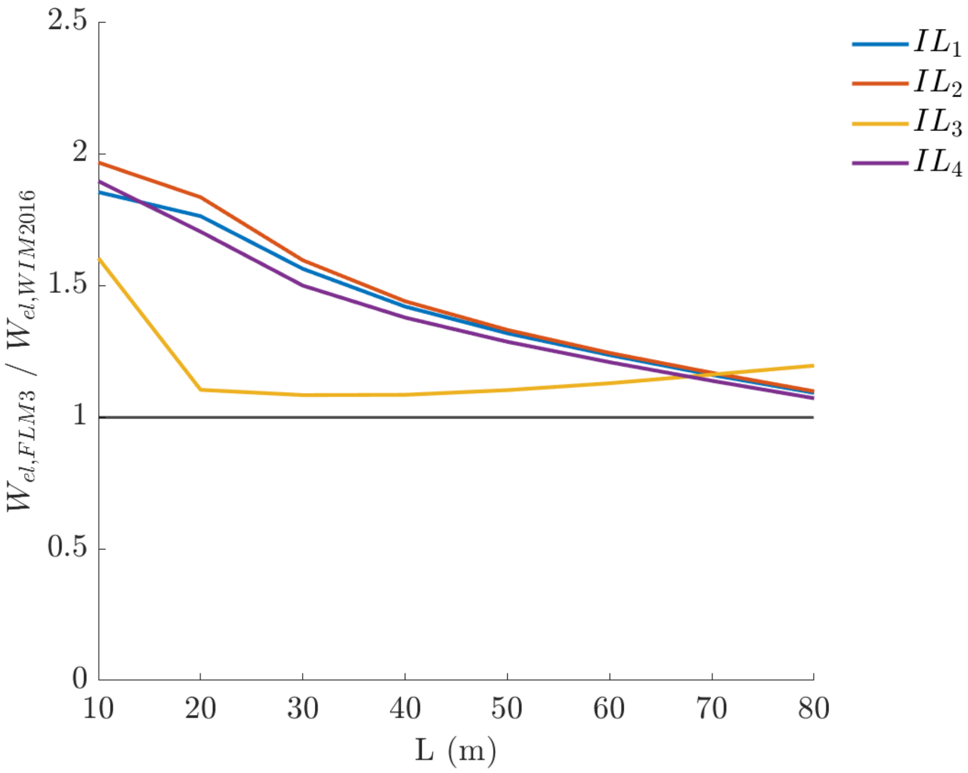

Figure 37. The ratio of the required $W_{,el}$ between FLM3 (Eurocode) and the 2016 B-WIM database.

4.5.4 Discussion

The small difference between the results obtained with Eurocode and the NCCI codes is due to almost similar λ_2 values. For span lengths of 30m or shorter, the difference is only slightly above 0,02. The difference increases with the span length. For span lengths of 70m and 80m, the difference increases to 0,1. This means that NCCI codes provide safer values for longer span lengths, while both methods still being conservative. While λ_2 in NCCI codes was calibrated by using Finnish traffic recorded in 2007, the results show a good safety level when compared to today's traffic. The calculation of sub-factor λ_1 also leads to very conservative results. This is due to its unrealistic capture of the span length influence (Maljaars, 2020). The difference in the damage equivalent factor λ between Eurocodes and NCCI codes is illustrated below, where Figure 38 a) shows λ obtained for the midspan section and b) for the support section.

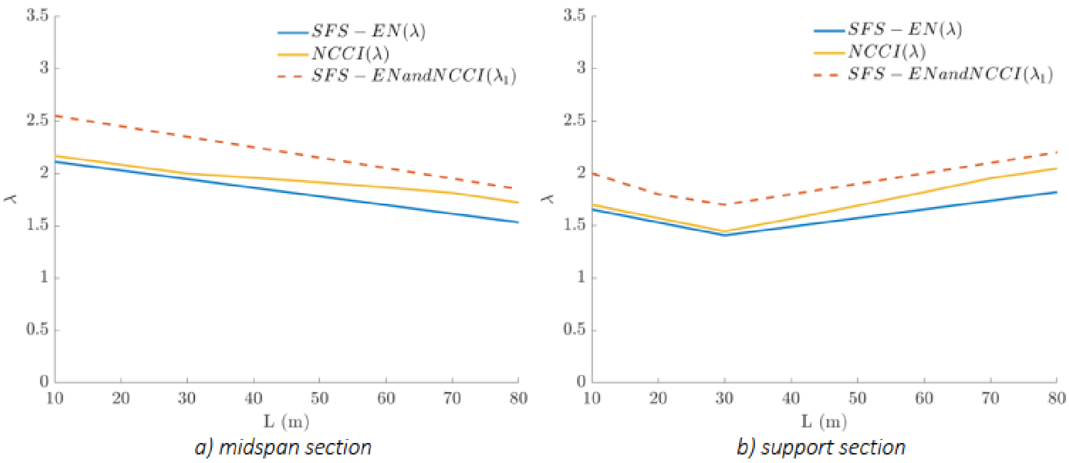

Figure 38. Illustration of λ for midspan and support section.

5 New Fatigue Load Model

As explained earlier, one of the goals of this thesis is to calibrate a new Fatigue Load Model that represents real traffic. From the above chapters, it can be concluded that the existing Load Models presented in the Eurocodes overestimate the required elastic section modulus. This means that a new FLM that represents real traffic can be calibrated. The new FLM is calibrated from the 2016 B-WIM data, as it closer represents today's traffic. The calibration of the new FLM and fatigue vehicle follows the principle introduced by Maljaars (2020). This means that the method and simplifications used in the calibration process are based on his work. The following simplifications and boundary conditions are considered for the calibration of the new fatigue vehicle.

- no influence lines will be considered,
- the stress ranges of each vehicle are assumed to be proportional to the vehicle weight, axle weight, or group axle weight under consideration,
- the calibration is done for a design life of 100 years,
- the calibration is done for a ratio of R=1.

The calibrated fatigue vehicle is illustrated in Figure 39. This fatigue vehicle is used with the calibrated FLM.

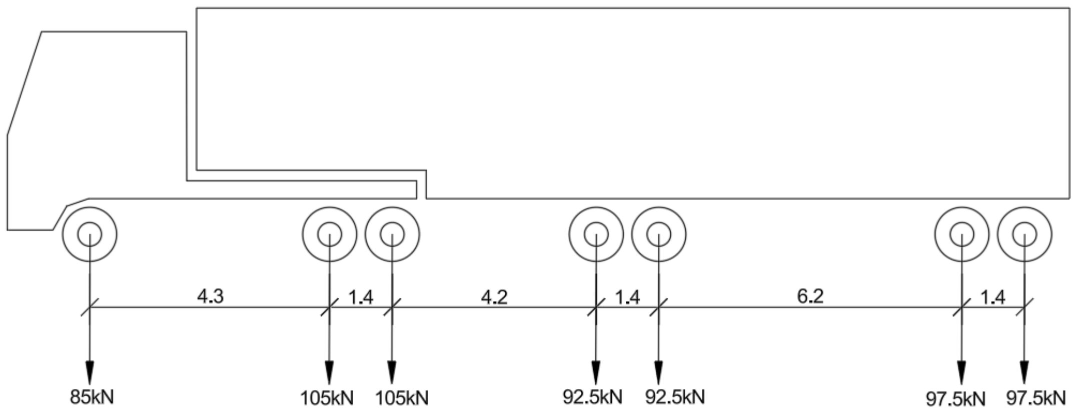

Figure 39. Illustration of the calibrated fatigue vehicle.

5.1 Calibration of the new fatigue vehicle

The calibration of the new fatigue vehicle is a multi-step process. The most unfavourable GVW, axle weights and vehicle configuration from the 2016 B-WIM database must be determined. This means that the different parameters should either be most frequently found in the database or contribute most to the damage, to be considered as most unfavourable. To simplify the process, vehicles are divided into vehicle types according to the number of axles. As the axle count ranges from 2-11 between the vehicles, a total of 11 different vehicle types were recorded during the 2016 measurement campaign. From these, vehicles with two or three axles appeared to be most frequently observed in the database, with 30% of all vehicles having two axles and 22% having three axles. However, the total load of 7-axle vehicles was the highest, contributing to 25% of the total load. Figure 40 shows the frequency of vehicle types and their total loads, where the columns illustrate the frequencies, and the plotted line shows the total loads. Similarly, the left vertical axis shows the number of different vehicle types, and the right vertical axis presents the total loads.

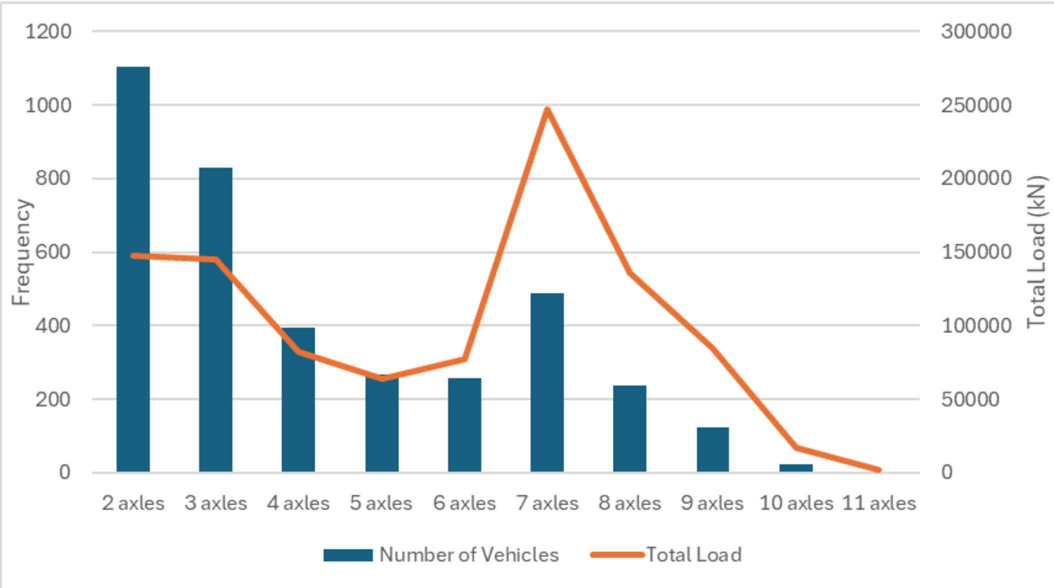

Figure 40. Frequency of vehicle types and their total loads.

The contribution to fatigue damage of all vehicle types is inspected to determine the optimal number of axles for the new fatigue vehicle. The calculation method is similar to the fatigue assessment performed for the B-WIM database explained in Chapter 4.3.2. However, after the total damage has been calculated, the code examines how much each vehicle type contributes to the total fatigue damage. As Figure 41, Figure 42, Figure 43, and Figure 44 shows, vehicles with seven axles contribute most to the damage. This is expected, as the total load of 7-axle vehicles is highest. Furthermore, the contribution to the total fatigue damage of vehicles with a higher axle count is overall greater. This is due to the large GVW of these vehicles. The contribution to the damage decreases for vehicles with five axles or less when the span length increases. This is due to the axle weights contributing less to the overall damage when span length increases, as explained in Chapter 4.4.3.

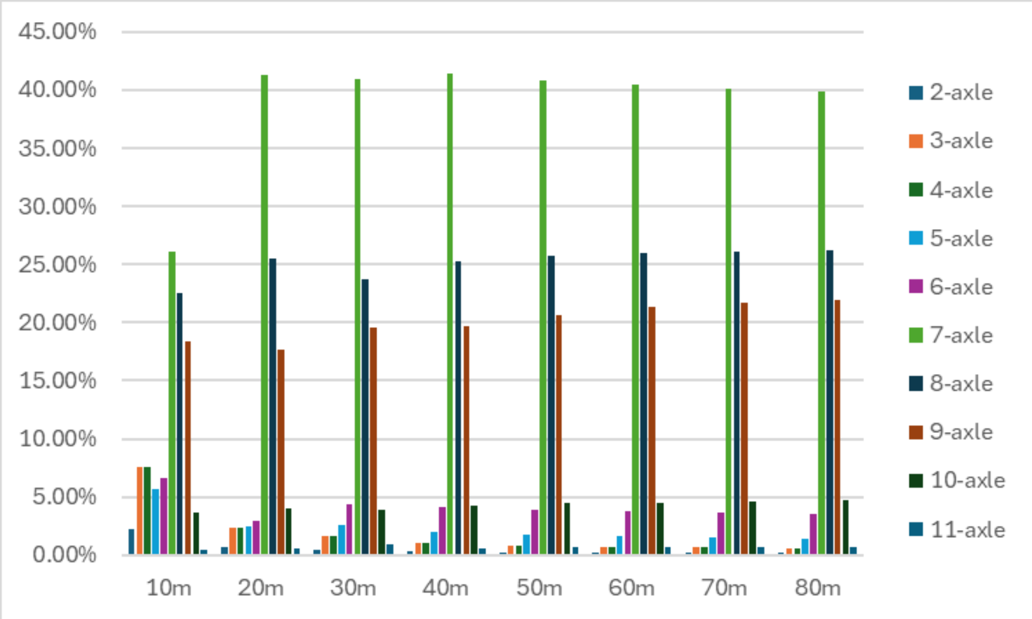

Figure 41. Contribution to fatigue damage of different vehicle types (IL_1).

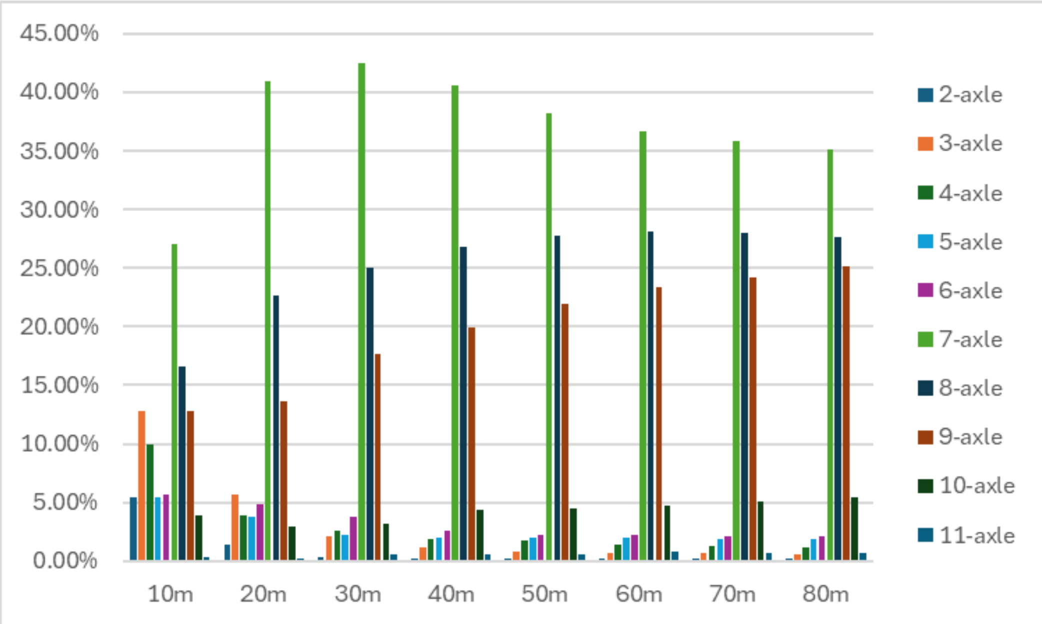

Figure 42. Contribution to fatigue damage of different vehicle types (IL_2).

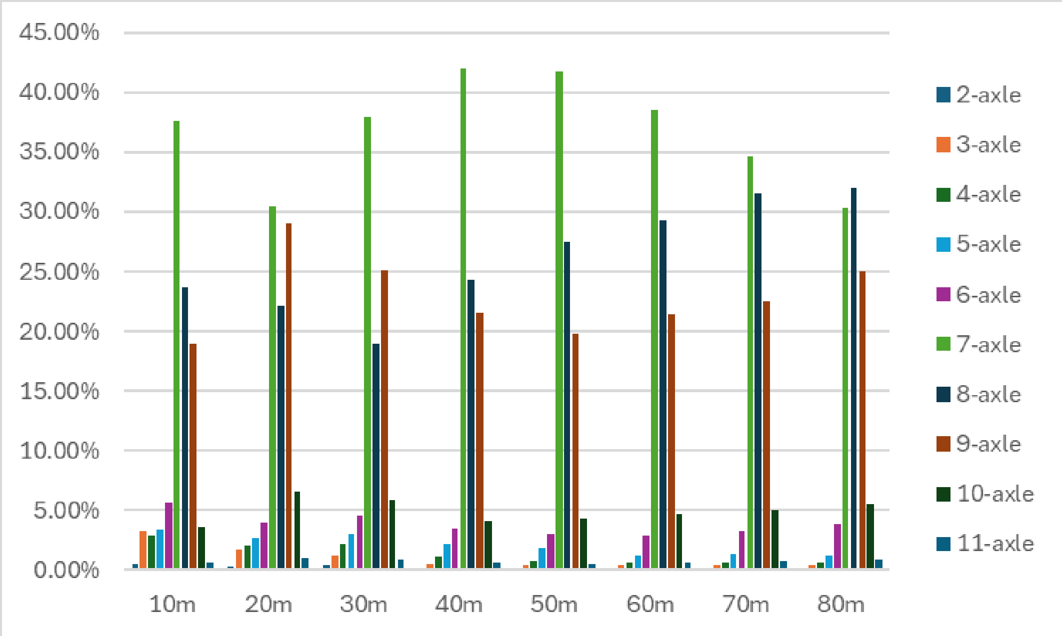

Figure 43. Contribution to fatigue damage of different vehicle types (IL_3).

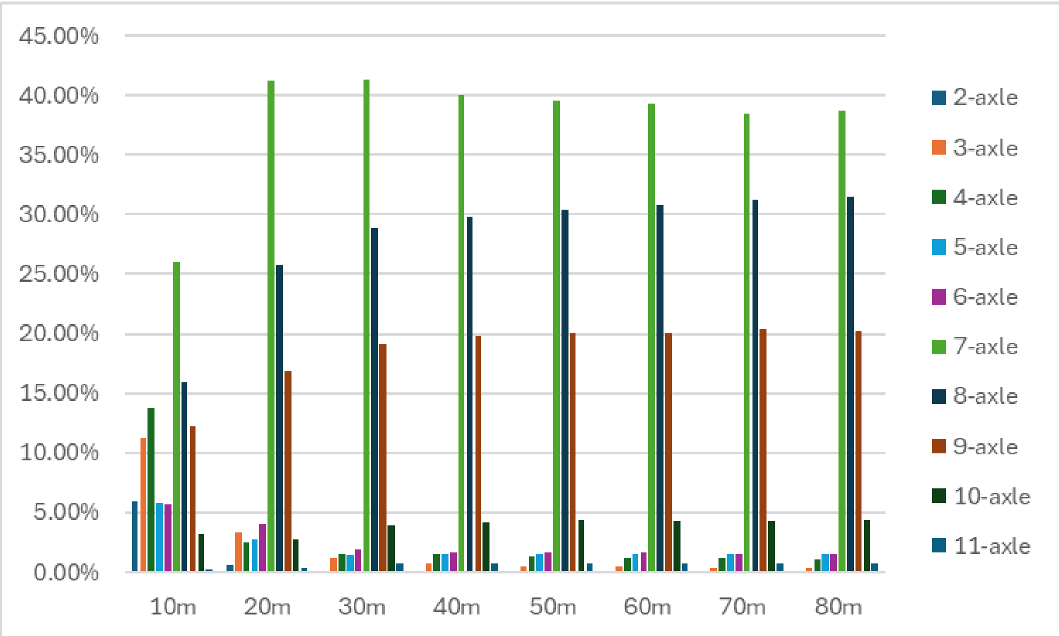

Figure 44. Contribution to fatigue damage of different vehicle types (IL_4).

To find the most unfavourable GVW, the damage contributions of all gross vehicle weights in the 2016 B-WIM database are inspected. This is done by assuming that the stress range is proportional to the GVW. Hence, no influence lines are used. As Figure 45 shows a GVW of 675kN contributes most to the damage. This is illustrated with a blue line showing the frequency of the weights and a red line showing how much each weight contributes to the damage. The horizontal axis shows the GVW, the left vertical axis represents the frequency of GVW, and the right vertical axis the damage contribution. This GVW of 675kN will be used as the weight of the new fatigue vehicle. Additionally, the calibrated weight aligns with the 7-axle vehicles found in the 2016 recorded traffic, as the database includes vehicles with seven axles with a similar GVW.

To further investigate how the regulation changes implemented in 2013 has affected, the GVW that contributes most to the damage from the 2014 database is found and compared to the calibrated weight of the new fatigue vehicle. The largest GVW in the 2014 database is 657kN, which means that the weight of the new fatigue vehicle obtained from the 2016 database exceeds the heaviest vehicle recorded in 2014. Hence, the GVW that contributes most to the damage from the 2014 database will be lower than that for 2016. Figure 46 show the frequencies and damage contributions for each GVW from the 2014 database. A GVW of 605kN contributes most to the damage from the 2014 recorded traffic. This is 70kN lower than the GVW obtained from the 2016 database. A lower GVW would lead to lower axle weights and the underestimation of today's traffic.

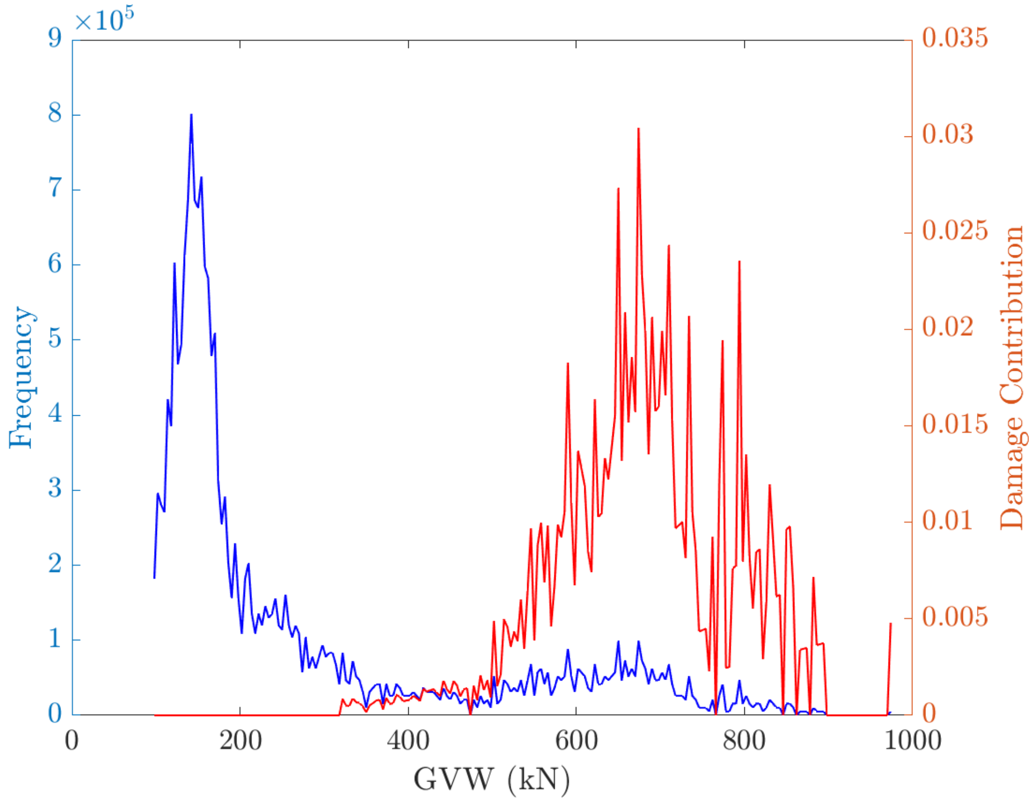

Figure 45. Fatigue damage contributions of the GVW in the 2016 B-WIM database. (Bin width=5kN).

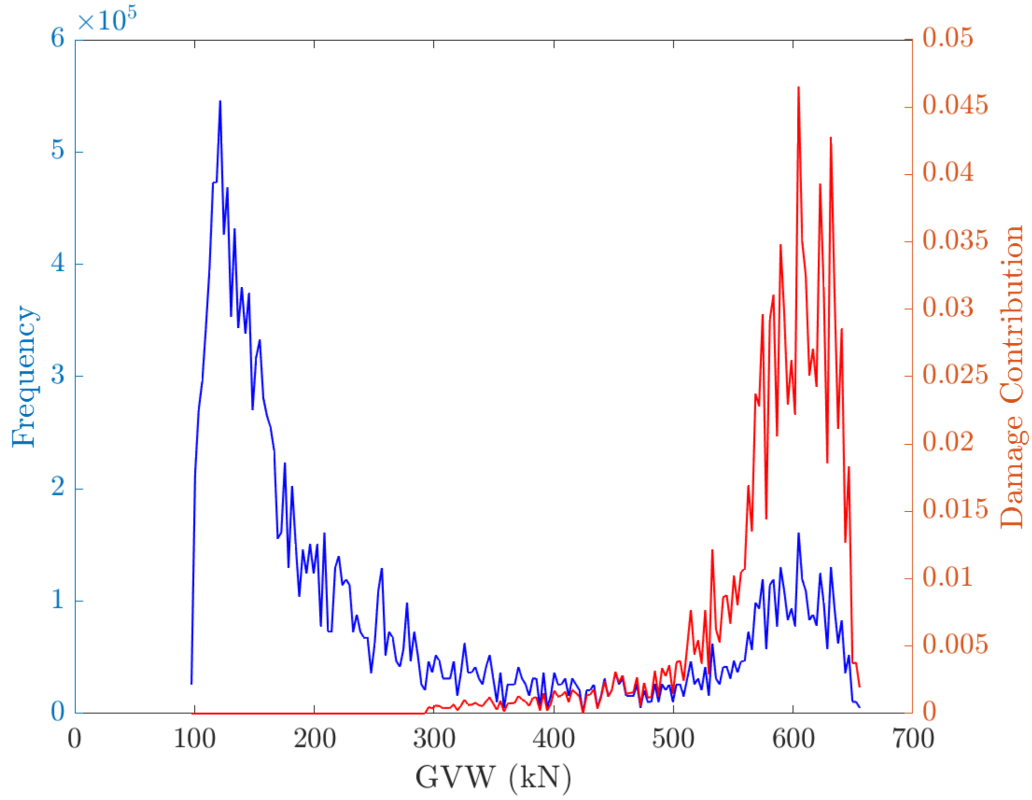

Figure 46. Fatigue damage contributions of the GVW in the 2014 B-WIM database. (Bin width=5kN).

5.1.1 Calibration of axle loads and axle spacings

The most dominant axle configuration, single axle weight, and axle group weights are determined according to their contribution to the total damage. The most frequently observed configuration with the largest total load in the 2016 database is a 1-2-2-2 configuration, where the first axle is a single axle, and the following six axles are tandems. It should be noted that only 7-axle vehicles are used to obtain the configuration of the new fatigue vehicle, as 7-axle vehicles were determined to contribute most to the damage. The weight of each axle is obtained by finding the weight that contributes most to the damage from their respective axles. The tandems are considered as groups, which means that the combined weight or group weight is determined.

The weight that contributes most to the damage of all first axles is 85kN. The value is also the same for all 7-axle vehicles. The contribution of the tandem axles depends heavily on their location in the configuration. From all 1-2-2-2 configurations in the 2016 database, the first tandem (axles 2 and 3) is heaviest 68% of the time. Meanwhile, the second tandem (axles 4 and 5) appears to be lightest 82% of the time. From all first tandem axles, a group weight of 210kN contributes most to the damage. Whereas, for second and third tandems the group weight that contributes most to the damage is 185kN and 195kN, respectively. These results align with the earlier observation that the first tandem is heaviest most of the time, followed by the third tandem and the second tandem. Figure 47 presents the damage contribution of a) the first axles and b) first group. Figure 48 shows the damage contribution for c) second group, and d) third group. The left vertical axis shows the frequency of said axles, whereas the right vertical axis shows the damage contribution. The horizontal axis presents the axle and group axle weights in kN.

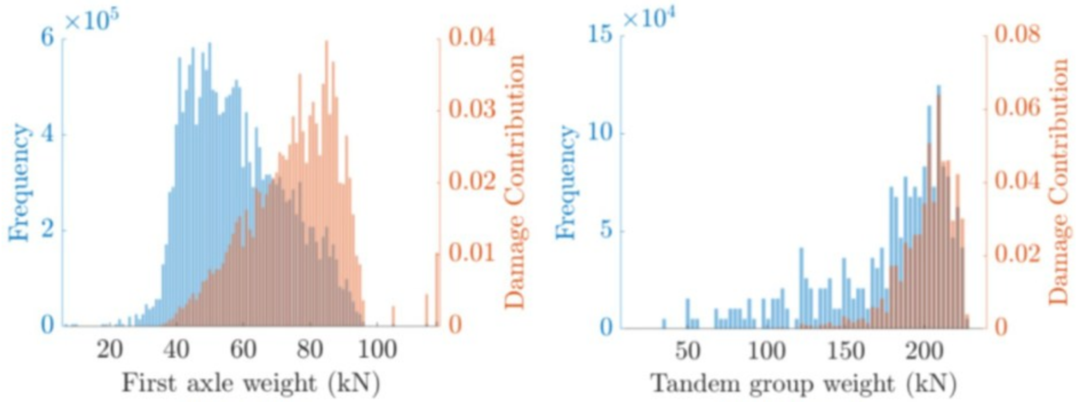

a) First Axle b) First Tandem

Figure 47. Damage contribution of a) the first axle, and b) first tandem. (First axle Bin width=1kN, tandem bin width=3kN).

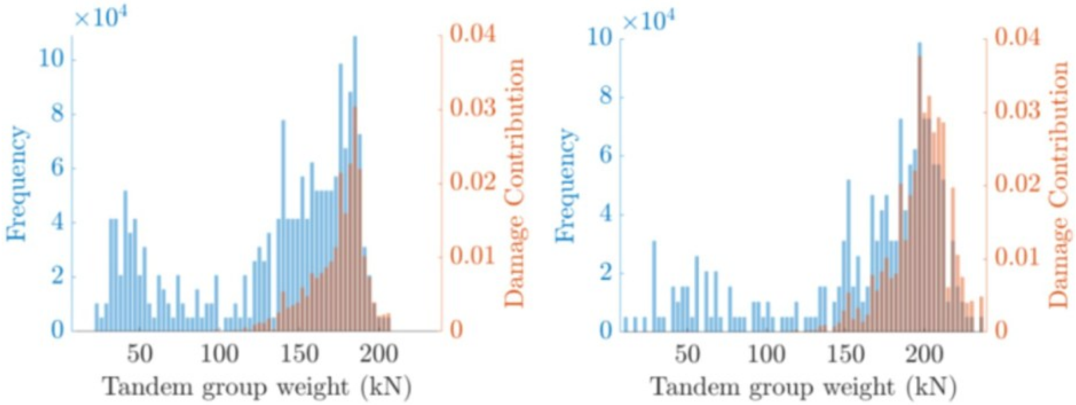

c) Second Tandem d) Third Tandem

Figure 48. Damage contribution of c) second tandem, and d) third tandem. (Bin Width=3kN).

The axle spacings are determined by finding the most frequent distances between the axles for the configuration of the new fatigue vehicle. That is the 1-2-2-2 configuration. As the new configuration consists of 3 tandem axles, the most common spacing between tandem axles is determined and used as the spacing for each tandem axle (1.4m). The distance between steering and traction (4.3m), 1st rear, and 2nd rear (4.2m), and 3rd rear, and 4th rear (6.2m) are determined by the frequencies from all 7-axle vehicles. Figure 49 illustrates the frequencies of the above-mentioned axle spacings. For the graph to show smoother results, the frequencies are multiplied with scaling factors.

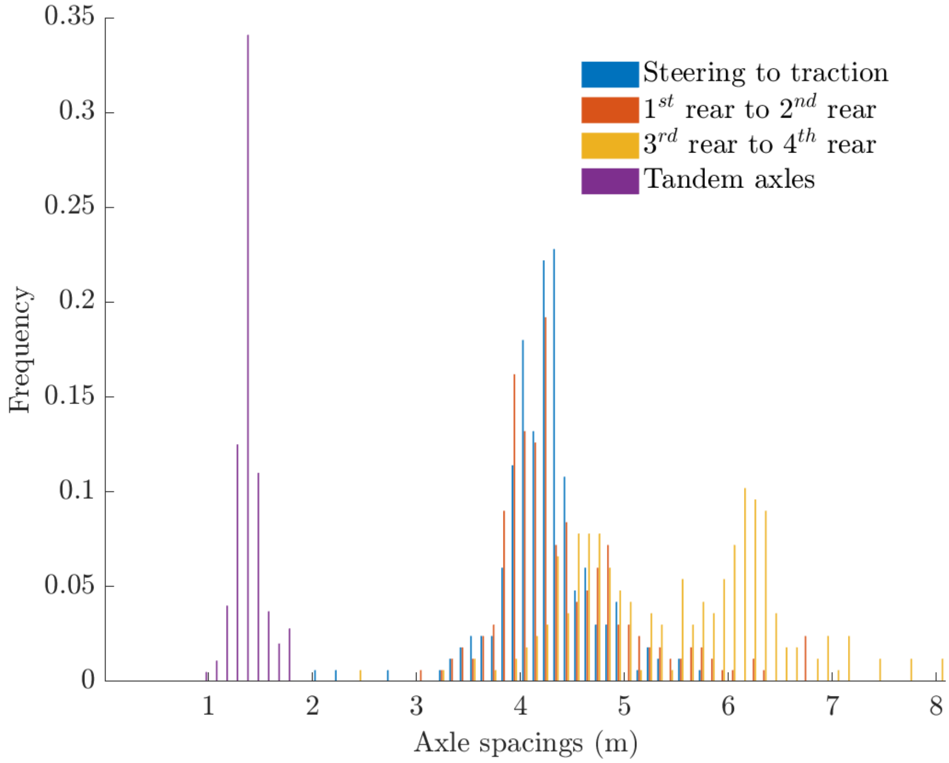

Figure 49. Distribution of the axle distances for 7-axle vehicles in the 2016 B-WIM database. (Bin width=0,1).

The frequencies of the axle spacings between years 2014 and 2016 B-WIM databases are similar, indicating that the overall vehicle configurations have remained while the weights have increased. This is because the regulation implemented in 2013 did not include the increase of vehicle lengths.

5.2 Calibration of the new Fatigue Load Model

In this chapter an improved Fatigue Load Model with improved accuracy compared to FLM3 and FLM4 is calibrated. As FLM3 is frequently used and is less complex and more practical than FLM4, it is taken as the basis for the new Fatigue Load Model. As λ_2 is the only factor that considers the annual traffic volume and vehicle weights, it will be updated to represent the new fatigue vehicle. Note that the N_{obs} used in λ_2 is the yearly traffic volume measured in Kaarina. Additionally, Q_{m1} is the equivalent weight of the Kaarina traffic. This way the new FLM is calibrated to represent the traffic in Kaarina. Hence, Q_{m1}=480,12kN and N_{obs}=193960, based on the Kaarina traffic. This leads to a λ_2=0.5886 for all span lengths, which is smaller than the values recommended in NCCI4 for span lengths longer than 30m.

Furthermore, λ_2 is smaller than that obtained with the fatigue vehicle used with FLM3. Additionally, new equations will be presented for the calculation of λ_1. These equations were introduced by Maljaars (2020). However, the equation for bending moment at midspan is modified slightly compared to the one the above author introduced. Due to the modification of λ_1 and λ_2, the damage equivalent factor λ will be updated. Therefore, the new damage equivalent factor can be expressed as:

$$\lambda = \lambda_1' \lambda_2' \, \lambda_3 \, \lambda_4 \tag{34}$$

where

$$\lambda_1' = \begin{cases} b + c \cdot L^d & \textit{For moment at midspan} \\ b' + c' \cdot L^{d'} & \textit{For moment at support} \end{cases} \tag{35}$$

$$\lambda_2' = \frac{Q_{m1}}{675} \left(\frac{N_{Obs}}{N_0} \right)^{\frac{1}{5}} \tag{36}$$

$$\lambda_3 = \left(\frac{t_{Ld}}{100} \right)^{\frac{1}{5}} \tag{16}$$

$$\lambda_4 = \left[1 + \frac{N_2}{N_1} \left(\frac{\eta_2 Q_{m2}}{\eta_1 Q_{m1}} \right)^5 + \frac{N_3}{N_1} \left(\frac{\eta_3 Q_{m3}}{\eta_1 Q_{m1}} \right)^5 + \cdots + \frac{N_k}{N_1} \left(\frac{\eta_k Q_{mk}}{\eta_1 Q_{m1}} \right)^5 \right]^{\frac{1}{5}} \tag{17}$$

Maljaars (2020) presented values for the calibration factors b…d' obtained from traffic measured in the Netherlands. However, these values give poor results when used against Kaarina traffic. Therefore, new calibration factors are determined and presented in this analysis. The calibration is done separately for influence lines concerning bending moment at midspan and bending moment at support. This means that factors b', c', and d', will be calibrated for IL_3, whereas factors b, c, and d for influence lines IL_1, IL_2, and IL_4. The calibration is performed by calculating the root mean square error (RMSE), between the required elastic section modulus obtained for B-WIM and the one for the new FLM. The goal is to minimise the error. RMSE is expressed as:

$$RMSE = \sqrt{\sum \left(\frac{W_{FLM} - W_{WIM}}{W_{WIM}} \right)^2} \tag{37}$$

To calibrate the new factors used with λ'_1, a MATLAB code is constructed that performs the RMSE calculation. With initial coefficients b…d', the code calculates the required elastic section modulus for all span lengths. This is done with the same principle as the fatigue analysis of FLM3. Furthermore, target values, in this case, the required elastic section modulus obtained for the 2016 B-WIM database, are added to the code. After the required $W_{,el}$ is determined for the new FLM, a generic algorithm, which is an in-built MATLAB function, is employed to find the factors that best fit the target values. This means that the elastic section modulus is recalculated over all span lengths with different factors, and the results are compared to the target ($W_{,el}$) values. The algorithm gradually improves the factors until the RMSE is minimised. Factors b…d' calibrated for Kaarina traffic are presented in Table 17. Additionally, the calibrated sub-factor λ'_1 is visualised for both the midspan and support section in Figure 50.

Table 17. Calibration coefficients for the new FLM.

b	c	d	b'	c'	d'
1.85	0.03	0.0019	1.8	0.019	0.33

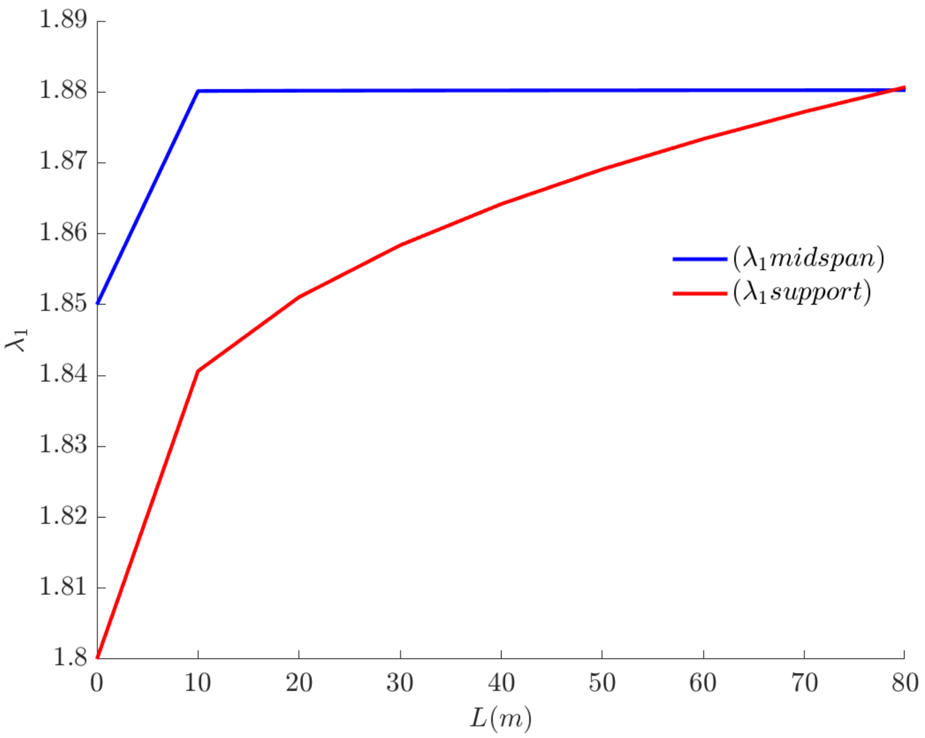

Figure 50. Illustration of sub-factor λ_1 for the new FLM.

5.2.1 Results from the analysis with the new Fatigue Load Model

Table 18 shows the required $W_{,el}$ for each span length and influence line obtained for the calibrated FLM. Each value represents the elastic section modulus needed for D=1 after 100 years. Additionally, Figure 51 shows the ratio between $W_{,el}$ for the new FLM and the $W_{,el}$ for the 2016 B-WIM data. The graph shows that the new FLM is more accurate than FLM3 and FLM4.

Notice that the new FLM is calibrated for a ratio of R=1. The unsafe results obtained for span lengths of 10m are due to the new fatigue vehicle exceeding the span length. Additionally, the new FLM slightly overestimates the required $W_{,el}$ for span lengths 20-80m. However, the overestimation is minimal (0-5%) depending on the span length and influence line. Nevertheless, the results obtained with the new FLM are promising.

The improvement in accuracy is due to the calibration of sub-factors λ'_1 and λ'_2. The first sub-factor now considers better the effect of the influence lines. Additionally, as Figure 50 shows, λ'_1 for the midspan section remains even for all span lengths. In Eurocodes and NCCI codes, this factor is obtained for a critical length from a decreasing line. For the support section, the sub-factor increases with the span length. This only occurs for span lengths longer than 20m in the design codes. Furthermore, due to the GVW of the new fatigue vehicle, sub-factor λ'_2 remains relatively low. This is because the new fatigue vehicle is heavier than the equivalent weight (Q_{m1}) of the Kaarina traffic.

Table 18. Required $W_{,el}$ for the new FLM corresponding to a fatigue damage of D=1 after 100 years (unit: m^3).

FLM (New)	10m	20m	30m	40m	50m	60m	70m	80m
IL_1	0.0111	0.0369	0.0736	0.1119	0.1501	0.1882	0.2264	0.2647
IL_2	0.0107	0.0370	0.0736	0.1121	0.1506	0.189	0.2274	0.2659
IL_3	0.0093	0.0232	0.0353	0.0519	0.0679	0.0835	0.099	0.1143
IL_4	0.01331	0.04641	0.0871	0.1285	0.1702	0.212	0.2539	0.2958

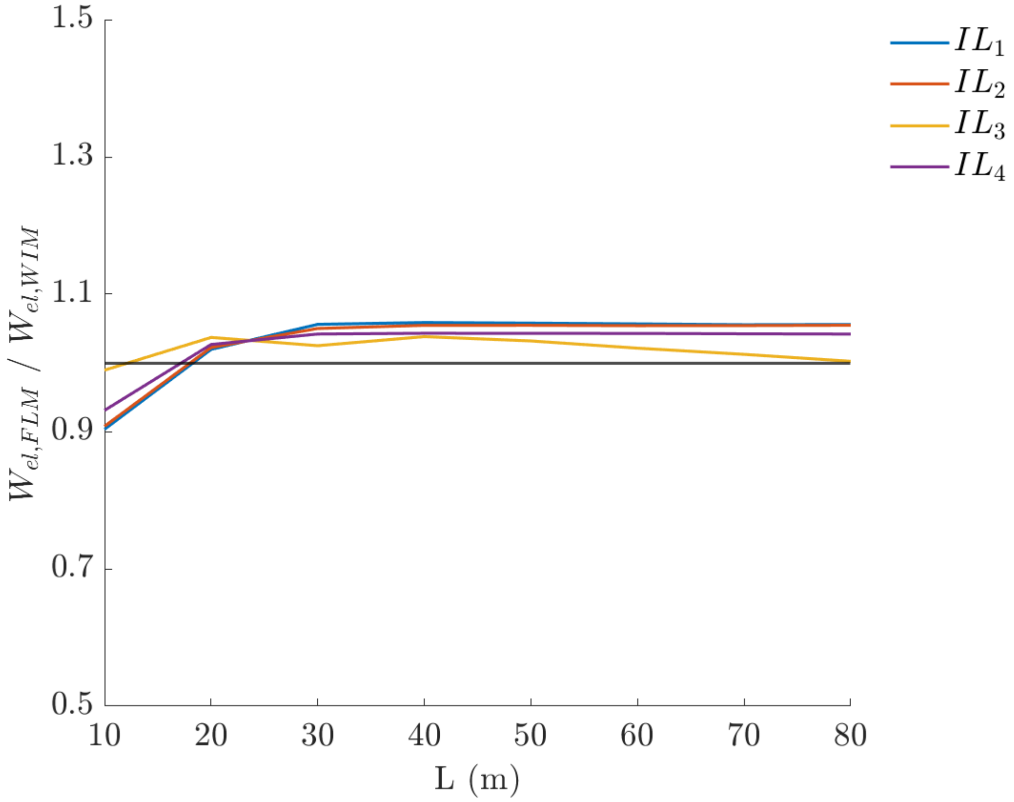

Figure 51. The ratio of the required $W_{,el}$ between the new FLM and the 2016 B-WIM database.

6 Summary and conclusions

The increase in vehicle weights has significance in the fatigue verification. This can be seen in the difference in the required $W_{,el}$ for 2016 recorded traffic compared to the 2014 recorded traffic. While the average GVW are similar between the two years, the heavier vehicles and higher number of vehicles in the latter year clearly increase the required $W_{,el}$. The effect of increased vehicle weights was also demonstrated by Aggarwal & Parameswaran (2015), Deng & Yan (2018) and Jang & Mohammadi (2018).

A new FLM was introduced based on Maljaars (2020) earlier work. The calculation of the damage equivalent factor and its sub-factors, λ'_1 and λ'_2, were improved and calibrated to the 2016 B-WIM database. The calibration of the new fatigue vehicle included the derivation of GVW, axle weights and group weights by finding the loads that contribute most to the damage. The axle spacings were determined by finding the most frequent distances between the axles from all 7-axle vehicles. The new fatigue vehicle is illustrated in Figure 39 in Chapter 5.

The comparison between actual traffic and Fatigue Load Models was made by calculating the required $W_{,el}$ for the 2016 B-WIM database and comparing it to the required $W_{,el}$ obtained for FLM3 and FLM4. A design life of 100 years was used in the analysis. The Fatigue Load Models used today clearly overestimate the required $W_{,el}$. The new FLM improves the accuracy substantially as shown in Figure 51. The improvement in accuracy is due to the calibration of sub-factors λ'_1 and λ'_2. Moreover, as λ'_2 is calibrated to Kaarina traffic, the change in flow rate or average GVW provides more accurate results when the new FLM is used. Additionally, the much heavier GVW of the new fatigue vehicle does not overestimate λ'_2. Hence, considering the goals presented in the Chapter 1.4, the following conclusions are drawn:

- The traffic recorded in 2016 induces higher stresses and more cycles and is, therefore, more unfavourable in terms of fatigue than the 2014 traffic. This can be observed from the higher elastic section modulus the latter year requires for a design life of 100 years. Additionally, for a bridge with a certain cross-section, the traffic from the latter year would cause a shorter fatigue life compared to the traffic recorded in 2014. Hence, the regulation changes have had an impact on bridge fatigue.

- The difference between the 2016 B-WIM data and Fatigue Load Models was inspected. FLM3 and FLM4 overestimate the required elastic section modulus compared to actual traffic, especially for shorter span lengths. However, while the vehicle weights have increased, the Fatigue Load Models give safe results. Furthermore, it should be noted that FLM3 and FLM4 overestimate the required section modulus slightly less for the 2016 traffic than the 2014 traffic. This is due to the 8-11% higher $W_{,el}$ required for 2016 B-WIM data compared to the 2014 B-WIM data. Hence, if 2014 traffic was used, the Fatigue Load Models would be 8-11% more conservative depending on the influence line and span length. This means that the increase in vehicle weights has slightly affected the safety rate of the Fatigue Load Models.

- A new FLM was introduced in this thesis that represents real traffic observed on the Finnish road network. The calibrated FLM increases the accuracy substantially compared to FLM3 and FLM4, giving similar results for all span lengths and influence lines. The new FLM was calibrated to represent a design life of 100 years.

- The set of equivalent lorries provided in SFS-EN 1991-2 appears to provide similar results as the vehicles in the 2016 B-WIM database when a traffic volume that is equal to the B-WIM data is used. Therefore, the inaccuracies obtained from FLM4 are due to the traffic volumes provided in the Eurocodes.

6.1 Limitations and future work

While the new FLM is derived for traffic measured in Kaarina, it does not fully represent real traffic, as the vehicles were considered to cross the bridge separately. Therefore, the new FLM may slightly underestimate the required $W_{,el}$. To further examine the accuracy of the new FLM, the required $W_{,el}$ of bridges where multiple vehicles are simultaneously on the bridge shall be studied. This could have an impact especially on longer span lengths. The effect of multiple vehicles crossing a bridge depends on how the vehicles are positioned along the span length. Furthermore, the length of the span influences the probability of multi-vehicle effect. The effect is clearly lower when two vehicles are travelling on the same lane compared to bidirectional crossing.

As the measurement period was only one week, the accuracy of the B-WIM data can be questioned. There are clear signs of heavier vehicles on today's road network, which is logical due to the new regulation presented in 2013. However, there may be a risk of the B-WIM database overestimating or underestimating the number of vehicles measured during the one-week measurement campaigns in 2014 and 2016, as there is no certainty of how well the one-week measurement period compares to possible one-year traffic. Therefore, the measurement periods could be longer to get a more accurate representation of real traffic. This way, the review of the Fatigue Load Models would be more accurate. Also, as the axle and vehicle weights are measured during motion, the actual axle weights may lack accuracy. The provided vehicle data did not include possible DAF coefficients or any information if the axle weights were multiplied with a DAF. Therefore, if DAF is included in the weight measurements, the provided B-WIM data presentation should give that information along with the DAF coefficients.

For verifying the accuracy and suitability of the new FLM, the coefficients b…d' presented in Table 17 should be tested against other measured traffics with similar characteristics as the Kaarina traffic. Qvisen (2020) and Hirvonen (2022) categorised measured traffic from multiple measurement sites as long distance, medium distance, and local traffic. As the traffic measured in Kaarina was classified as medium distance traffic, the calibration factors should be tested against other traffic measurements categorised as such. Moreover, due to the categorisations, different calibration factors can be calibrated separately for long distance and local traffic types if needed.

References

Aggarwal, V., & Parameswaran, L. (2015). *Effect of Overweight Trucks on Fatigue Damage of a Bridge*. In Advances in Structural Engineering, p.2483-2491. DOI: DOI 10.1007/978-81-322-2187-6_190

Al-Emrani, M. & Aygul, M. (2014). *Fatigue design of steel and composite bridges*. Department of Civil and Environmental Engineering, Division of Structural Engineering, Steel and Timber Structures. Chalmers University of Technology. Göteborg, Sweden, Report 2014:10. ISSN 1652-9162

Al-Qadi, I., Wang, h., Ouyang, Y., Grimmelsman, K., & Purdy, J. (2016). *LTBP Program's Literature Review on Wigh-in-Motion Systems*. U.S. Department of Transportation. Report No. FHWA-HRT-16-024, 42p. Retrieved from https://rosap.ntl.bts.gov/view/dot/35735

ASTM E1049-85. (2017). *Standard Practices for Cycle Counting in Fatigue Analysis*. ASTM International. DOI: https://doi.org/10.1520/E1049-85R17

Brady, S. P., O'Brien E. J., & Znidaric, A. (2006). *The Effect of Vehicle Velocity on the Dynamic Amplification of a Vehicle crossing a Simply Supported Bridge*. Journal of Bridge Engineering. Volume 11, Issue 2, pp.241-249 (March/April 2006). DOI: http://dx.doi.org/10.1061/(ASCE)1084-0702(2006)11:2(241)

Bruls, A. Calgaro, J-A, Mathieu & H. Prat, M. (1996). ENV 1991 part 3: The main models of traffic loads on road bridges: background studies. DOI: https://doi.org/10.5169/seals-56073

Chan, T.H., Law, S.S., Yung, T.H., & Yan, X.R. (1999). *An interpretive method for moving force identification*. Journal of Sound and Vibration 219(3): 503–524. DOI: https://doi.org/10.1006/jsvi.1998.1904

Chatzis, M., & Lilja, H. (2012). *Calibrating Eurocode's Fatigue Load Model 3 to Specific National Traffic Composition*. Structural Engineering International, Volume 22, 2012, Issue 2, p. 232-237. DOI: 10.2749/101686612X13291382991128

Constantinescu, A., Van, K. D., & Maitournam, H. (2022). *A unified analysis for low and high cycle fatigue based on shakedown concepts*. Fatigue and Fracture of Engineering Materials and Structures, 2003, 26, pp.561-568. DOI: https://doi.org/10.1046/j.1460-2695.2003.00675.x

Cottrell, B. H. (1992). *The Avoidance of Weigh Stations in Virginia by Overweight Trucks*. Virginia Department of Transportation, Virginia Transportation Research Council, Report No. FHWA/VA-93-R2, 1992, pp, 33. Retrieved from https://rosap.ntl.bts.gov/view/dot/19321

COUNCIL DIRECTIVE 96/53/EC. (1996). Weights and Dimensions Directive rules. Retrieved from https://eur-lex.europa.eu/eli/dir/1996/53/oj

Croce, P. (2001). *Background to fatigue load models for Eurocode 1: Part 2 Traffic Loads*. Progress in Structural Engineering and Materials 3(4):335-345. DOI: 10.1002/pse.93

De Ceuster, G., Breemersch, T., Van Herbriggen, B., Verweij, K., Davydenko, I., Klingender, M., Jacob, B., Arki, H., & Bereni, M. (2008). *Effects of adapting the rules on weights and dimensions of heavy commercial vehicles as established within Directive 96/53/EC*. Final Report, European Commission. Directorate-General Energy and Transport, Brussels. 315 p. Issue Number: TREN/G3/318/2007. Retrieved from http://ec.europa.eu/transport/themes/strategies/studies/doc/2009_01_weights_and_dimensions_vehicles.pdf

Deng, L., & Yan, W. (2018). *Vehicle Weight Limits and Overload Permit Checking Considering the Cumulative Fatigue Damage of Bridges*. Journal of Bridge Engineering. Vol. 23, Issue 7. DOI: 10.1061/(ASCE)BE.1943-5592.0001267

EN 1990 (2002). *Eurocode – Basis of structural design*. The European Union Per Regulation 305/2011, Directive 98/34/EC, Directive 2004/18/EC. Retrieved from https://eurocodes.jrc.ec.europa.eu/EN-Eurocodes/eurocode-basis-structural-design

Fatemi, A., & Yang, L. (1998). *Cumulative fatigue damage and life prediction theories: a survey of the state of the art for homogeneous materials*. International Journal of Fatigue, Vol. 20(1), January 1998, p.9-34. DOI: https://doi.org/10.1016/S0142-1123(97)00081-9

Fernandes, R. Oliveira, L. & Henriques, N. (2020). *Growing Evolution of the Electrification Rate on Heavy Vehicles*. In International Congress on Engineering-Engineering for Evolution, KnE Engineering, pages 896–907. DOI: 10.18502/keg.v5i6.7108

Finnish Transport Agency, (2018). *Bridge WIM Overview Report: Year 2013-2017*. Research reports of the Finnish Transport Agency, 29/2018-Retrieved from: https://www.doria.fi/handle/10024/164063

Fiorillo, G., & Ghosn, M. (2015). *Application of influence lines for the ultimate capacity of beams under moving loads*. Department of Civil Engineering, The City College of New York/CUNY, 160 Convent Avenue, New York, NY 10031, United States. Engineering Structures 103 (2015) 125–133. DOI: http://dx.doi.org/10.1016/j.engstruct.2015.09.003

Hectors, K. & De Waele, W. (2021). *Cumulative Damage and Life Prediction Models for High-Cycle Fatigue of Metals: A Review*. Metals 2021, 11, 204, DOI: https://doi.org/10.3390/met11020204

Hirvonen, J. (2022). *Fatigue assessment of a bridge expansion joint utilizing traffic data*. Master's thesis. Aalto University, School of Engineering, Building Technology, pp. 116. Retrieved from https://aaltodoc.aalto.fi/items/d10f59af-54bf-4193-b5d9-49ad86208cda

Hobbacher, A., Fricke, W., Haagensen, P. J., Huther, M., Iida, K., Lierurade, H.P., Maddox, S. J., Marguis, G., Miki, Ch., Niemi, E., Ohta, A., Ørjasæter, O., Petershagen, H. J., & Sonsino, C. M. (2008). *RECOMMENDATIONS FOR FATIGUE DESIGN OF WELDED JOINTS AND COMPONENTS*. International Institute of Welding, doc. XIII-2151r4-07/XV-1254r4-07. Paris, France, October 2008

Jacob, B., & La Beaumelle, V. (2010). *Improving truck safety: Potential of weigh-in-motion technology*. IATSS Research Volume 34, Issue 1, July 2010, pages 9-15. DOI: http://dx.doi.org/10.1016/j.iatssr.2010.06.003

Jang, B., & Mohammadi, J. (2018). *Significance of Fatigue Damage from Overloaded Trucks on Bridge Load Rating*. MATEC Web Conf. Volume 165, 2018, 12th International Fatigue Congress (FATIGUE 2018). pp, 6. DOI: https://doi.org/10.1051/matecconf/201816510005

Karim, M., Ibrahim, N., Saifizul, A., & Yamanaka, H. (2012). *Effectiveness of vehicle weight enforcement in developing country using weign-in-motion sorting system considering vehicle by-pass and enforcement capability*. IATSS Research Volume 37, Issue 2, March 2014, p. 124-129. DOI: http://dx.doi.org/10.1016/j.iatssr.2013.06.004

Kim, J., Jung, Y., Utebayeva, A., Kamaliyeva, Z., Collins, N., Sarbassov, D., Sagin, J., & Amanzhlova, R. (2021). *HIGH-PERFORMANCE HIGH-SPEED WIM FOR SUSTAINABLE ROAD LOAD MONITORINGUSING GIS TECHNOLOGY*. TRANSPORT PROBLEMS 2021 Volume 16 Issue 4, p. 149-162. DOI: 10.21307/tp-2021-067

Kulovic, M., Injac, Z., Davidovic, S., & Posavac, I. (2017). *MODELLING TRUCK WEIGH STATIONS' LOCATIONS BASED ON TRUCK TRAFFIC FLOW AND OVERWEIGHT VIOLATION: A CASE STUDY IN BOSNI AND HERZEGOVINA*. Promet – Traffic&Transportation, Vol. 30, 2018, No. 2, 163-171. p, 166. DOI: 10.7307/ptt.v30i2.2423

Law, S. S., Chan, T. H. T. & Zeng, Q. H., (1997). *Moving force identification: A Time domain method*. Journal of Sound and Vibration. Vol. 201:1. p. 1-22. ISSN: 0022-460X

Law, S. S., Chan, T. H. T. & Zeng, Q. H., (1999). *Moving Force Identification—A Frequency and Time Domains Analysis*. Journal of dynamic systems, measurement, and control. Vol. 121:3. p. 394-401. ISSN: 0022-0434

Lee, S. H., An, L. S., Park, Y. C., & Kim, H. K. (2022). *How to Use BWIM Data in Fatigue Evaluation of a Medium-span Steel Bridge*. In: International Journal of Steel Structures (2022) 22(6):1817-1828. DOI: https://doi.org/10.1007/s13296-022-00661-8

Lee, Y., Pan, J., Hathaway, R., & Barkey, M. (2005). *Fatigue Testing and Analysis (Theory and Practice). 416 p.* ISBN: 0-7506-7719-8. DOI: https://doi.org/10.1016/B978-0-7506-7719-6.X5000-3

Li, K., Gu, L., Wang, X., Wang, J., Wang, R., Gu, H., Zhang, X., & Tu, S. (2023). *A unified rule for high-cycle and low-cycle fatigue life prediction in multi-scale framework*. International Journal of Fatigue 179 (2023) 107512. DOI: https://doi.org/10.1016/j.ijfatigue.2023.107512

Ludescher, H., & Bruhwiler, E. (2009). *Dynamic Amplification of Traffic Loads on Road Bridges*. Article in Structural Engineering International, 10(2): 190-197, May 2009. DOI: 10.2749/101686609788220231

Lydon, M., Taylor, S.E., Robinson, D., Mufti, A., & O'brien, E.J. (2016). *Recent Developments in Bridge Weigh in Motion (B-WIM).* In Journal of Civil Structural Health Monitoring, Volume 6, pages 69-81, (2016). DOI: 10.1007/s13349-015-0119-6

Maddah, N. (2013). *Fatigue Life Assessment of Roadway Bridges based on Actual Traffic Loads*. PhD dissertation at EPFL, Lausanne, 2013. Retrieved from 10.5075/epfl-thesis-5575

Maljaars J. (2020). *Evaluation of traffic load models for fatigue verification of European road bridges*. In Engineering Structures 225 (2020): 111326. TNO, The Netherlands, Eindhoven University of Technology. DOI: 10.1016/j.engstruct.2020.111326

Manson, S. (1964). *Interpretive Report on Cumulative Fatigue Damage in the Low Cycle Range*. NASA Lewis Research Center Cleveland, OH, United States. Accession No. 64N30606. Retrieved from https://ntrs.nasa.gov/

Manson, S. & Halford, G. (1980). *PRACTICAL IMPLEMENTATION OF THE DOUBLE LINEAR DAMAGE RULE AND DAMAGE CURVE APPROACH FOR TREATING CUMULATIVE FATIGUE DAMAGE*. NASA Technical Memorandum 81517. Accession Number: 80N23684. Retrieved from https://ntrs.nasa.gov/citations/19800015193

Marco, S. M. & Starkey, W. L. (1954). *A Concept of Fatigue Damage*. Trans. ASME. May 1954, 76, 627-632. DOI: https://doi.org/10.1115/1.4014922

Mayer, R.M., Poulikakos, L.D., Lees, A.R., Heutschi, K. Kalivoda, M.T., & Soltic, P. (2010). *Reducing the environmental impact of road and rail vehicles*. Environmental Impact Assessment Review 32 (2012) 25-32. DOI: 10.1016/j.eiar.2011.02.001

Mertz, D. (2022). *Steel Bridge Design Handbook. Chapter 12: Design for Fatigue*. National Steel Bridge Alliance, a division of the American Institute of Steel Construction. Publication No. B912-22, 36 p. Retrieved from https://www.aisc.org/nsba/design-and-estimation-resources/steel-bridge-design-handbook/

Miner, M. A. (1945). *Cumulative damage in fatigue*. J. Appl. Mech. Sep 1945, 12(3): A159-A164. DOI: https://doi.org/10.1115/1.4009458

Moses, F., (1979). *Weigh-in-motion system using instrumented bridges*. Journal of Transportation Engineering. Vol. 105:3. p. 233-249. DOI: https://doi.org/10.1061/TPEJAN.0000783

NCCI 1, (2017). *Eurokoodin soveltamisohje: Siltojen kuormat ja suunnitteluperusteet* – NCCI 1 (6.12.2017). ISBN: 978-952-317-486-3

NCCI 4, (2016). Eurokoodin soveltamisohje: Teräs- ja liittorakenteiden suunnittelu – NCCI 4 (25.8.2016). ISBN: 978-952-317-306-4

Norman, O., & Hopkins, R. (1952). *Weighing Vehicles in Motion*. Highway Research Board Bulletin, Issue 50, Highway Research Board, 1952

O'Brien, E., Znidaric, A., Baumgärtner, W., Gonzalez, A., McNulty, P., & et al. (2001). *Weighing-in-Motion of Axles and Vehicles for Europe (WAVE)*. WP.2: Bridge WIM Systems. Dublin, Ireland: University College Dublin. ISBN: 961-90366-1-1

O'Connor C. & Chan Tommy, H. T. (1988). *Dynamic Wheel Loads From Bridge Strains*. Journal of Structural Engineering. Vol. 114:8. p. 1703-1723. DOI: 10.1061/(ASCE)0733- 9445(1988)114:8(1703)

Ojio, T. & Yamada, K. (2002). *Bridge weigh-in-motion systems using stringers of plate girder bridges*. In: Third International Conference on Weigh-in-Motion (ICWIM3). Iowa Orlando, USA. 13-15 May 2002. p. 209-218

Ojio, T. & Yamada, K. (2005). *Bridge WIM by reaction force method*. In: Fourth International Conference on Weigh-In-Motion (ICWIM4). Taipei, Taiwan. 20-23 February 2005

Palmgren, A. (1924). *Die Lebensdauer von Kugellagern*. VDI-Zeitschrift 68, 1924, pp. 339-341

Pedersen, M. (2018). *Introduction to Metal Fatigue – Concepts and Engineering Approaches*. Aarhus University, Department of Engineering. DOI: 10.13140/RG.2.2.25216.28163

Peres, N. (2004). *Fracture Mechanics*. Springer New York. DOI: https://doi.org/10.1007/b118073

Peters, R. J. (1984). *AXWAY – a system to obtain vehicle axle weights*. In: Proceedings of the 12th Australian road research board conference. Hobart, Australia. 27-31 August 1984. Vermont South, Australia: APRB Group Limited. Vol. 12:1. p. 10-18. ISSN: 0005-0164

Peters, R. J., (1986). *CULWAY – an unmanned and undetectable highway speed vehicle weighing system*. In: Australian Road Research Board Proceedings. Hobart, Australia. 25-29 August 1986. Vermont South, Australia: APRB Group Limited. Vol. 13:6. p 70–83

Pöyskö, T. Sirkiä, A & Lapp, T. (2014) Elinkeino-, liikenne- ja ympäristökeskus. Raskaan liikenteen uudet enimmäismitat ja – massat. (Finnish). ISBN 978-952-314-005-9 (PDF)

Qvisen, J. (2020). *Standardised Bridge Weigh-in-Motion data and its applications in bridge engineering*. Master's thesis. Aalto University, School of Engineering, Building Technology. Espoo. pp. 87. Retrieved from https://aaltodoc.aalto.fi/items/647a1f1c-03cd-49e7-b577-32bb62504ad4

Rauhanen, M. (2015). *Ajoneuvoasetuksen muutos 2013*. In: Kuntatekniikan päivät. (Presentation). 21-22.5.2015. Available at: https://kuntatekniikka.fi/wp-content/uploads/sites/2/2015/06/SKTY_Ajoneuvoasetukse-muutos_Rauhanen_ Turku2015.pdf

Richardson, J., Jones, J., Brown, S., O'Brien, E., & Hajializadeh, D. (2014). *On the use of bridge weigh-in-motion for overweight truck enforcement*. International Journal of heavy vehicle systems IJHVS 21(2):83-104. DOI: 10.1504/IJHVS.2014.061632

Richart, F. E. & Newmark, N. (1975). *An Hypothesis for the Determination of Cumulative Damage in Fatigue*. In Civil Engineering Classics; Newmark, N.M., Ed.; ASCE: Reston, VA, USA, 1948; pp. 279–312

Roylance, D., (2001). *Fatigue*. Department of Materials Science and Engineering, Massachusetts Institute of Technology, Cambridge, MA 02139, May 1, 2001.

Russo, F., Mertz, D., Frank, K., & Wilson, K. (2016). *Design and Evaluation of Steel Bridges for Fatigue and Fracture*. U.S. Department of Transportation. Federal Highway Administration. Publication No. FHWA-NHI-16-016, December 2016. 310 p. Retrieved from https://rosap.ntl.bts.gov/view/dot/42864

Rygula, A., Brzozowski, K., & Maczynski, A. (2019). *Limitations of the effectiveness of Weigh in Motion systems*. Open Eng. 2020; 10:183-196. DOI: https://doi.org/10.1515/eng-2020-0020

Schütz, W. (1996). *A HISTORY OF FATIGUE*. Engineering Fracture Mechanics, Vol. 54. No. 2, pp. 263-300, 1996. DOI: https://doi.org/10.1016/0013-7944(95)00178-6

Silvennoinen, A. (2007). *Terässiltojen väsymismitoitus EUROCODE-standardin pohjalta*. TEKNILLINEN KORKEAKOULU, RAKENNUS- JA YMPÄRISTÖTEKNIIKAN OSASTO. Master's Thesis. retrieved from: https://urn.fi/URN:NBN:fi:aalto-2020120553979

Sivakumar, B., Ghosn, M., & Moses, F. (2011). *Protocols for collecting and using traffic data in bridge design*. National Academy of Sciences, 2011, 116 p., ref. National Cooperative Highway Research Program NCHRP Report 683 - NCHRP Project 12-76(01). ISSN 0077-5614

SFS-EN 1991-2. (2006). *Eurocode 1. Actions on structures. Part 2: Traffic loads on bridges*. The Finnish Standard Association SFS. Retrieved from https://online.sfs.fi/

SFS-EN 1992-1-1. (2005). *Eurocode 2. Design of concrete structures. Part 1-1: General rules and rules for buildings*. The Finnish Standard Association SFS. Retrieved from https://online.sfs.fi/

SFS-EN 1993-1-9. (2005). *Eurocode 3. Design of steel structures. Part 1-9: Fatigue*. The Finnish Standard Association SFS. Retrieved from https://online.sfs.fi/

SFS-EN 1993-2. (2006). *Eurocode 3. Design of steel structures. Part 2: Steel Bridges*. The Finnish Standard Association SFS. Retrieved from https://online.sfs.fi/

Skoglund, O. (2021). *An Introduction to Fatigue of Civil Engineering Structures*. KTH Royal Institute of Technology, Stockholm 2021. Department of Civil and Architectural Engineering, Division of Structural Engineering and Bridges. Retrieved from URN: urn:nbn:se:kth:diva-305468

Skoglund, O. (2022). *Fatigue life estimation based on LEFM and the study of initial parameters*. KTH Royal Institute of Technology, Stockholm 2021. Department of Civil and Architectural Engineering, Division of Structural Engineering and Bridges. ISBN: 978-91-8040-018-3

Skoglund, O., & Leander, J. (2022). *Initial parameters to estimate the fatigue strength of welded structures using a fracture mechanical model*. Division of Structural Engineering and Bridges, KTH Royal Institute of Technology, Stockholm, Sweden. In Engineering Structures Volume 260, 1 June 2022, 114185. DOI: https://doi.org/10.1016/j.engstruct.2022.114185

Tompuri, V. (2023). *Kruunuvuorensilta on Suomen suurin*. Infra ja Ympäristörakentaminen, NRO 1/2023. Retrieved 20 7, 2024, from https://betoni.com/lehti/2023/03/03/kruunuvuorensilta-on-suomen-suurin/

Toikka, J. & Virtala, P. (2015). *Akselimassatutkimus 2013–2015: projektin loppuraportti*. Helsinki, Finland: Liikennevirasto, tekniikka ja ympäristö -osasto. Liikenneviraston tutkimuksia ja selvityksiä 67/2015. ISBN: 978-952-317-179-4

Väylävirasto. (2023). *Siltojen toimintalinjat*. Väyläviraston ohjeita 9/2023. (Finnish). VÄYLÄ/1479/06.04.01/2023. Retrieved from: https://vayla.fi/etusivu

Väylävirasto (2024): *Bridge maintenance*. Retrieved 10 10, 2024 from https://vayla.fi/en/maintenance/road-network/bridge-maintenance

Walbridge, S., Fischer, V., Maddah, N., & Nussbaumer, A. (2013). *Simultaneous Vehicle Crossing Effects on Fatigue Damage Equivalence Factors for North American Roadway Bridges*. In Journal of Bridge Engineering, Vol. 18, No. 12, December 1, ASCE, 2013.18:1309-1318. DOI: 10.1061/(ASCE)BE.1943-5592.0000482

Wang W., Deng, L., & Shao, X. (2015). *Number of stress cycles for fatigue design of simply supported steel I-girder bridges considering the dynamic effect of vehicle loading*. In Engineering Structures 110 (2016) 70-78. Key Laboratory for Wind and Bridge Engineering of Hunan Province, Hunan University, Changsha, Hunan 410082, China. DOI: http://dx.doi.org/10.1016/j.engstruct.2015.11.054

Willets, L. (2024). *EU amends HGV weights limits*. Retrieved 2 9, 2024, from https://truckandbusbuilder.com/article/2024/03/14/eu-amends-lorry-transportation-weight-limits

Yarnold, M., Shi, S., Barden, C., Hurlebaus, S., Mander, J. Walubita, L., & Middleton, D. (2023). *DEVELOP BRIDGE WEIGH-IN-MOTION APPROACH TO MEASURE LIVE LOADS ON TEXAS HIGHWAYS: TECHNICAL REPORT*. TEXAS A&M TRANSORTATION INSITUTE COLLEGE STATION, TEXAS. Technical Report 0-7038-R1. Retrieved from https://rosap.ntl.bts.gov/view/dot/73202/dot_73202_DS1.pdf

Ye, X. W., Su, Y.H., & Han, J.P. (2014). *A State-of-the-Art Review on Fatigue Life Assessment of Steel Bridges*. Hindawi Publishing Corporation. Mathematical Problems in Engineering. Vol. 2014, Article ID: 956473, 13 pages. DOI: http://dx.doi.org/10.1155/2014/956473

Yu, Y., Cai, C. S. & Deng, L., (2016). S*tate-of-the-art review on bridge weigh-in-motion technology*. In Advances in Structural Engineering 19(9): 1514-1530. DOI: 10.1177/1369433216655922

Appendices

Appendix A – Fatigue Load Model calibration with DAF=1,0

A. Fatigue Load Model calibration with DAF=1,0

As there is no certainty of DAF being included in the recorded axle forces, the required $W_{,el}$ for the years 2014 and 2016, as well as calibration factors for λ'1, will be introduced in this appendix. The results are from calculations where DAF=1,0.

Table 19 and Table 20 shows the required $W_{,el}$ for the years 2014 and 2016. As expected, the difference is 20% across all span lengths and influence lines compared to calculations where DAF=1,2.

Table 19. Required $W_{,el}$ for year 2014. (DAF=1,0).

2014	10m	20m	30m	40m	50m	60m	70m	80m
IL1	0.0092	0.0274	0.0531	0.0805	0.108	0.1355	0.163	0.1907
IL2	0.0089	0.0274	0.0534	0.081	0.1086	0.1364	0.164	0.1917
IL3	0.0072	0.017	0.026	0.038	0.0501	0.0621	0.0744	0.0866
IL4	0.0107	0.0344	0.0636	0.0937	0.124	0.1545	0.185	0.2156

Table 20. Required $W_{,el}$ for year 2016. (DAF=1,0).

2016	10m	20m	30m	40m	50m	60m	70m	80m
IL_1	0.01018	0.0302	0.0581	0.0881	0.1183	0.1484	0.1787	0.2089
IL_2	0.00981	0.0302	0.0584	0.0886	0.119	0.1494	0.1798	0.2101
IL_3	0.00781	0.0187	0.0287	0.0417	0.0549	0.0682	0.0815	0.0951
IL_4	0.01187	0.0377	0.0697	0.1027	0.136	0.1694	0.203	0.2366

The calibration factors derived with DAF=1,0 are presented in Table 21. Additionally, Figure 52 shows the ratio between the required $W_{,el}$ for the new FLM and the required $W_{,el}$ for 2016 B-WIM data, with DAF=1,0. With these calibration factors, the ratios obtained for different span lengths and influence lines resemble the result obtained with DAF=1,2.

Table 21. Calibration coefficients for λ_1. (DAF=1,0).

b	c	d	b'	c'	d'
1.35	0.25	0.0007	1.2	0.31	0.058

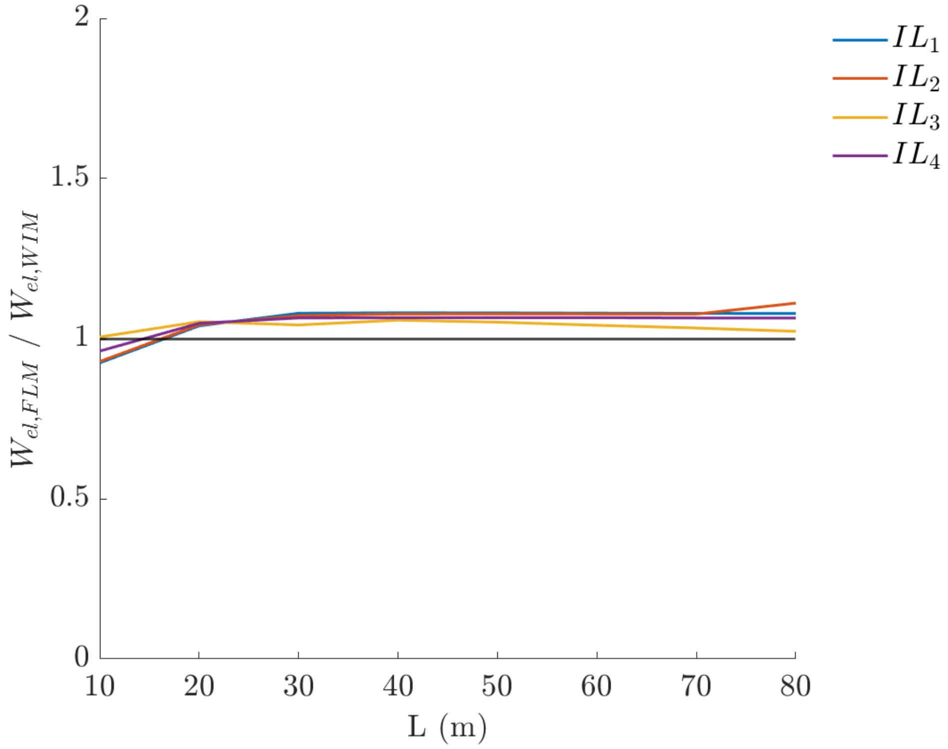

Figure 52. The ratio of the required $W_{,el}$ between the new FLM and the 2016 B-WIM database. (DAF=1,0).